Enhanced Active Power Control of Photovoltaic Systems

Fyali Jibji-Bukar

Department of Electronic and Electrical Engineering

University of Strathclyde

A thesis submitted for the degree of Doctor of Philosophy

May 2020

Declaration

This thesis is the result of the author's original research. It has been composed by the author and has not been previously submitted for examination which has led to the award of a degree.

Acknowledgement

First, I am grateful to God for his grace, love and mercy.

I would like to thank my supervisor, Prof Olimpo Anaya-Lara for his guidance, technical support and invaluable feedback over the course of my studies. I am also grateful his patience and moral support. I would also like to thank my second supervisor, Dr. Alasdair McDonald, for his advice at the beginning of my PhD.

I will like to thank Parents and my brothers for their love, prayers, financial and moral support I have consistently received from them.

Finally, I will like to thank all my friends who provided me with support and encouragement throughout the period of my PhD studies.

This thesis is dedicated to my parents:

Wasa and Elizabeth Jibji

Abstract

The share of electrical power generation from renewable energy sources is increasing and is expected to keep on increasing as various countries intensify their efforts to reduce CO_2 emissions. Differences in the nature and characteristics of some renewable generation affect the ability of power systems to maintain frequency stability. This is because some renewable generation sources do not have inertia or are converter connected and decoupled from grid frequency.

Solar Photovoltaic system do not have any stored inertia and usually operate at maximum power. There is need for control method for solar PV systems to contribute to frequency stability. This thesis proposes operation methodologies for photovoltaic (PV) systems to carry out active power control functions - including frequency control and proposes a framework for comparing frequency support ability of different generation sources.

First, a modification to the conventional Perturb and Observe (P&O) maximum power point tracking (MPPT) algorithm is proposed to avoid leftward and rightward from maximum power. Results presented show that PV systems employing P&O with the proposed modification avoid both leftward and rightward drift when subjected to rapidly increasing irradiance, sinusoidal irradiance, and real irradiance. This drift-free P&O enables the PV system to participate in active power control function at rapidly increasing irradiance. An offline MPPT that uses the characteristics of PV modules to determine the maximum power point offline and reduce online computation is proposed for frequency support. Two methods for achieving de-loaded operation of a PV system using the offline MPPT are presented and compared for accuracy. The ability of offline MPPT and the P&O with proposed modification to maintain a power reserve under different irradiance conditions are compared.

Second, this thesis examines the ability of a PV system to contribute to frequency support. Different methods for frequency support from a PV power plant under different penetration levels are examined. Results show with the appropriate amount of reserve and support parameters, PV systems can contribute to frequency support. The results also show that PV power plants with the proper support parameters

can adequately compensate for the loss of inertia with regards to its effect on the nadir of frequency response. A variable droop control method for frequency support is proposed to reduce the amount of reserve required for frequency support. The effect of MPPT choice on frequency support is evaluated by comparing responses from PV systems with the offline MPPT, P&O with proposed modification, and the constant voltage MPPT.

Lastly, this thesis proposes a framework for comparing the frequency support ability of different generating units based on their response speed and support parameters. Different response speeds are emulated by changing one the time constant of a Second-order system. The effect of response speed, support method, and support parameters on the nadir of frequency response and maximum power increase are evaluated for different response speeds. A method for comparing support ability by considering the economic cost and benefit for support is also presented.

Table of Contents

List of Figures

List of Acronyms

BESS	Battery Energy Storage System
CAES	Compressed Air Energy Storage
CV	Comparison Value
DFIG	Doubly Fed Induction Generator
DHL	Dynamic High Low
DSR	Demand Side Response
ESO	Electricity System Operator
EU	European Union
FESS	Flywheel Energy Storage
FF	Fill Factor
FFR	Fast Frequency Response
IEEE	Institute of Electrical and Electronics Engineers
IV	Current-Voltage
LFC	Load Frequency Control
LFS	Low Frequency Static
MPP	Maximum Power Point
MPPT	Maximum Power Point Tracking
P&O	Perturb and Observe
p.u.	Per Unit
PEV	Plug-in Electric Vehicle
PHES	Pumped Hydro Energy Storage
PI	Proportional Integral
PMSG	Permanent Magnet Synchronous Generators
PV	Photovoltaic
PVPP	Photovoltaic Power Plant
PWM	Pulse Width Modulation
ROCOF	Rate-of-change of frequency
SCES	Supercapacitor Energy Storage System
UK	United Kingdom

APC	Active Power control
ANN	Artificial Neural Network

List of Symbols

η	Efficiency (%)
τ	Time constant (s)
D	Damping coefficient
D_g	Droop gain
E	Energy (J)
H	Inertia Constant (s)
I_0	Saturation Current (A)
I_{mp}	Maximum power current (A)
I_{sc}	Short-circuit current (A)
k	Boltzmann constant ($J.K^{-1}$)
q	Elementary Charge (C)
S	Apparent power (W)
V_{mp}	Maximum power voltage (V)
V_{oc}	Open-circuit voltage (V)
T	Temperature (K)
R_s	Series Resistance (Ω)
R_{sh}	Shunt Resistance (Ω)

Chapter 1 : Introduction

1.1 Background

The average annual global temperature of the Earth's surface has been increasing over the last several decades, with nineteen of the warmest years on record occurring in the previous twenty years [1, 2]. This has resulted in changes in the earth's weather and climate collectively referred to as climate change. The adverse effect of climate change is expected to increase as the earth's temperature increases [3]. The increase in the earth's temperature has been attributed to human activities that lead to a rise in the concentration of greenhouse gases [4, 5].

Of the greenhouse gases, CO_2 emission contributes the most to global warming. Figure 1.1 shows the sources of greenhouse gases by gas for the last few decades [5]. CO_2 concentration in the atmosphere has increased from 280 parts per million (ppm) in 1870 to about 412 ppm in January 2020 [6]. It had not increased by more than 300 ppm in the previous 800,000 years before 1910 [7]. Figure 1.2 gives various sources of greenhouse gas emission by multiple industries [5]. The primary source of CO_2 emission is the burning of fossil fuels for electricity and transportation. Concerns about the effects of climate change have resulted in a drive to meet the world's energy needs from renewable sources.

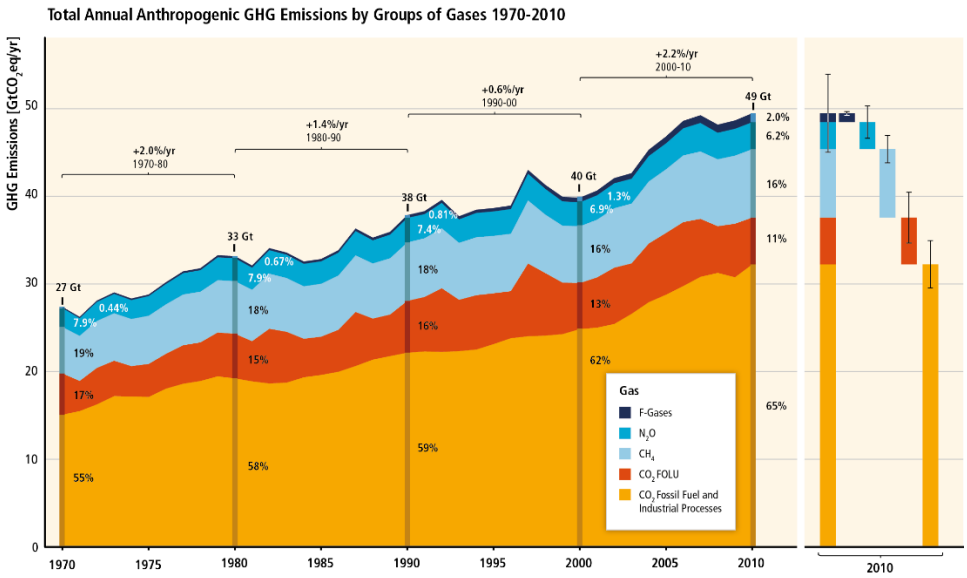

Figure 1.1: Sources of Greenhouse Gas [5]

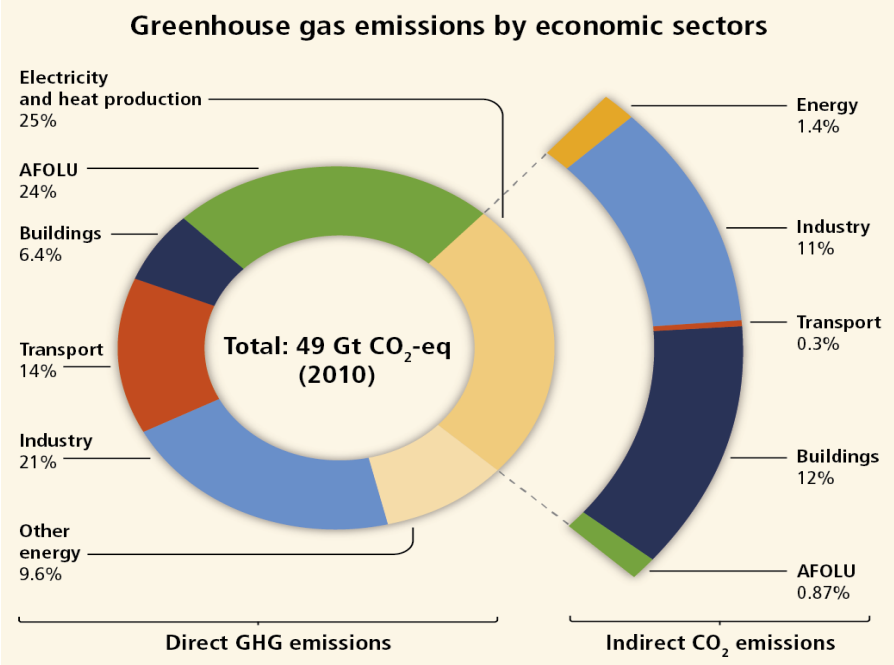

Figure 1.2: Sources of Greenhouse gas by industry [5]

To this end, various countries have made legal commitments to increase their use of renewable sources to meet their energy needs. The EU renewable directive which required member countries to meet a renewable energy goal of 20% by 2020

has been revised to 32% by 2030 [8]. As a result, the share of renewable energies in power systems globally has experienced steady growth over the last few decades. In the UK renewable generation has been steadily rising in recent years. Renewable energy accounted for about 39.6% of all generation in the last quarter of 2019 [9, 10]. The increase in renewable generation globally primary comes from wind, solar and hydro.

In the literature, various control and operation strategies have been proposed to maintain frequency stability in systems with high renewable penetration. Response from both renewable generation and load is used to compensate for the loss of inertia resulting from reducing the share of generation from synchronous generators. Frequency support form wind turbines, storage systems and demand control have been extensively discussed in the literature [11-13]. Support methods usually involve droop control and inertia emulation. With support contribution from varying generation forms, the need for a common framework for quantifying frequency support arises. Both droop and inertia support from non-synchronous sources are affected by the speed of response. The effect of varying response speed is a factor that influences considerably the performance of a generation source in the provision of frequency response.

Solar photovoltaics is one of the renewable energy technologies driving the increase in renewable energy penetration. Figures 1.3 shows the global installed solar PV since 2000 and the projected growth from in installed solar PV according to the International Energy Agency (IEA) [14]. Solar PVs do not have any rotating parts and thus no stored kinetic energy that could be used to contribute to power systems inertia. With solar PV capacity expected to continue to grow, methods for frequency support from solar PV systems are instrumental to attaining higher solar PV penetration.

The aim of this thesis can be broadly divided into two as:

1. Control of solar PV system to respond to frequency events effectively.
2. Design a framework to compare frequency support from different generation sources.

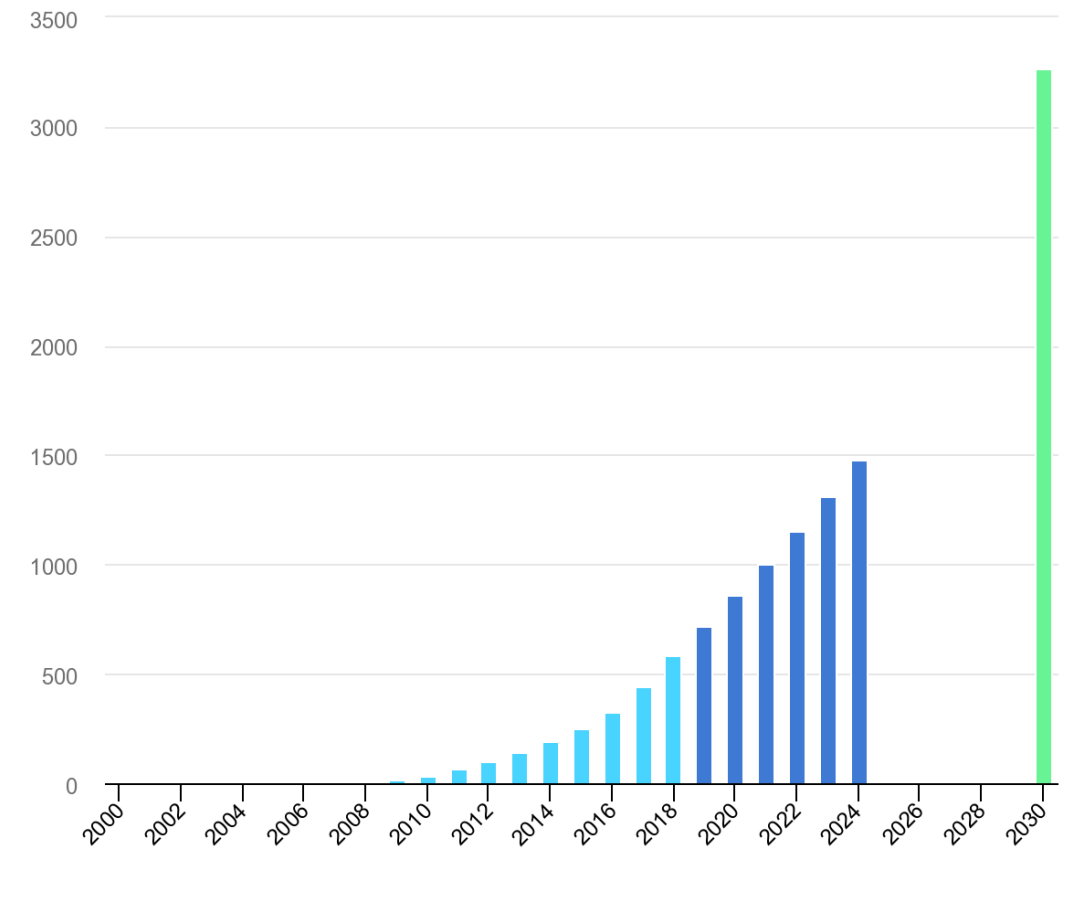

Figure 1.3: Historical and Forecasted solar PV capacity in TWh [14]

1.2 Power System Stability

The IEEE/CIGRE joint taskforce on stability terms and definitions define power system stability as the ability of a power system to regain equilibrium after experiencing a disturbance [15]. The ability to maintain system stability affects the reliability of power systems as instability can lead to blackouts [16]. Maintaining stability is essential in power systems irrespective of the size and the makeup of generation sources of the system. Due to the increase in converter-connected generation sources in power systems, system inertia has been reduced. Converter-connected sources are not synchronously connected to the grid and will not naturally respond to a generation-load imbalance. In wind generation technologies, the converters are decoupling the generator frequency from the system frequency. In solar PV systems, they are no rotating masses and therefore they cannot contribute to system

inertia. Increasing PV penetration leads to a reduction in system inertia. Maintaining stability is essential in systems with reduced inertia and increased generation variability to ensure continued integration of converter-connected renewable energy sources as they do not normally contribute to system inertia.

The IEEE/CIGRE joint taskforce on stability terms and definition classify stability based on nature, size and timescale into rotor angle stability, frequency stability and voltage stability [15]. The classification of stability is given in Figure 1.4.

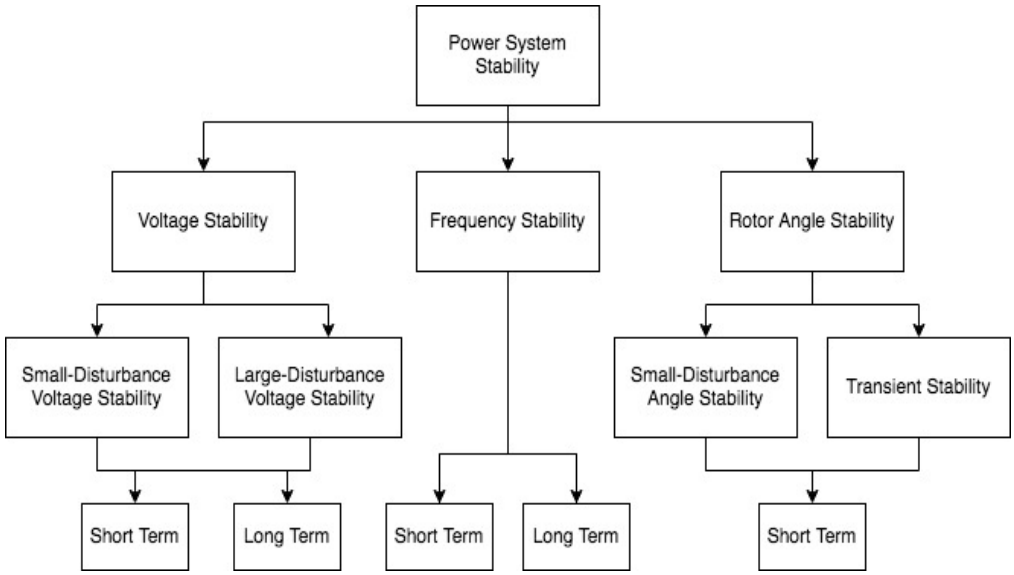

Figure 1.4: Stability classification [15]

1.2.1 Frequency Stability

Frequency stability is the ability of a power system to maintain system frequency as constant as possible within necessary limits in the event of a generation-load imbalance [17]. The power system frequency is an indicator of the generation-load balance. The power system frequency decreases when the generation is less than the load and increases when the generation is greater than the load. Although the frequency is continuously changing transmission system operators are legally required to maintain power system frequency within operational limits. Various power system operators have limits for the maximum instantaneous and steady-state frequency

deviation. The National Grid – the UK ESO – aim to keep system frequency in normal operation around $\pm 0.2Hz$ and have a statutory limit of $\pm 0.5Hz$ [18, 19]. The ability of ESOs to meet their frequency requirements depends on the generation reserves and load resources available and how quickly they can be deployed. The response in different timeframes after a generation-load imbalance determines the rate-of-change of frequency (ROCOF), the maximum deviation and the steady-state deviation. An example of a frequency response in the event of a generation-load unbalance is given in Figure 1.5. The ROCOF is usually dependent on the inertia of the power system. The Nadir is the lowest point on the response, and its value is determined by both the system inertia and the speed of the generating units participating in primary frequency response.

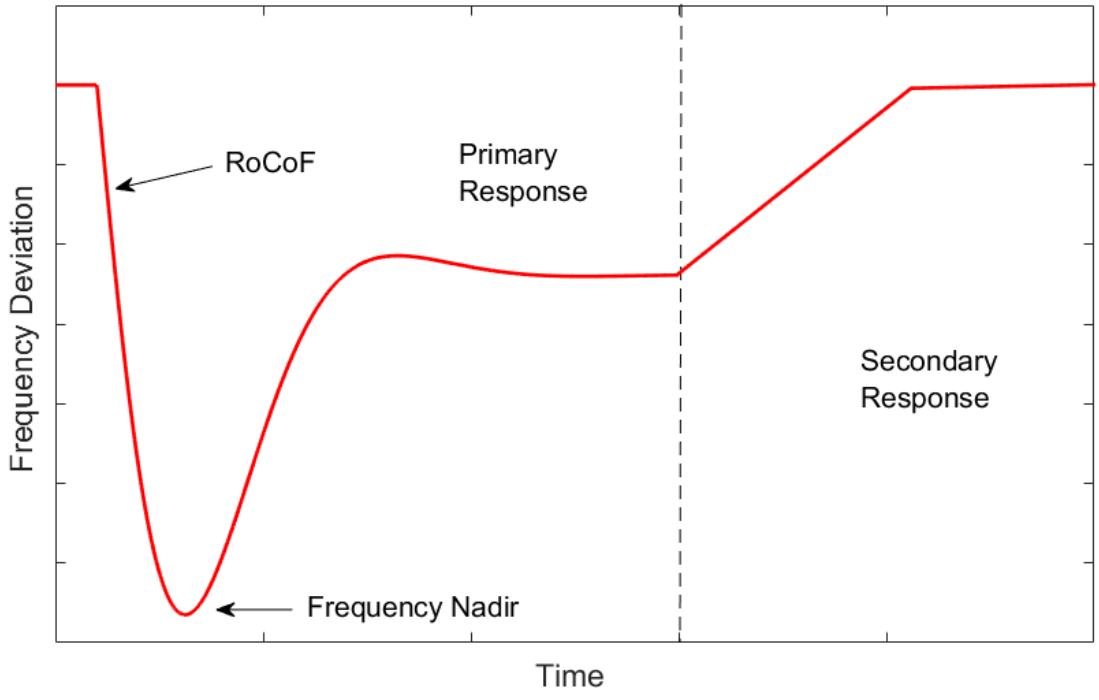

Figure 1.5: Frequency response evolution

1.2.2 Types of Frequency Response

Frequency response provision is grouped into the dynamic and non-dynamic frequency response by the National Grid [20].

- Dynamic Frequency response: This is a continuous frequency response, and response is usually proportional to the ROCOF or change of the frequency.
- Non-Dynamic Frequency Response: This is a one-time change in power output at a defined frequency deviation.

The frequency response services provided by the national grid include Firm Frequency response, Dynamic containment, mandatory response services and Low Frequency Static (LFS) and Dynamic Low High (DLH). Both LFS and DLH are trial products.

- ***Firm Frequency Response:*** This is a frequency response is obtained through bids by the providers. Bids are accepted by National Grid after economic consideration and consideration of the quality and quantity of the response. The speed of response from the provision of firm frequency response can vary from bid to bid and can include both dynamic and non-dynamic responses [21]. This response can also be provided by generators, storage systems and by aggregated demand response [21].
- ***Dynamic Containment:*** This is a new frequency response service from National Grid designed to mitigate the effect of reducing inertia and the increasing rate of generator-load imbalance occurrence [22]. The frequency response is post-fault, and participating units have to be fast responding. This frequency response service has to be dynamic and proportional to the frequency deviation but is only activated when frequency deviates by $\pm 0.2\ Hz$ [22].
- ***LFS and DHL:*** LFS is a frequency response service that is triggered when the frequency drops below 49.6Hz. The increase in power is delivered in 1 second and lasts 30 minutes [23]. The DHL is a dynamic response service that delivers equal primary, secondary and high response [23].
- ***Mandatory Frequency Response:*** This is the automatic change in output power in response to a frequency deviation [24]. The requirement of this response is usually based on the size and location of the provider. This response

is decided in the connection agreement [24]. This response service can be offered as a primary, secondary or high-frequency response.

The provision of a response service is classified based on the response speed and duration of response into:

- ***Primary Response:*** This response is provided within 10 seconds of a power imbalance and sustained for 20 seconds [21].
- ***Secondary Frequency Response:*** This response is provided within 30 seconds of a generation-load imbalance and sustained for 30 minutes [21].
- ***High Frequency Response:*** This is a reduction in power in response to a frequency event [17]. This response is provided within 10 seconds and sustain indefinitely [21].

1.3 Research Motivation

Photovoltaic systems are a major technology driving the increase in renewable generation in power systems but also a major reason for the loss of inertia in power systems. However, with the proper controls, frequency support from photovoltaic systems can help reduce the burden of frequency support from conventional generation and other renewable sources. In order to do so, there are various challenges that first need to be addressed in the way Solar PV systems are controlled. The MPPT techniques used by PV systems are typically designed for performance in dynamic conditions without consideration for network support functions. Hence, to enable a solar PV system to provide support to system operation, MPPT should be designed to accommodate the system requirements. It is also important to evaluate the effectiveness of PV systems in providing support and to determine the amount of de-loading needed for a given loss of system inertia.

Many operation and control methods have been proposed for frequency response from the majority of renewable sources, including wind turbines and storages systems to assist in ameliorating the effect of reduced system inertia. A framework for comparing and quantifying the frequency support capability of different generation sources, storage systems and demand management techniques is needed. The ability

to quantify support ability enables optimization of de-loading amount and the factoring of economic consideration in frequency support.

1.4 Contributions from this thesis

1. An offline MPPT which does not require any online computation for use in PV system participating in frequency response. The MPPT combines drift-free and fast-tracking. Frequency response from PV system is also implemented.
2. The development of two de-loading methods for use with the offline MPPT.
3. A variable droop control method is used for the PV system to provide frequency support is developed.
4. A drift-free P&O algorithm is proposed. This was developed to enable comparison of the P&O and other MPPT in for PV system providing frequency response.

1.5 Thesis structure

This thesis contains six chapters. A brief summary of each chapter is as follows the details of:

- ***Chapter 1***

This chapter presents the background and an introduction to frequency control types.

- ***Chapter 2***

This chapter discusses the role of inertia in power systems. The effect of inertia on the ROCOF and nadir of a frequency response is discussed. Both wind turbine and photovoltaic generation technologies are explained along with a review of frequency support methods for wind turbines. Review of various energy storage systems including flywheel energy storage system (FESS), battery energy storage system (BESS), compressed air energy storage (CAES) and pumped hydro energy storage (PHES) is conducted based on their suitability for frequency support is carried out in this chapter. Lastly, a review of demand side response (DSR) and the different DSR based strategies for frequency response is presented.

- ***Chapter 3***

  This chapter investigates the effect of MPPT on Active Power Control and develops an offline MPPT for fast active power control. First, common MPPT methods are reviewed, and how deloading can be achieved with them is discussed. A modification to the basic P&O MPPT algorithm is proposed for the avoidance of leftward and rightward drift. The P&O with proposed modification is then tested in dynamic irradiance. A description of the operation of the offline MPPT for maximum power and deloaded operation is presented. Some MPPTs are then compared for reserve maintenance. Finally, two deloading methods are presented for the offline MPPT in both percentage deloading and fixed-power deloading.

- ***Chapter 4***

  This chapter evaluates frequency support from a photovoltaic power plant. A PV system is operated with some power reserve using the offline MPPT proposed in chapter 3. Conventional frequency support methods like inertia emulation and droop control are impleneted. The performance of PV frequency support is evaluated for different penetration scenarios and support method. Support from PVPP is also compared to support from a synchronous generator. Variable droop control is proposed for more effective frequency control and better reserve management. The effect of MPPT is also evaluated by comparing response from the PVPP employing the offline MPPT to other common MPPTs.

- ***Chapter 5***

  This chapter presents a framework for comparing frequency support from diverse generation sources by comparison to a Second-order system. The effect of different combination of support method, support parameters, response speed and system inertia on the frequency response is presented. The nadir is used as the basis for comparison. Comparison of response based on maximum power increase is also presented. A method for comparing generating sources' value for frequency response based on economic considerations is presented.

- ***Chapter 6***

  A summary of previous chapters is presented. Areas for possible research are suggested.

1.6 Publications

1.7.1 Conference Publication

- **Fyali Jibji-Bukar**, Olimpo Anaya-Lara.: 'Offline photovoltaic maximum power point tracking'. International Conference on Power and Renewable Energy, 2018, Berlin

1.7.2 Journal Publications

- **Fyali Jibji-Bukar,** Olimpo Anaya-Lara.: 'Frequency control from a photovoltaic power plant with offline maximum power point tracking and variable droop control'. In IET Renewable Power Generation, vol. 13. no. 13, pp. 2278-2286, 2019.

Chapter 2 : Frequency Support by Renewable Energy Sources

2.1 Introduction

The proliferation of renewable energy sources in electrical systems in response to climate change has resulted in new frequency stability challenges. Most of the increase in renewable generation globally in the last decade has come from hydro, wind turbines (offshore and onshore), solar PVs, and other converter connected sources [25]. In the UK, this growth in renewable is driven by wind and solar [26]. Solar PV, in particular, is forecasted to provide more than 50% of the expected growth in renewables [27].

Some renewable sources usually do not naturally add to system inertia and have to track maximum power as they are subject to the variability of environmental conditions. The loss of system inertia and maximum power tracking from renewable reduces the resources required for maintaining frequency stability. As explained in Chapter 1, maintaining adequate frequency response ability is necessary to prevent high RoCoFs and large nadirs, which could lead to under frequency shutdowns [16]. The adverse effect of reduced inertia on frequency response is known to be one of the main obstacles to higher renewable generation penetration [28].

For power systems to continue the trend of increasing renewable penetration, various system operation techniques have been proposed to enable adequate frequency

response in high renewable penetration systems. Frequency support from wind turbines and wind farms have been extensively covered in literature [29, 30]. Various types of storage systems have been used to augment renewable energy penetration and provide frequency support [12]. Demand has also been used as a resource for maintaining frequency stability [11, 31].

This chapter provides a wide-ranging review of electricity generation from renewable sources, including Solar PV, Wind turbines. It also provides a summary of various types of energy storage systems. Frequency support from renewable generation sources, storage systems, and demand management are also reviewed. In Section 2.2, the role of inertia in power systems is discussed. Section 2.3 presents a review of Solar PV and wind turbines technologies for power generation and frequency support. Section 2.4 presents a review of energy storage technologies and their capability for frequency support. Section 2.5 presents a discussion of frequency support from demand response. Section 2.6 gives the concluding remarks.

2.2 Inertia and Frequency Response

The frequency of power systems indicates the balance between generation and load [32]. Power system operators aim to maintain system frequency between a defined range. Frequency deviations from desired limits could lead to under-frequency load shedding [33]. Conventionally, power systems mainly rely on the inertia of generators and governor actions to keep frequency within permissible limits.

Inertia is the ability to resist change [34]. In power systems, the inertia of generators refers to the ability of the rotating masses to resist a change in speed as a result of generation load imbalance. The energy stored in the rotating mass of generators is given as [35]:

$$E = \frac{1}{2} J\omega^2 \tag{2.1}$$

where J is the moment of inertia in kgm^2 and ω is the angular velocity in rad/s. The moment of inertia J is given as [36]:

$$J = \sum_{i=1}^{n} m_i r_i^2 \tag{2.2}$$

where m_i is the mass of a particle and r_i is the radius of a particle from the axis. n is the number of particles in the body. The inertia constant *H*, of a generating unit or a power system, is the time the stored rotational energy can provide the apparent base power of the generating unit or the power system [37]. The inertia constant is given as:

$$H = \frac{E}{S} = \frac{1}{2S} J\omega^2 \tag{2.3}$$

Where *S* is the apparent power. The value of *H* usually ranges from 2-9s [36]. The inertia constants for different types of generators can be found in reference [37].

From the swing equation which describes the motion of rotating masses, the ROCOF will become [37]:

$$\frac{d\Delta\omega}{dt} = \frac{\Delta P_G - \Delta P_L}{2H} \tag{2.4}$$

where $\Delta\omega$ is the change in frequency, ΔP_G is change in generation and ΔP_L is the change in load. Frequency sensitive loads such as devices which include a motor can change the power imbalance. This is usually represented by a load damping coefficient *D*. The damping coefficient represents the degree by which the load is affected by a change in frequency [38]. The addition of changes in power caused by frequency-sensitive loads, (2.4) then becomes (2.5) [37].

$$\frac{d\Delta\omega}{dt} = \frac{\Delta P_G - \Delta P_L - (D \times \Delta\omega)}{2H} \tag{2.5}$$

In the Laplace domain, the change in frequency is given as:

$$\Delta\omega = \frac{\Delta P_G - \Delta P_L}{2Hs + D} \tag{2.6}$$

The schematic diagram in Figure 2.1 shows the block diagram representation of the effect of the inertia and damping coefficient on the frequency.

Power systems consist of synchronous generators with differing sizes and inertia. The inertia of the system is given as:

$$H_{sys} = \frac{\sum_{i=1}^{n} S_i H_i}{S_{sys}} \tag{2.7}$$

where n is the number of synchronous generators in the system. H_i and S_i are the inertia and base power of a given generator and S_{sys} is the base power of the system.

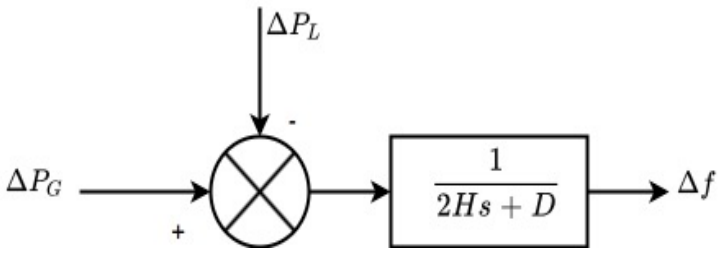

Figure 2.1: Aggregate system inertia

From (2.6), it can be seen that the inertia primarily determines the RoCoF and change in frequency immediately following generation-load imbalance. Although generation action will begin shortly after the imbalance – particularly mandatory frequency response - the speed with which synchronous generators adjust their output power varies between generators. Most conventional generators are usually not fast enough to prevent the rapid fall of frequency in the first few seconds after a frequency deviation event. Declining inertia in power systems implies that frequency stability will be challenged. The increasing generation from photovoltaics and wind turbines will result in reducing system inertia. Many countries in the EU have experienced a significant reduction in inertia in the last several decades, with Denmark experiencing over 50% reduction in inertia from 1996 to 2016 [37].

Although the initial RoCoF is solely dependent on the inertia, the RoCoF from the onset of the imbalance to the nadir can be affected by other low inertia mitigation efforts. The performance of low inertia mitigation methods and their comparison to conventional inertia is useful in quantifying frequency support ability of high renewable penetration systems. Unlike inertia response from synchronous generators which is instantaneous, emulated inertia will be affected by the response speed of the generating unit. This creates a challenge in quantifying frequency support ability with a system that maintain RoCof limits with a combination of inertia and emulated inertia. This will be addressed in detail in Chapter 5.

2.3 Frequency support from renewable energy

In this section, the generating mechanism of different renewable sources is covered. This section also presents a review of frequency support from renewable generation sources. Also, a summary of other methods of frequency support, such as demand-side response and energy storage, is discussed.

2.3.1 Wind Turbines

Wind turbines are one of the leading technologies driving the increasing penetration of renewable energy in electric power systems. Wind turbines work by converting the energy in the wind to electrical power. The energy of the wind lifts the turbine blades, which then turns an electrical generator.

The most common types of wind turbines are type 3 and type 4 wind turbines. Type 3 and 4 wind turbines are preferable because they can operate efficiently in a wide range of wind speeds. The DFIG (type 3) is the most common because it is cheaper than the type 4 (Fully rated converter). DFIG based wind turbines cost less than FRC based wind turbines because its converter capacity is about 30% of rated power [39]. The schematic of the control of a DFIG based wind turbine and the permanent magnet synchronous generator wind turbine with full converter is given in Figures 2.2 and 2.3.

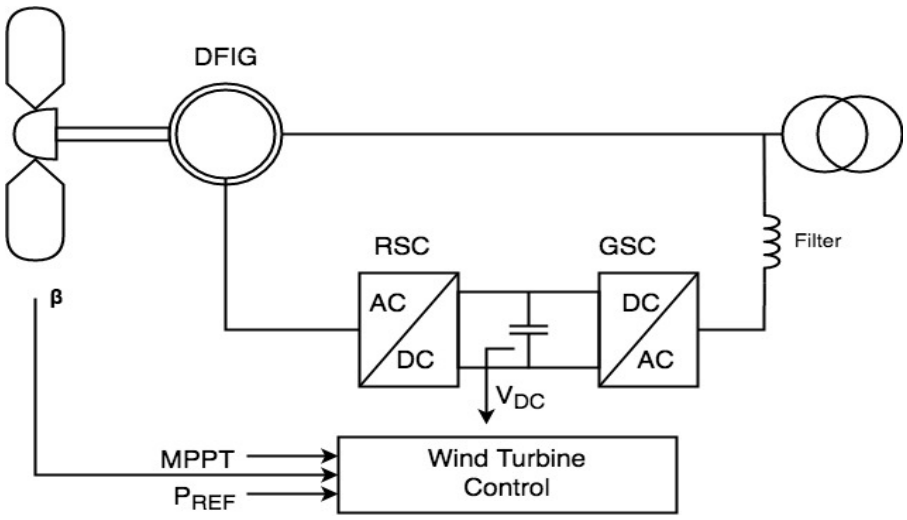

Figure 2.2: Schematic of DFIG based wind turbine

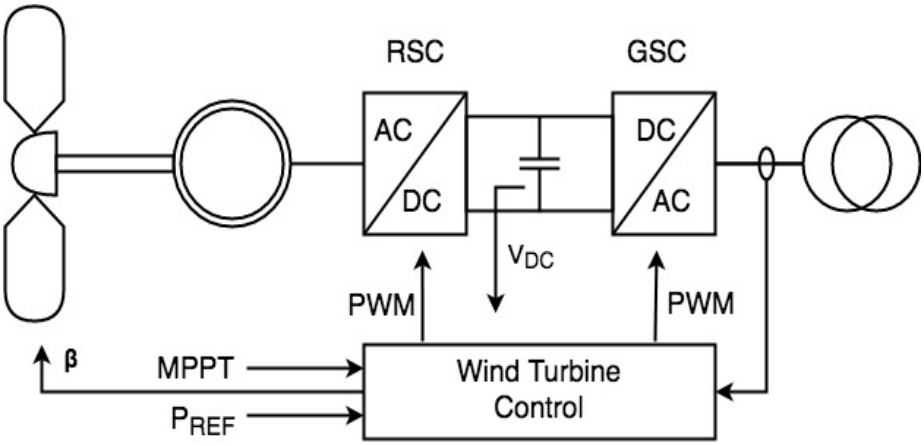

Figure 2.3: Schematic of PSMG based wind turbine

Although the rotor of DFIG has stored kinetic energy, this inertia cannot be delivered to the grid because the rotor is decoupled from the network by electronic power converters [40]. Without supplementary control to extract wind turbine inertia, increasing wind converter-connected turbines will lead to a reduction in power system inertia. In literature, several methods for wind turbines to participate in both inertia support and primary frequency control have been proposed. The methods by which wind turbines provide inertia support is broadly classified into two.

In the first method, the wind turbine reference power is increased to a value higher than maximum power. This will result in the rotor slowing down, and the stored kinetic energy released [29, 41]. The additional power for inertia support can be determined by the RoCoF [42] or by the change in frequency [43]. The power reference could also be increased by a fixed amount in response to frequency deviation [41, 44]. A drawback of this method is that a secondary frequency dip can occur as a result of a drop in power when the rotor is recovering to normal speed [13]. In reference [45], variable droop control is used to prevent a secondary frequency drop. In [46], a second drop is prevented by augmenting wind turbine support with dynamic demand control. The main advantage of this method is that wind turbines can provide this support while operating at optimum power.

The second method is overspeeding the turbine rotor such that it operates at a higher C_p than the optimum C_p. Operating at a higher rotor speed than optimum

increases the available inertia but also leads to loss of power. During a frequency event, the rotor speed is reduced to maximum power value, releasing stored kinetic energy [29]. The main drawback of this method is the loss in power resulting from deviation from maximum power point [47].

Wind turbines can also provide primary frequency support as with conventional generators. Wind turbines have to operate below maximum power point at all times to maintain a reserve for primary frequency support. Both percentage de-loading and delta de-loading can be implemented for primary frequency support [29]. De-loading can be achieved by changing the value of C_p to correspond with the desired reserve. The primary way de-loading is achieved is by pitch angle control. Pitch angle control is usually used to limit the speed of wind turbines in high wind speeds [48]. The pitch angle is increased from for a given wind speed to achieve deloading. Deloaded wind turbines can provide primary frequency support by implementing droop control [39]. In [49, 50], inertia support is combined with droop control to provide primary frequency support.

Deloading wind turbines for primary frequency control can also be achieved by overspeeding the wind turbines, which is operating at a higher speed than the maximum power speed. Deloading can also be achieved by reducing the rotor speed. The over-speeding method is usually preferred to the under-speeding method [51]. This is because when providing frequency support from under-speeding, the wind turbine will use some of the support power to increase the stored kinetic energy and thus reducing the effectiveness of the support provided [51]. The main disadvantage of deloading by over-speeding is that the speed must not exceed the maximum speed limit. This limits the maximum amount of power that can be reserved [29].

In literature, inertia support is usually augmented with droop support from deloaded wind turbine or other mechanisms to provide primary frequency support. In [46], dynamic demand control is used together with inertia support to deliver both inertia support, primary frequency support and prevent a secondary frequency drop. In [52], coordination and simultaneous implementation of pitch angle control and rotor speed control are used to increase the speed range of the rotor and to increase the speed of active power control from wind turbines.

2.3.2 Solar Photovoltaics

The basic unit of a solar photovoltaic system is the solar cell. Solar cells generate electricity by converting the energy in the sun light to electricity by the use of a phenomenon known as the photovoltaic effect [53]. The photovoltaic effect, which was first discovered by Edmund Becquerel in 1839, is the generation of electricity by some materials when exposed to light [53]. In a photovoltaic cell, a semiconductor material (usually about $0.1m^2$) absorbs light, which excites the electrons of the materials to a higher energy state. The electrons are then fed to an external circuit to produce a voltage difference between the contacts of the cell. The main difference between the photovoltaic cell and the photoelectric effect is that in the photoelectric effect, the excited electrons escape the material. The efficiency of solar cells depends on the semiconductor material used and the external circuit. The most common solar cell types are crystalline silicon solar cells, amorphous silicon solar cells, thin-film solar cells, and organic solar cells. Primarily due to research, the efficiencies of various solar cells have been improving over past decades [54]. The efficiency of a solar cell is how much light energy is converted into electricity.

PV cells behave like a diode in the dark and will generate a current in the opposite direction to the photogenerated current when a load is present in the cell terminals [53]. The current flowing through the terminals of the PV cell is the difference between the photogenerated current and the dark current. The current-voltage (IV) characteristics of PV cells is determined by the dark current and as a result, has a non-linear relationship. The IV and PV curves of a PV cell are given in Figure 2.4.

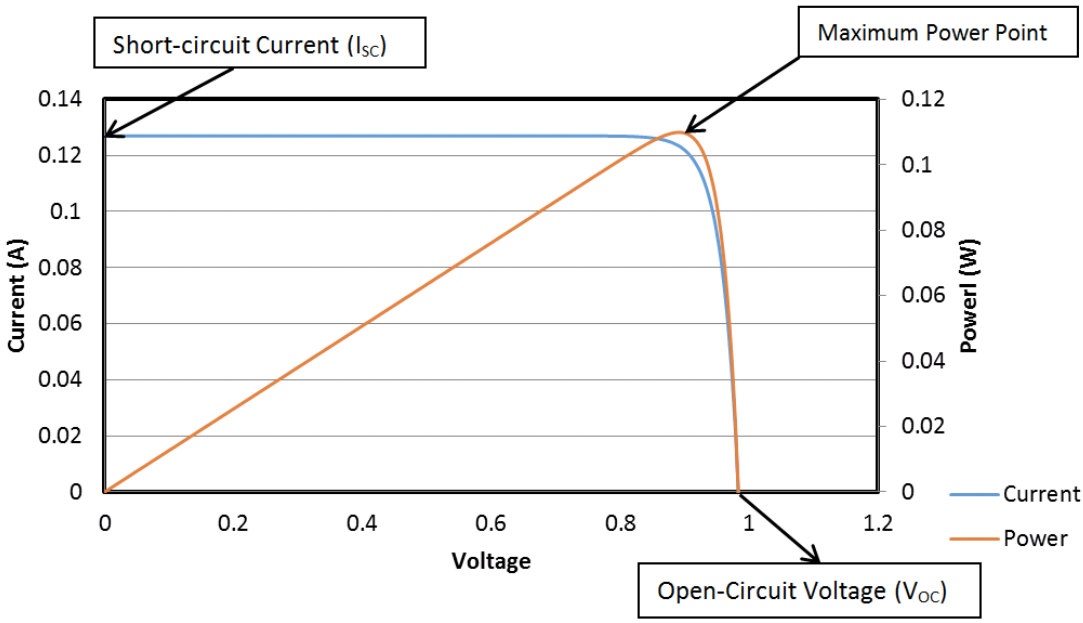

Figure 2.4: PV and IV curves

The performance of a PV cell is determined by the following parameters:

- ***Short-circuit current:*** This is the current that flows through the terminals of the PV cell when there is a load. Ideally, the short-circuit current and light generated current will be of the same value but are usually very close in value. The short-circuit current also has a direct relationship with irradiance incident on the PV cell.
- ***Open-circuit voltage:*** This is the voltage across the terminals of the PV cell when they are separated. The open-circuit voltage is determined by the dark current.
- ***Fill Factor (FF):*** The fill factor is a measure of the squareness of the IV curve. It is given by equation (2.8). The FF is used to measure the quality of the PV cell.

$$FF = \frac{I_{mp}V_{mp}}{I_{sc}V_{oc}} \tag{2.8}$$

I_{mp} and V_{mp} are the maximum power current and maximum power voltage respectively. I_{SC} and V_{OC} are the short-circuit current and open-circuit voltage respectively

- ***Efficiency:*** The efficiency of a PV cell is the ratio the maximum power obtainable from the cell to the incident light power [33]. The efficiency of a solar cell is given by equation (2.9). It should be noted that the efficiency of the cell is different from the efficiency of a PV system as the PV system includes other components that contribute to power loss. The efficiency is given as:

$$\eta = \frac{I_{mp}V_{mp}}{P} \tag{2.9}$$

P is the incident light power on the cells. The performance of PV modules is usually specified in the datasheet at standard testing condition (STC) which is at an irradiance of 1000w/m^2 and temperature of 25°C.

Solar PV cell or modules can be modelled as the equivalent circuit in Figure 2.5.

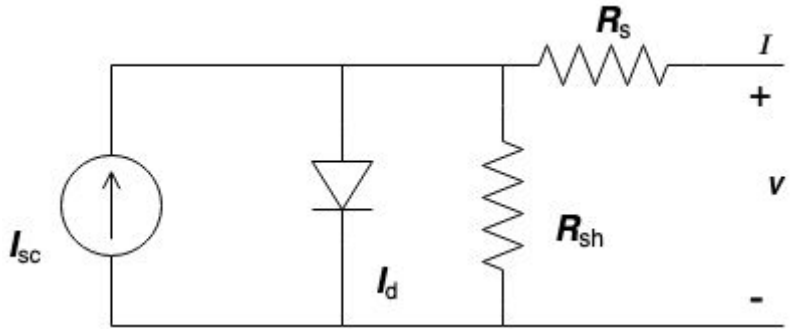

Figure 2.5: Five parameter model of solar cell

The current through the terminals of the PV module is given by equation (2.10) [53].

$$I = I_{SC} - I_0\left[exp\left(\frac{q(V + I * R_s)}{N_s KT}\right) - 1\right] - \left[\frac{V + I * R_s}{R_{sh}}\right] \tag{2.10}$$

Where, I_{SC} is the short-circuit current, I_0 is the saturation current, q is the electric charge, k is the Boltzmann constant, T is the temperature, V is the voltage across the terminal of the module, N_S is the number of cells in series, R_S is the series resistance and R_{SH} is the shunt resistance.

PV cells are combined, usually in series, to make a PV module with higher output power and modules are connected in series and parallel to create a larger

PV system. Figures 2.6 and 2.7 gives the schematic of a PV module and the connections of modules for a PV system, respectively.

Due to the dependence of the IV curve on photogenerated current - which is determined by the irradiance - and the dark current – which is affected by the temperature of the cell, the IV curve changes with changing irradiance and temperature. This implies that the maximum power point also varies with irradiance and temperature. PV systems employ a maximum power point tracking technique to operate at maximum power as irradiance and temperature changes. As a result of using an MPPT technique, the voltage from PV systems varies during operation. A converter is used to produce a constant output voltage from PV systems. The power from a PV module combination is DC and has to be converted to AC before grid connection. The schematic of a grid-connected PV system is given in Figure 2.8.

The overall efficiency of a PV system will be affected by the efficiency of the PV cell, the MPPT and the DC to AC conversions.

The PV MPPT techniques differ with respects to efficiency, computational effort, and response speed, ability to track dynamic conditions and cost [55]. Some MPPT methods may require irradiance and temperature measurements. MPPT techniques also differ in ease of obtaining a deloaded operation. While some can be directly deloaded by modifying parameters in the algorithm, some have to be deloaded indirectly. Since the power output from PV systems depend on environmental conditions, the resulting variability could lead to more generation-load imbalance events and rapid rise or drop in power depending on cloud and shading conditions. As a result, active power control of PV systems which include deloading, ramp-rate control is required to maintain system stability. Some grid codes now require PV systems to participate in grid regulations [56-57]. In Puerto Rico, PVPP are required to provide a 5% droop response to frequency deviation and also provide ramp rate control [56].

Although frequency support from PV system has been explored in [58-60], very little attention has been paid to the deloading technique and the role of the MPPT in frequency support. Frequency response from PV power plants is still a developing field, and more research is required to optimise and quantify frequency support from

PV systems. Also, because PVPP is expected to replace conventional generators and provide support using methods similar to conventional generators, a framework for comparison between PV and synchronous generators is necessary. The Chapters 3 and 4 of this thesis will address:

- How Active Power Control (APC) can be achieved in a PVPP by MPPT modification.
- How frequency support can be achieved with a PVPP.

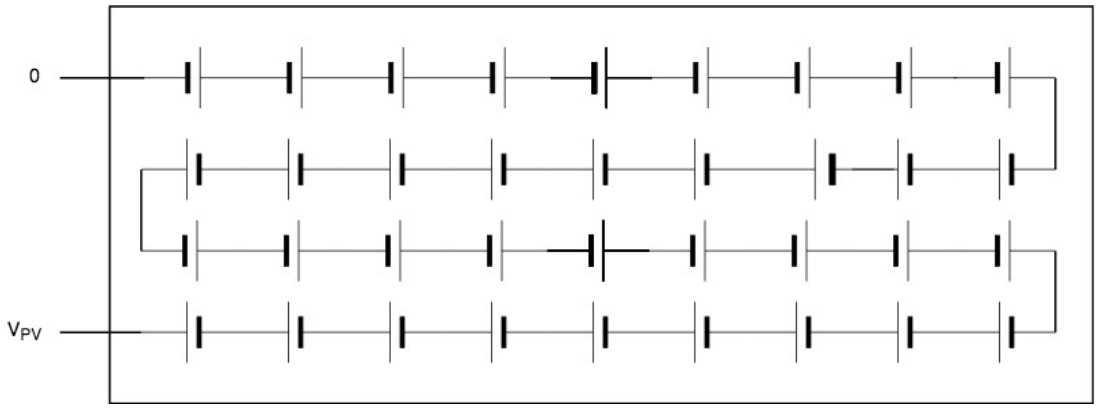

Figure 2.6: Connection of cell in module

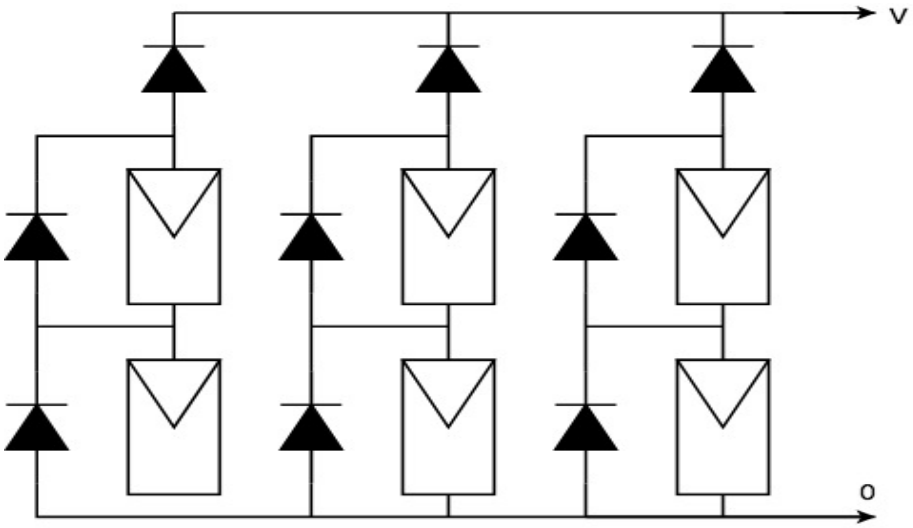

Figure 2.7: Connection of modules

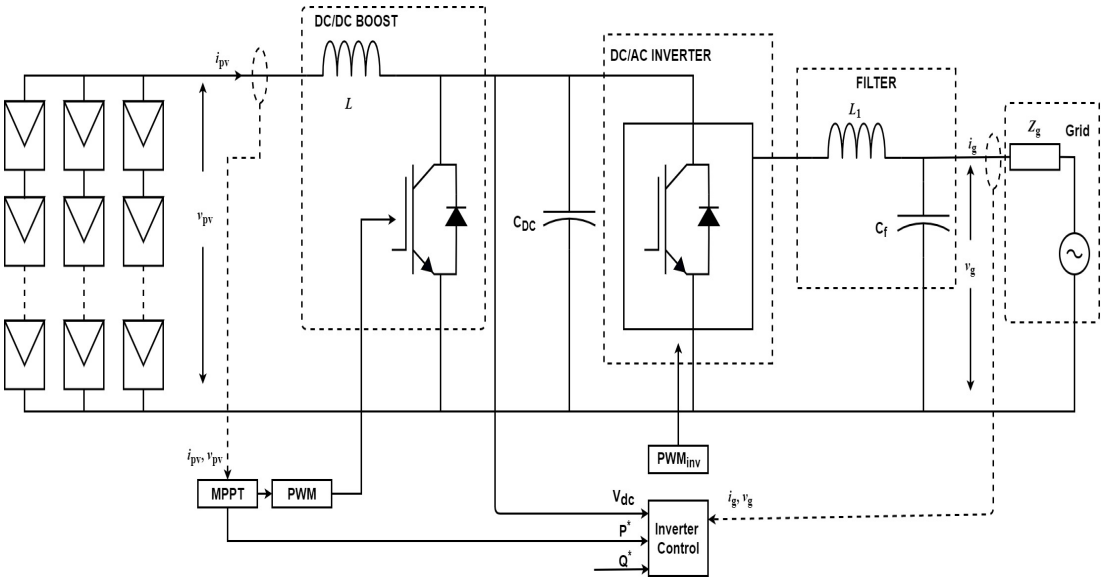

Figure 2.8: Grid connected PV system

2.3.3 Storage Systems and Frequency Support

Energy storage systems play an essential role in the transition to renewable energy. Energy storage systems can help to maintain supply when output from intermittent sources is lower than required. They can also help improve the overall efficiency of some renewable generation sources and can also contribute to primary frequency support when they are fast-responding. Energy storage systems can be classified into mechanical, electrical, thermal and chemical [61]. The various energy storage systems have different advantages and disadvantages in price, energy density, efficiency and response speed. This section reviews various energy storage technologies and their suitability and their use and suitability for frequency support.

1. Battery Energy Storage System (BESS)

Batteries are made up of electrochemical cells which store energy in chemical form [62]. Cells are connected in series and parallel to in increase battery capacity. A cell contains an anode, cathode and an electrolyte. Batteries differ from one another based on the material used for the electrodes and the electrolyte [62]. BESSs are generally fast-acting and can participate in frequency support at the primary and secondary support timescale to varying degrees of effectiveness. Battery storage systems have been used for frequency support in USA, Germany, Puerto Rico and Spain [12, 62]. Lead Acid batteries are the most common type of electrochemical storage due to their

low cost [63], but lithium-ion batteries are preferred in portable electronics due to their high energy density [64].

With respect to frequency support, the battery lifecycle and the response speed are two parameters that can affect the suitability of a BESS technology for frequency support. Lithium-ion batteries are suggested in [12] as the best BESS technology to provide frequency response services. The most common system of BESS providing frequency support is in combination with a variable generation source such as PVPP or Wind farm. In [65], BESS is used in to provide frequency support for a power system with PV penetration. In [66, 67] battery storage is used to augment frequency support provision by a wind farm. The control methods for frequency support in systems with BESS is either the conventional droop control or more complex methods like the fuzzy-logic based method in [66].

2. Flywheel energy storage system

The main components of a flywheel energy storage system include a flywheel, reversible electric motor/generator and electronic converter. Figure 2.9 gives the basic FESS. Flywheel storage system (FES) stores energy as kinetic energy [68]. When the rotor is accelerated, the energy stored in the flywheel increases. FESs are classified into low-speed FES which rotates below 6×10^3rpm and high-speed FES which can reach 10^5rpm [69]. The FES releases energy by decelerating.

FESS can provide frequency support by reducing the speed of the flywheel in response to a frequency deviation. FESS can participate in primary control because of its fast response speed [69]. FESS can independently provide frequency support or can coordinate support provision with a variable generation source – usually a wind or PV power plant. In reference [70], coordinated support of FESS and wind turbines is used to provide frequency support and eliminate the need for de-loading of wind turbines to provide primary frequency support. In [71], droop control is proposed as one of the strategies for FESS to provide frequency support.

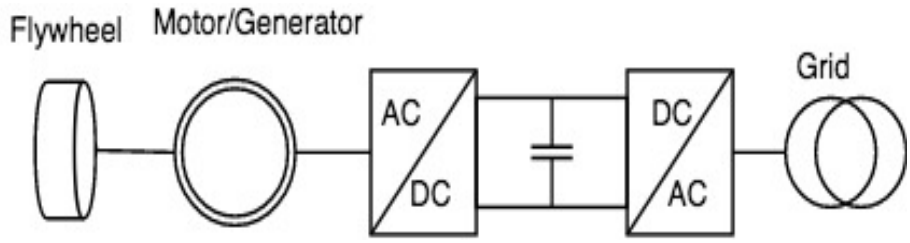

Figure 2.9: Basic FESS

3. Pumped Hydro Energy Storage (PHES)

PHES is the most common storage system in power systems [62]. A PHES system consists of two reservoirs separated by a height. Energy is stored by pumping water from the lower level reservoir to the higher level reservoir. Electricity is generated from the stored energy by running down water in the higher level reservoir to turn a turbine which powers electric generators. PHES is one of the most cost-effective storage systems, and large amounts of power can be stored [72]. However, it is affected by geography due to the need for a water source and high ground [72]. A company are pioneering a method that uses pumps to move the water to a pressurised underground well instead of the higher-level reservoir [73]. This will reduce the geography constraint of PHES.

PHES are primarily used to store excess power when demand is low and provide additional generation when demand is high. PHES can provide frequency support usually, in coordination with a variable generation. In [74], PHES provides frequency support in a system with high wind penetration enabling wind turbines to operate at MPP. An advantage of PHES in frequency provision is that they contribute to the system inertia [75]. PHES however, have a slower response speed compared to most BESS technologies [62].

4. Supercapacitor (Ultracapacitors) energy storage (SCES)

Supercapacitors consist of two electrodes, an electrolyte and a separator [76]. Supercapacitors store energy as charges between the electrode and electrolyte [62]. The amount of energy stored by supercapacitors depends on the surface area of the electron and electrolyte interface [77]. Activated carbon is usually used as the electrode material to increase the surface and thus increase energy density [58]. The

main advantages of the SES are that it provides very fast charging and discharging and long cycling time [76]. The main disadvantage of SES is that they have low energy density and are not suited for long term applications [62, 76].

5. Compressed Air Energy Storage

CAES like the PHES is used to store power when there is excess production and provide additional power when demand is high. CAES stores energy as compressed air, usually in an underground cavern which is then sealed at high pressure [78]. A motor drives compressors, which drives air into the cavern [62]. When the energy is to be used, the air is released and burned with fuel which increases its efficiency [62, 79]. It is then used to turn the turbine and generate power. While CAES can store a large amount of power, it is relatively slow responding compared to other storage systems.

Sometimes two or more energy storage systems are combined to better meet some functions like frequency support or for more economical operation. These systems are called hybrid storage systems [12]. In [80], coordination of SCES and PHES is used to provide frequency support in a power system. The proposed support strategy uses PHES to provide support for some time after support from SCES has stopped due to fast discharging essentially providing support in both the inertial and primary support timescales. In [81], a frequency support strategy for wind turbine to provide primary and secondary support is proposed by combining support from a lead-acid battery and ultracapacitor. The ultracapacitor provides support by emulating inertia response while the lead-acid battery provides primary support using droop control. The multilevel method used here takes advantage of the ultracapacitors long cycles by using it for support that requires fast discharge of power. The multilevel method also reduces the amount of power required from the lead acid battery per time and thus increasing its lifespan.

While frequency support can be provided by some storage systems – independently or in coordination with other generation units – their suitability for frequency response and the type of response they can provide varies. Although factors like the energy density, power density, cost, number of cycles and geography dependence determine the best storage technology for frequency response services,

only the response time technically and directly affect the frequency response from a storage system. Table 2.1 gives the response speed for various energy storage systems and the frequency support service they can provide.

Table 2.1: Response Service of Storage Systems [62, 63]

Storage Technology	Response time	Comments on FR Service
Lithium-ion Battery	Milliseconds	Inertia Emulation
Lead Acid Battery	Milliseconds	Primary Frequency control. Not suitable for inertia Support due to low power density and low cycling times
Superconducting Magnet	Milliseconds	Inertia Emulation
Supercapacitor	Milliseconds	Inertia Emulation
Compressed Air	Minutes	Can provide a slow-primary response and secondary frequency
Pumped Hydro	Minutes	Inertia, Primary and Secondary Frequency response
Flywheel	Seconds	Primary Frequency Response

2.3.4 Demand Side Response

Frequency response aims to keep system frequency from rapidly deteriorating following a power imbalance that can be caused by either the generation side or the load side. Generation is usually adjusted to respond to a frequency event, but changes to the load can also be used to influence frequency response. Demand side response (DSR) can help increase the resources available for power system to maintain frequency stability, particularly in systems with increasing MPPT and reducing inertia. DSR can also help reduce the need for addition generation for frequency support and can also be cost effective than support from generation [82]. The advancement of smart grid technology is a key enabler of frequency support by DSR.

For frequency support, DSR can either employ centralized, decentralized or hybrid control [11]. In centralized control, a control center automatically controls load depending on frequency deviation [11]. This method requires communication channels and is associated with high cost [83]. Centralized control is better suited for small power systems [83]. A downside of a centralized DSR is that the delay caused by the communication of the support signal can reduce the response time for frequency support [11]. Decentralized control is the most common control method for DSR. In decentralized control, the load responds to frequency deviation independent of the system operator. A decentralized control method has a downside of not providing adequate proportionate to a frequency deviation. The hybrid control (semi-controlled) method combines the centralized and decentralised control [11]. The load that participate in DSR are made up of thermostatically controlled loads (freezers, fridges, water heaters and air conditioning) and distributed storage systems like electric vehicles.

In [82], dynamic FFR is provided by decentralized control of an aggregate of heat pumps and fridges. An algorithm is developed to trigger the heat pumps on and off depending on the frequency variation. The performance of the algorithm is evaluated for the Great Britain power system. In [84], an aggregate of water heaters is used for frequency regulation using a centralized controller. As a result, a two-way communication channel was needed to implement the control algorithm. Adaptive hill control is used by the central controller in [85] when the frequency deviates by $> \pm 0.05Hz$ to turn off and on electric water heaters. A decentralized DRS using a frequency response controller similar to droop control of generators is proposed in reference [86]. The method in [86] uses the time evolution of frequency response to determine how much load will be switched on or off. Reference [87] describes a mechanism for DSR provision similar to generator droop by adjusting the thermostat of thermostatically controlled load in proportion to frequency change. DSR using electric vehicles have been reported in [88].

The major downside of DSR for frequency support is that the amount of load available for will vary depending on environmental changes and consumer behaviour

and thus limited in how much it can compensate for increasing renewable penetration and low system inertia

2.4 Summary

In this chapter, the effect of inertia in power system frequency stability is discussed. Increasing converter-connected generation sources in power systems is shown to have results in low inertia which results in higher RoCoFs. The reduction in system inertia is driven by the steady increase in generation from wind turbines and solar photovoltaics. The generation mechanism of wind turbines and solar photovoltaics is explained. Wind turbines can provide inertia with additional control to release inertia hidden in the rotors. Wind turbines can provide primary support by deloading the wind turbine with pitch regulation. Also, storage systems are increasing in power system and are primarily used to store power from intermittent sources. Storage systems are also used to provide frequency support. Storage systems usually provide frequency support in coordination with intermittent energy sources. DSR is also discussed as a source of frequency support. Frequency support from PVPP can be achieved by deloading, but the mechanism for deloading PV is not much discussed in the literature. Also, the effect of the PV MPPT on frequency response and reserve maintenance needs to be explored.

It is observed from the literature review that frequency support from wind turbines, storage and DSR are provide mostly by inertia emulation and droop control. However, the control of PV system and operation of PV MPPT to provide frequency support have not been explored. The ability to compare between support sources will be valuable in designing frequency support schemes for power systems.

Chapter 3 : PV MPPT and Active Power Control

3.1. Introduction

As discussed in chapters 1 and 2, the participation of renewable energy sources in maintaining system stability is essential in increasing their penetration in electrical power systems. For generating units to contribute to system stability, they have to be able to increase or decrease their output power in response to system events. Typically, PV systems employ an MPPT technique to operate at maximum power. A modification of the MPPT and PV operation is required to enable the PV systems to operate below maximum power. Hence the need for a de-loading technique.

Furthermore, power from a photovoltaic power plant (PVPP) can fluctuate quickly due to changes in environmental conditions [89]. Ramp rate control of PV systems is required to control the rate of change of the power output from a PV system [90]. Implementing ramp rate control will also require the PV system to keep a reserve or can also be achieved by combining PV operation with an energy storage system [90]-[92]. PV systems may also be required to participate in frequency support, as increasing PV penetration results in the reduction of system inertia. Hence, Active Power Control (APC) of PV systems is necessary to increase the functionality of PVPP in power systems.

APC of PV systems has been explored in literature. Authors in [93] proposed strategies for achieving reserve operation, power limiting operation, and ramp-rate control by perturbing forward or backward, the reference voltage from the MPPT algorithm is determined based on the difference between the desired values and current values. The methods used in [93] can result in oscillation around the operation point even when an MPPT that does not result in oscillation around MPP is used. In [58] and [94], frequency support from a PVPP is achieved by controlling the reference voltage. How control of the reference voltage is achieved and the effect of the MPPT choice are not explored. Currently, APC of PV systems is carried out by combining it with a storage system [94], [95, 96]. Deloading PV systems will likely become more attractive as the efficiency of PV modules increases, and the cost of PV modules declines.

The differences in response speed of different MPPT techniques imply that they take different times to reach their operating point. When there is a fast-changing irradiance condition, differences in tracking speed could result in more significantly different performances. This chapter examines the ability of different MPPT techniques to maintain a reserve and their performance in fast-changing irradiance conditions. Because the P&O is widely noted to drift in from MPP in fast-changing irradiance [97, 98], it is not suited for APC in fast-changing irradiance. This chapter also proposes and tests a modification to the P&O algorithm that avoids drift in fast-changing irradiance. The proposed P&O is tested by simulation in fast-increasing and sinusoidal irradiance conditions. Lastly, this chapter proposes an offline MPPT technique for improved performance in fast-changing conditions. The offline MPPT technique makes use of the characteristics of the PV module to determine the MPP voltage and current offline. The offline determination of the PV operating point results in reduced online computation and fast-response. This chapter also describes how APC functions such as reserve maintenance and frequency support can be achieved in a PV system using the offline MPPT.

The rest of the chapter is structured as follows: 3.2 gives a review of conventional MPPT techniques and describes how a reserve operation can be achieved. 3.3 examines the performance of selected MPPT techniques in reserve maintenance under fast-chaining irradiance. Section 3.4 explains the drift associated with the P&O

MPPT technique, proposes and tests a modification to the P&O. Section 3.5 describes the working an offline MPPT technique. Section 3.6 gives the concluding remarks.

3.2. MPPT Review and De-loading operation

3.2.1. Perturb and Observe (P&O)

The Perturb and Observe is a widely popular MPPT primarily because it is easy to implement and has a low cost [97]. The P&O algorithm works by searching the Power-Voltage (PV) curve. Due to the non-linear characteristics of the IV curve of a PV module at any irradiance or temperature [53], the maximum power voltage lies between 0 and the open-circuit voltage. The P&O algorithm perturbs the voltage or duty cycle in a particular direction (increasing or decreasing) as long as the measured change in power after each perturbation is positive. The algorithm will only change direction once the resulting change in power from the last perturbation is negative. As a result, the Perturb and Observe algorithm does not settle on a voltage even at steady irradiance but will oscillate around MPPT. When a large perturbation step is used, the oscillation can result in loss of power, but when a small perturbation step results in slow tracking speed. The constant perturbation of the P&O algorithm makes it difficult to achieve de-loaded operation. Direct manipulation of the output voltage will be difficult due to the constant search for MPP by the P&O algorithm. Also, the maximum available power is not known so reserve cannot be maintained by limiting the maximum voltage of the P&O.

This chapter proposes an approach to enable the de-loaded operation of PV systems using the P&O algorithm by using a model of the module and measurement of irradiance and temperature to generate the maximum power voltage for the PVPP. In practice, a dedicated module can be operated at MPP using the P&O to generate the MPP voltage. The manipulation of the MPP voltage can be used to implement APC functions. Figure 3.1 shows the operation strategy to achieve de-loaded operation with the P&O. In this case, the PVPP is not directly operating with the P&O. The P&O algorithm is used to generate the operating voltage for the PVPP. Operating the PVPP with voltage from a model or dedicated module will still result in oscillation around the operating point. However, the efficiency will be affected by the measurement of the irradiance and temperature.

3.2.2. Incremental Conductance

Like the P&O MPPT technique, the Incremental Conductance MPPT technique searches for the MPP in real-time. The significant difference is that the incremental conductance MPPT does not adjust the operating voltage when already at MPP. The main principle of the incremental conductance MPPT is that at MPP, the slope of the power-voltage curve is zero [99]. Which implies that:

$$\frac{dP}{dV} = 0 \tag{3.1}$$

Eq. (3.1) can be written as

$$\frac{d(I \times V)}{dV} = 0 \tag{3.2}$$

From the product rule of derivatives, Eq. 3.2 becomes:

$$V \times \frac{dI}{dV} + I \times \frac{d(V)}{dV} = 0 \tag{3.3}$$

The incremental conductance becomes:

$$\frac{dI}{dV} = -\frac{I}{V} \tag{3.4}$$

Eq. (3.4) implies that at maximum power, the incremental conductance is equal to the negative conductance. The Incremental conductance algorithm perturbs the voltage or duty cycle until the condition in Eq. 3.4 is met. The incremental conductance like the P&O cannot be de-loaded by directly modifying the MPPT due to the constant search for MPP. The algorithm increases the voltage if the incremental conductance is greater than the negative instantaneous conductance and reduces the voltage if the incremental conductance is less than the negative instantaneous conductance. This process of increasing and reducing the voltage will continue until the incremental conductance and the negative instantaneous conductance are equivalent. A de-loaded operation can be achieved by using the same method proposed for the P&O.

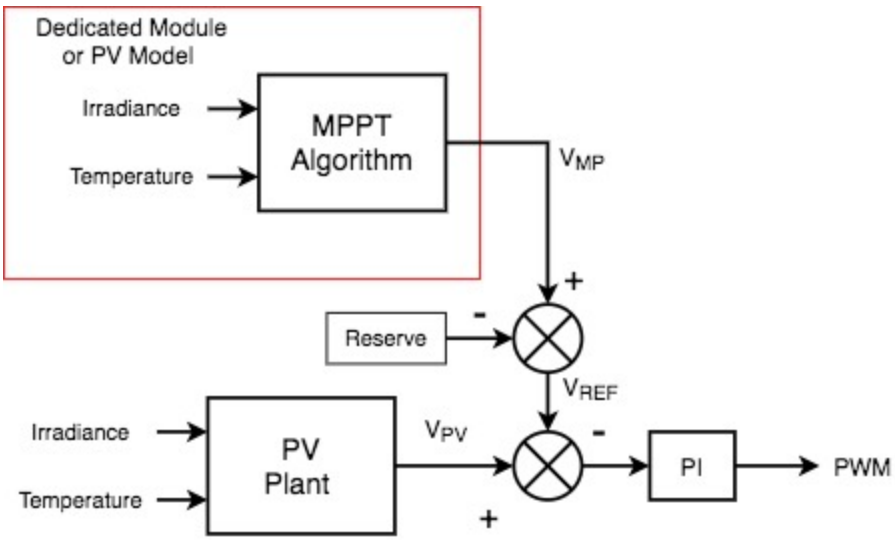

Figure 3.1: Deloading mechanism for P&O MPPT

3.2.3. Open-Circuit Voltage and Short-Circuit Current

This MPPT technique operates with a fixed percentage of the open-circuit voltage or the short-circuit current as the maximum power voltage or current [100]. This technique is based on the fact that the ratio of the maximum power voltage and current to the open-circuit voltage and short-circuit current respectively does not vary widely with changing irradiance and temperature. Loss resulting from the regular measurement of short-circuit current and open-circuit voltage is the main drawback of this MPPT technique. A de-loaded operation can be achieved with this technique by manipulating the MPP voltage or current.

Because the short-circuit voltage and open-circuit current MPPT drive the output power of the PV system to zero, it is not suitable for APC. The significant fluctuation in power can affect frequency support function if the open-circuit voltage or short-circuit current measurement occurs when PVPP is participating in frequency response.

3.2.4. Constant Voltage

This MPPT technique operates the PV system at a fixed voltage for all irradiance and temperature. This method requires no computation and is very fast. It is also cheap as it does require any sensors for temperature or irradiance measurement. As expected, this method results in the loss of significant power and is less efficient

than other MPPT methods [101]. This method is suitable for APC because the voltage can be directly manipulated. This method can be used in combination with a more efficient MPPT.

3.3. Drift Free Perturb and Observe

Conventional P&O algorithm can result in a deviation from the maximum power path while in operation - particularly at fast increasing irradiance [99, 100]. Despite being one of the higher efficiency MPPT techniques, the tendency of the P&O to deviate from MPP results in lower operational efficiency.

During a deviation from the maximum power path, it is difficult to predict the output power of the PV system. This deviation makes it difficult for a PV system employing a conventional P&O algorithm to participate in APC in a power system. Notably, it will be difficult for PV systems with conventional P&O to participate in frequency support when the irradiance is fast changing. This is because frequency support requires the adjustment of active power output by a value defined by the support parameters. The probability of drift from a PV system with P&O makes attaining a defined power output from a PV system difficult.

Many modifications to the conventional P&O algorithm for drift avoidance have been proposed in the literature. The adaptive P&O [97, 99], varies the perturbation size based on the rate of change of environmental conditions. In [97], the author achieves drift-free operations by tracking the change in power resulting from the oscillations around MPP. If the change in power rises above a defined threshold, then the perturbation size is increased. In this method, the change in power is used to detect changes in irradiance. Generally, drift from MPP in PV systems with P&O is achieved in varying the perturbation size. However, varying the perturbation size can lead to a significant swing in power in fast-increasing irradiance. This swing in power can affect the performance of a PV system when carrying out active power control functions such as frequency response. They can also be very complex and require higher computational power than conventional P&O [99]. In order to prevent drift from MPP without causing large fluctuations in output power of a PV system and improve the predictability of PV power output, a drift-free P&O MPPT technique that does not require a change in perturbation size is required.

The drift associated with the conventional P&O algorithm results from the confusion of a path of power increase to be the path of maximum power increase. A drift will begin to occur when the P&O algorithm experiences power increase in a particular direction, which is not the direction of power increase. Two scenarios could lead to the beginning of a drift from MPP. Figure 3.2 gives the illustration of the drift occurrence.

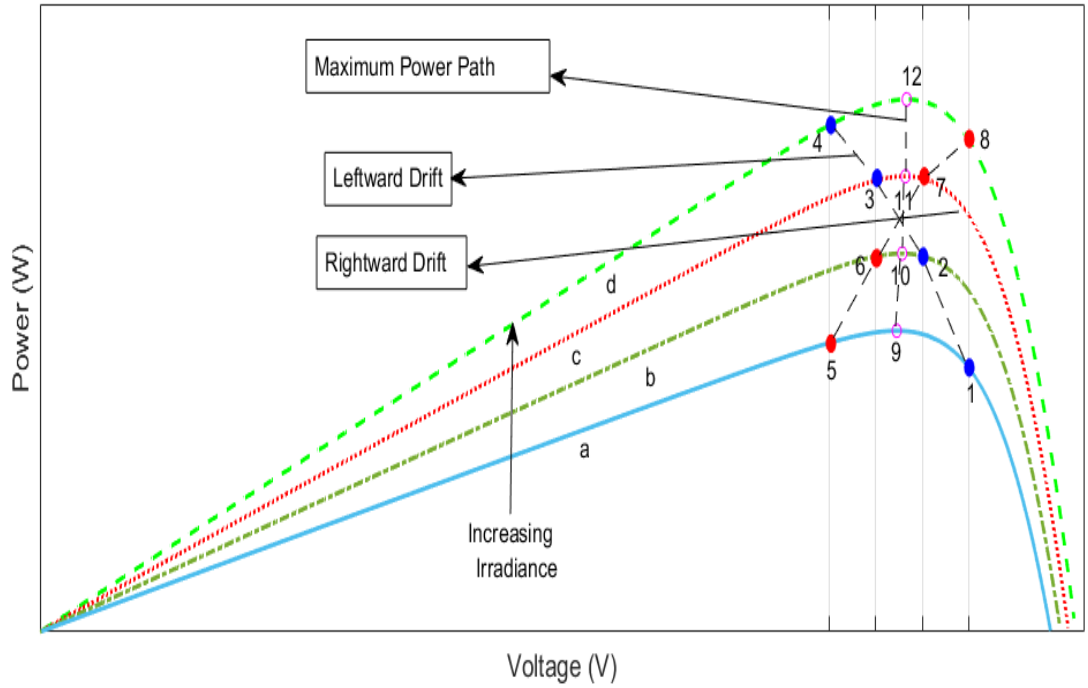

Figure 3.2: Drift analysis of P&O MPPT

Scenario 1: From Figure 3.2, at a given irradiance, the MPP for the PV curve (a) is at point (9), and the PV operating point is at point (1). If the irradiance moves the PV curve from (a) to (b), the MPP moves from (9) to (10). Assuming the previous step of the MPPT was reducing the voltage and assuming it led to a power increase, the P&O algorithm will move from point (1) to point (2) and will result in a power increase. If the irradiance increases and moves the PV curve from (b) to (c), the MPP will move from (10) to (11), and the next perturbation step will move the operating voltage from point (2) to point (3). The move from (2) to (3) represents a power increase, but the power at (3) is less than the MPP at (11). If the PV curve then moves from (c) to (d), the MPP moves from (11) to (12). The P&O algorithm will move the operating point from point (3) to point (4) because the previous step resulted in a power increase. This will lead to a larger deviation. The algorithm will keep in this direction

until a step results in a decrease in power. This will be called a leftward drift as a reduction in operating voltage is resulting in a drift in operating point to the left of the PV curve and maximum power path.

Scenario 2: In Figure 3.2, at a given irradiance, the PV curve of the solar PV system is given in (a). The MPP of (a) is at point (9). Assuming the operating point of the PV system is at (5). If the irradiance increases and moves the PV curve from (a) to (b), the MPP moves from point (9) to (10). Assuming the previous perturbation step was a voltage increase and resulted in a power increase, the P&O algorithm will move the operating point from point (5) to point (6), resulting in a power increase. If an increase in irradiance then moves the PV curve from (b) to (c), the MPP moves to point (11). The P&O algorithm will them move the operating point from point (6) to point (7), resulting in a power increase. The move from point (6) to (7) begins a drift from maximum power since the maximum power voltage lies between point (6) and point (7). As the PV curve moves from (c) to (d), the P&O algorithm will move the operating point from (7) to (8) and thus continue the deviation. The deviation will continue until the algorithm experiences a decrease in power. Deviation resulting from this scenario will be called rightward drift as an increase in voltage is resulting in a drift to the right of the PV curve and maximum power path. For both scenarios 1 and 2, it is assumed that the change in the PV curve from (a)-(b)-(c)-(d) and the change in perturbation step is happening very fast and at the same time. The P&O algorithm with the proposed loop is given in Figure 3.3.

The authors in [102] proposed a modification to the P&O algorithm that does not require any manipulation of the step size. In [102], the addition of a loop that measures the change in current is proposed. The change in current is measured when there is an increase in power and voltage. When there is an increase in power, voltage, and current from the previous step, the algorithm will reduce the voltage instead of increasing the voltage. Otherwise, the algorithm is the same as conventional perturb and observe. The additional loop ensures that the algorithm does not continue to increase the voltage (or decrease duty cycle) when the irradiance increases but also checks both voltage increase and decrease while remaining in a path of power increase. This will ensure that the algorithm follows the path that will result in the most power increase when the voltage is increasing. This additional loop proposed in [102] only

checks for the change in current when power and voltage increase, assuming that the drift will only occur when there is a positive change in voltage and irradiance. As explained in scenario 1, drift can occur with increasing irradiance while the perturbation is reducing the voltage or increasing the duty cycle. Therefore, the inclusion of a current loop measurement, only when there is a power and voltage increase only helps eliminate the possibility of rightward drift. In such a situation, a leftward drift can still occur. Which implies that drift solution proposed in [102] will still result in a drift in certain condition leading to power loss and making it inadequate for frequency support.

A current measurement loop is added to the algorithm when there is an increase in PV current irrespective of the direction of perturbation is proposed. This will eliminate the possibility of both leftward and rightward drift. This is implemented by adding a current measurement loop in the P&O algorithm when there is an increase in power and a negative change in voltage from the last perturbation step. The proposed loop is in addition to the loop proposed in [102]. The additional loop will increase the voltage (or decrease duty cycle) when there is an increase in power, a decrease in voltage, and a positive change in PV power.

The proposed modification is tested using a PV system which produces 100kW at STC. The schematic of the system is given in Figure 3.4. A linearly increasing and sinusoidal irradiance is used to evaluate the effectiveness of the proposed additional loop.

First, an irradiance increasing linearly from 200-600w/m^2 in 10s is used to as input to simulate a rapidly increasing irradiance. The PV system is then operated with the conventional perturb and observe, perturb and observe with loop proposed in [102] and the additional proposed loop. Figure 3.5 gives the output power and Figure 3.6 gives the output voltage for all three MPPTs tested. In Figure 3.5, the conventional P&O deviates massively from the expected output power. The conventional P&O experiences a sudden increase in power when the voltage limit is reached. This is because the voltage prevents the MPPT algorithm from continuing in the drift path. This deviation is expected as the irradiance is increasing fast, and drift is possible in at any point. When the loop proposed in [102] is included in the MPPT, there is an

increase in the output power from the output power with the conventional P&O but still a substantial deviation from expected output. It is observe in Figure 3.6 that with the loop proposed in [102] a rightward drift was avoided but a leftward drift occurred. P&O with the additional proposed loop, the gives the closest output power to the expected power in Figure 3.5. As observed in 3.6, the additional loop keep the voltage from drifting in any direction while the irradiance is increasing.

The PV system is subjected to sinusoidal irradiance of 1.5rad/s and 2rad/s. The output power is given in Figures 3.7 and 3.8. The P&O with the proposed additional loop results in expected output power for both sinusoidal irradiance of 1.5rad/s and 2rad/s. The output power with P&O with the single loop proposed in [102] and with conventional P&O resulted in deviation when the irradiance is increasing and then catches up with the proposed P&O after the irradiance begins to declines. The drift from the conventional P&O is larger than drift from P&O with the loop in [102]. This is because the slope of the PV curve is steeper to the right of the MPP than to the left of the MPP. A drift of the same voltage will result in a larger loss of power for a rightward drift than for a leftward drift.

Figures 3.5, 3.6 and 3.7 shows that the drift results in more loss in power for the conventional P&O and is smallest for P&O with proposed additional loop when compared with the maximum power. Other than in a drift situation, the three P&O methods track maximum power the same way. Results from Figures 3.5, 3.7, 3.8 show that only a drift-free MPPT without a large swing in power is appropriate for APC. This is because the change in power as a result of drift is not known, thereby making APC difficult. The difference between PV power and expected power increases with increasing irradiance.

It should also be noted that the drift does not occur in a particular situations with conventional MPPT. The drift will not occur if the MPPT is already moving in a direction which also happens to be the direction of maximum power increase when the irradiance is increasing. This implies that the drift will not happen in every instance of increasing irradiance.

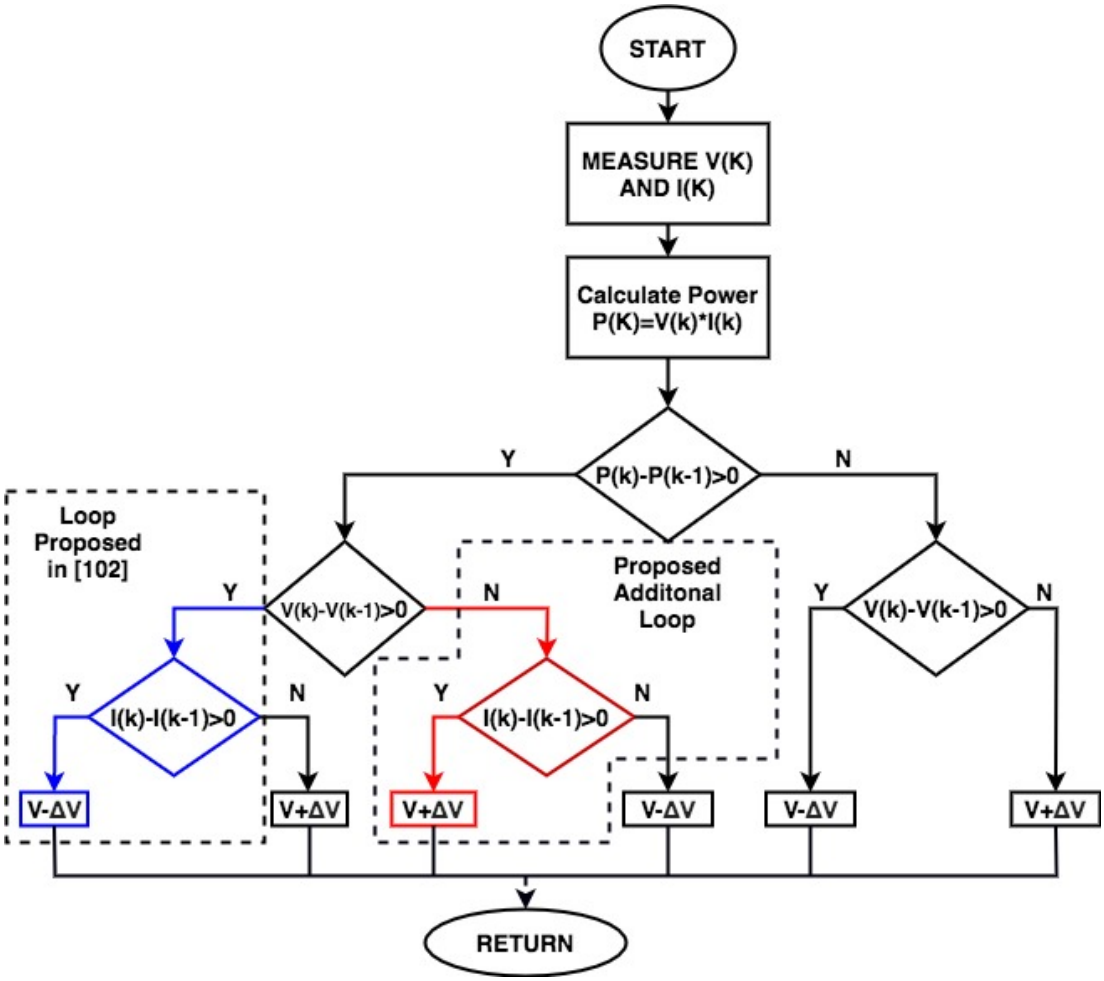

Figure 3.3: P&O flowchart with proposed loop

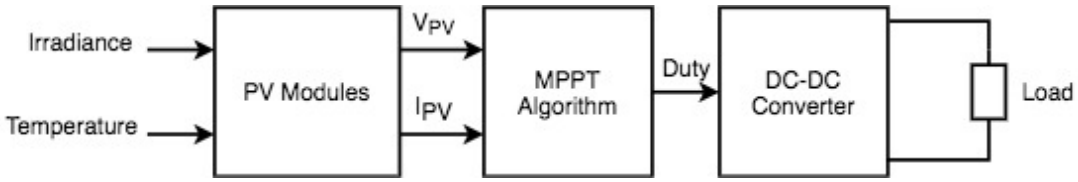

Figure 3.4: Schematic of P&O test system

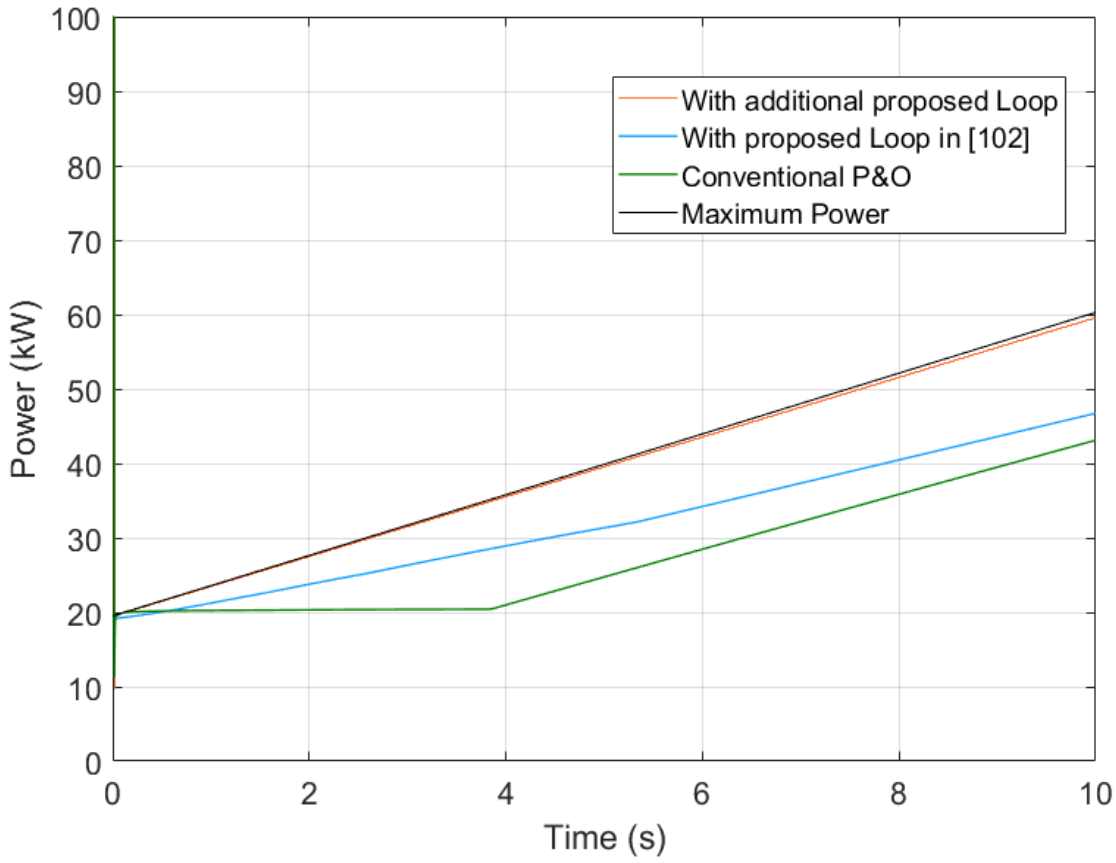

Figure 3.5: Power output for increasing irradiance

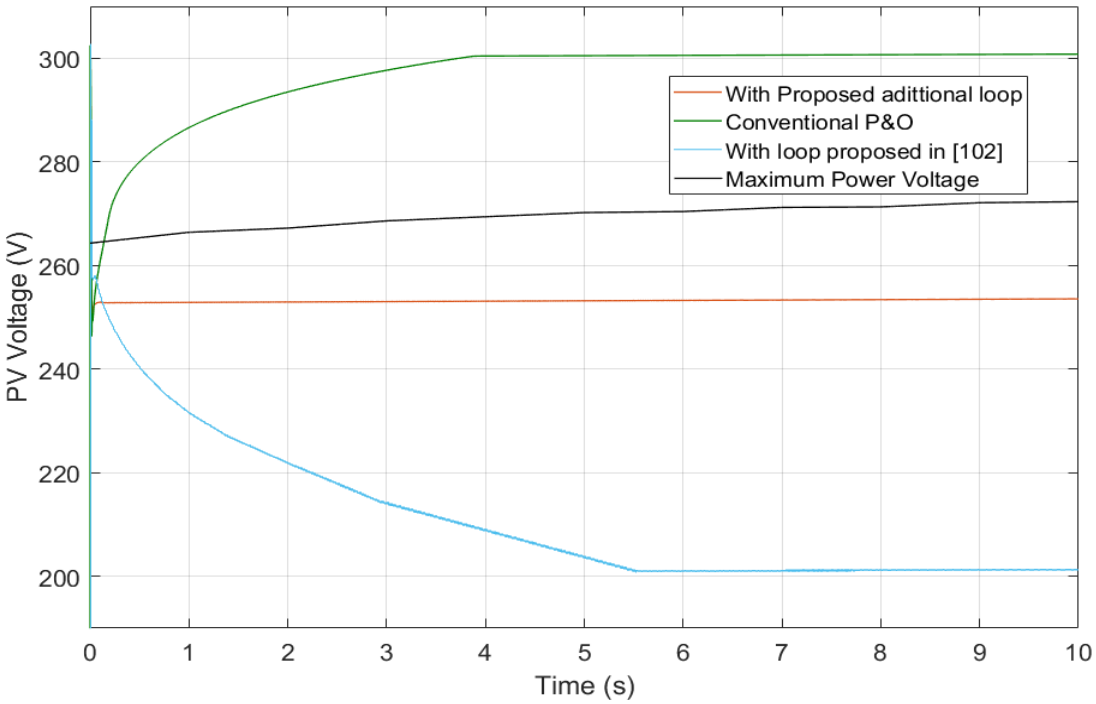

Figure 3.6: Voltage output for increasing irradiance

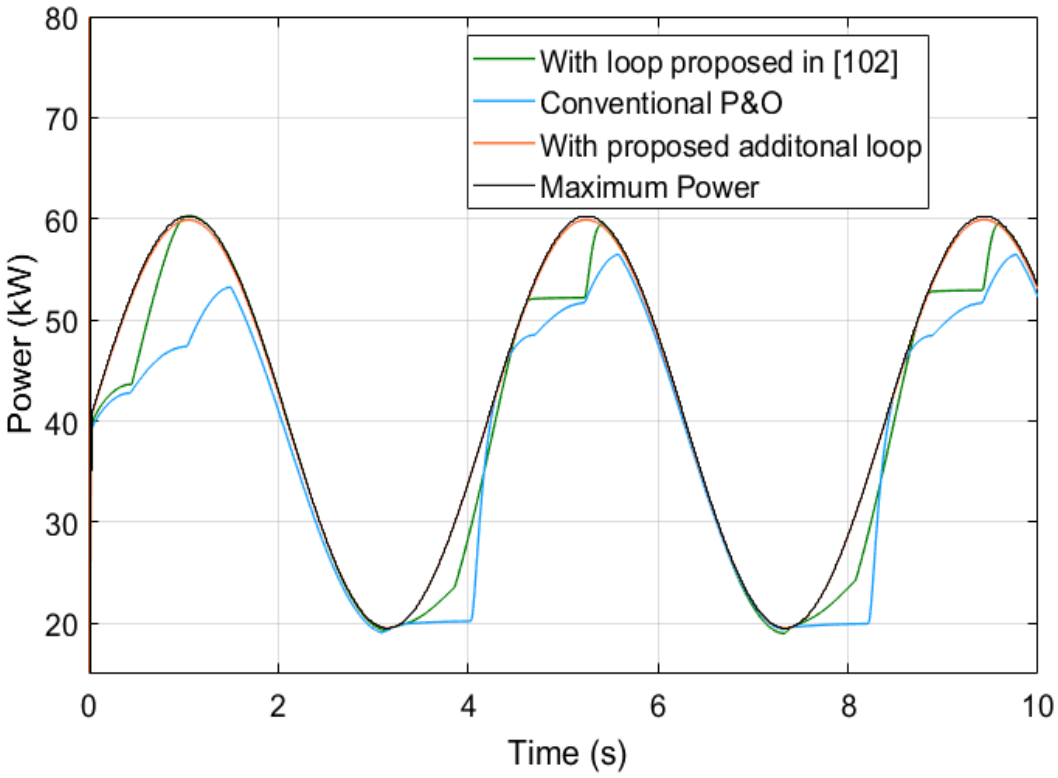

Figure 3.7: Power output for sinusoidal irradiance (1.5rad/s)

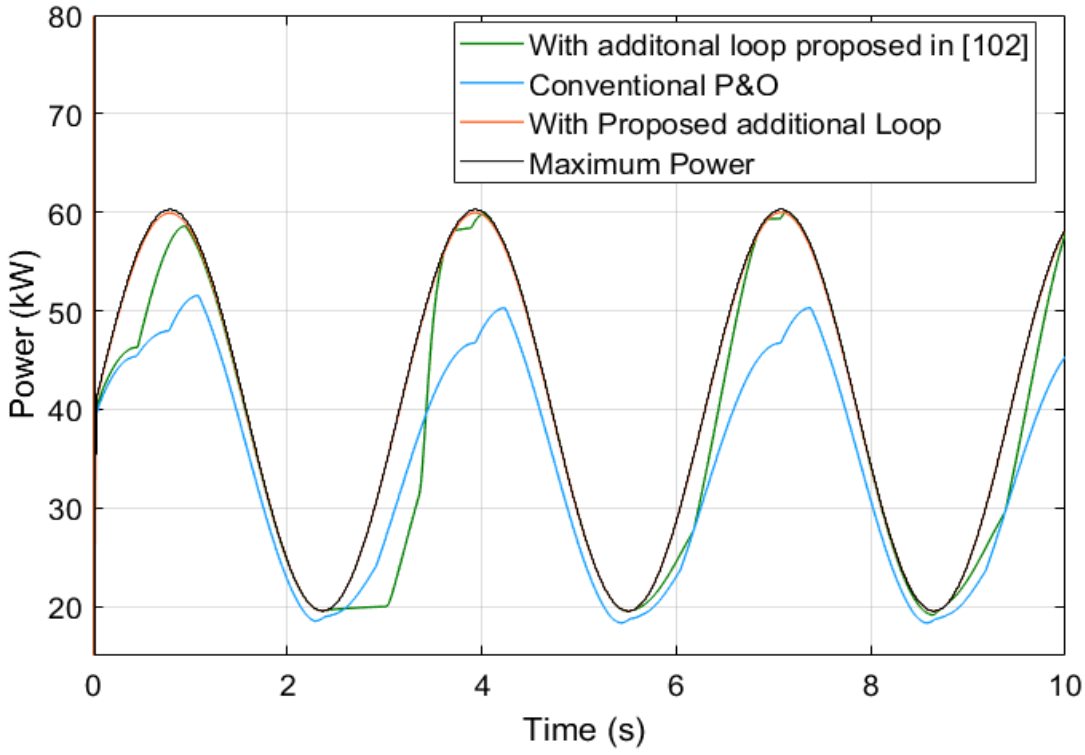

Figure 3.8: Power output for sinusoidal irradiance (2rad/s)

3.4. Offline MPPT

Apart from their efficiency, the tracking speed is another significant difference between MPPTs. It will be shown in section 3.5 that the differences in tracking speed contribute to differences in performance for reserve maintenance at fast-changing irradiance. The effect of tracking speed for some APC functions is exacerbated in fast-changing irradiance conditions. For frequency support function, the speed of response of a generating unit determines the quality of support – this will be discussed in detail in chapter 5. As noted in [103], most MPPT techniques are not designed for fast APC. Most improvements to convention MPPT techniques have been focused on increasing efficiency and tracking speed. While some MPPT techniques to improve tracking speed have been proposed, they are usually not designed with the consideration of APC for frequency support. They usually may involve an on-line variation of the duty cycle which could cause large swings in power and affect frequency support and may require a separate mechanism for de-loading and active power control.

Artificial neural networks (ANN) MPPT technique is generally considered to be fast [104]. Because ANN method outputs a voltage or current and its input is based on environmental conditions, it is easy to achieve de-loaded operation. ANN algorithm, however, requires training and the efficiency of this MPPT depends on the training. The P&O with additional current measurement loops proposed in section 3.4 and the optimised dP-P&O in [105] are able to track maximum power in fast-changing irradiance but combined with a de-loading mechanism may become more expensive making it less suitable for frequency support. The tracking speed of other MPPT techniques can be improved by using more computation power but this could result in an increase in cost [106]. To improve the ability of a PVPP to participate in frequency support in any irradiance condition, a low-cost, fast-response, drift-avoiding and easy to de-load MPPT is required.

The offline MPPT is proposed for fast-tracking and high-efficiency. The offline MPPT requires the offline determination of the MPP voltage and current to use as a reference in the PV operation. Because the calculation is done offline, all computation is eliminated, resulting in a fast operation with no oscillation around MPP. PV module characteristics are given in the datasheet. Using the information on the datasheet and the characteristics of the solar module, the IV curve for any

combination of irradiance and temperature can be obtained. The maximum power voltage or current can be readily obtained from the IV curve. The duty cycle for the converter can be obtained from the maximum power voltage.

3.5.1. Calculating R_s, R_{sh}, and I_0

The saturation current, I_0 can be obtained from (3.6). R_S and R_{SH} can be calculated using the method described in [107]. The values of R_S and R_{SH} are determined by (3.5) at STC and Nominal Operating cell Temperature (NOCT). The combination of R_S and R_{SH} that results in the closest maximum power at STC and NOCT is chosen as the values of the module resistances. The values obtained for Trina Solar TSM 310PD14 is 0.3Ω for R_S and 425Ω for R_{SH}.

$$I_0 = \frac{1}{e^{qV_{OC}/kT}-1} \times \left[I_{SC} - \frac{V_{OC}}{R_{sh}}\right] \tag{3.5}$$

3.5.2. Calculating I_{SC}

Every combination of irradiance and temperature will result in a different IV curve. Each IV curve will have its own open-circuit voltage and short-circuit current. I_{SC} is given by (3.6) [21].

$$I_{sc} = \frac{S}{1000} \times \left[I_{sc,STC} + \alpha_{SC} \times (T - 25)\right] \tag{3.6}$$

where S is the irradiance, $I_{SC,STC}$ is the short-circuit current at STC, α_{SC} is the temperature coefficient of the short-circuit current. Figure 3.9 shows the short-circuit current for a wide operating range. The effect of changing temperature on the IV curve and the power-voltage curve is given in figures 3.10 and 3.11, respectively. The effect of changing irradiance on the IV curve and power voltage curve is given in Figures 3.12 and 3.13, respectively.

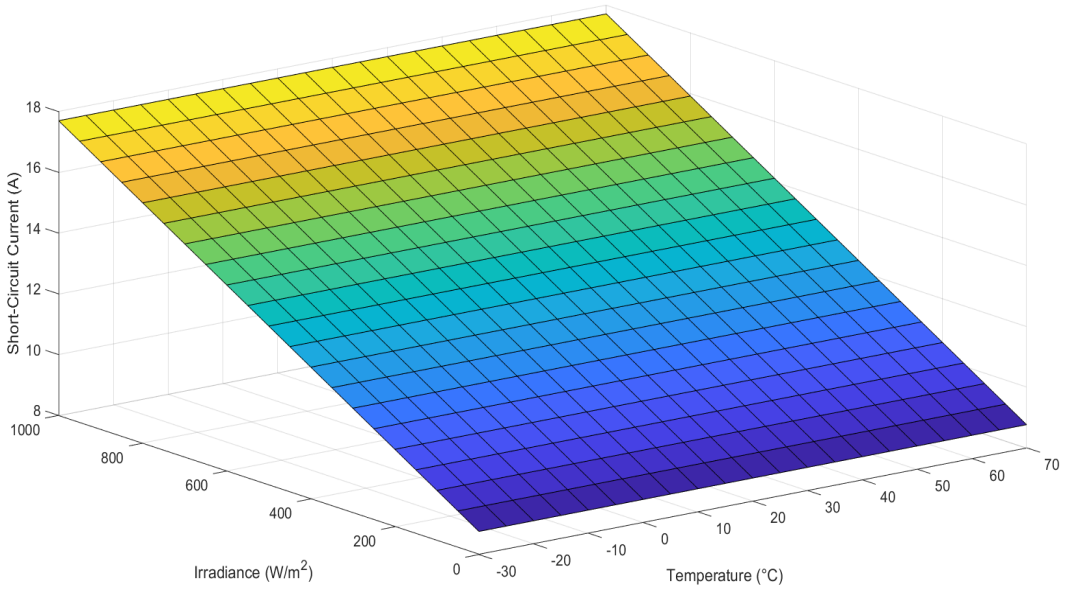

Figure 3.9: Short-circuit current for PV module

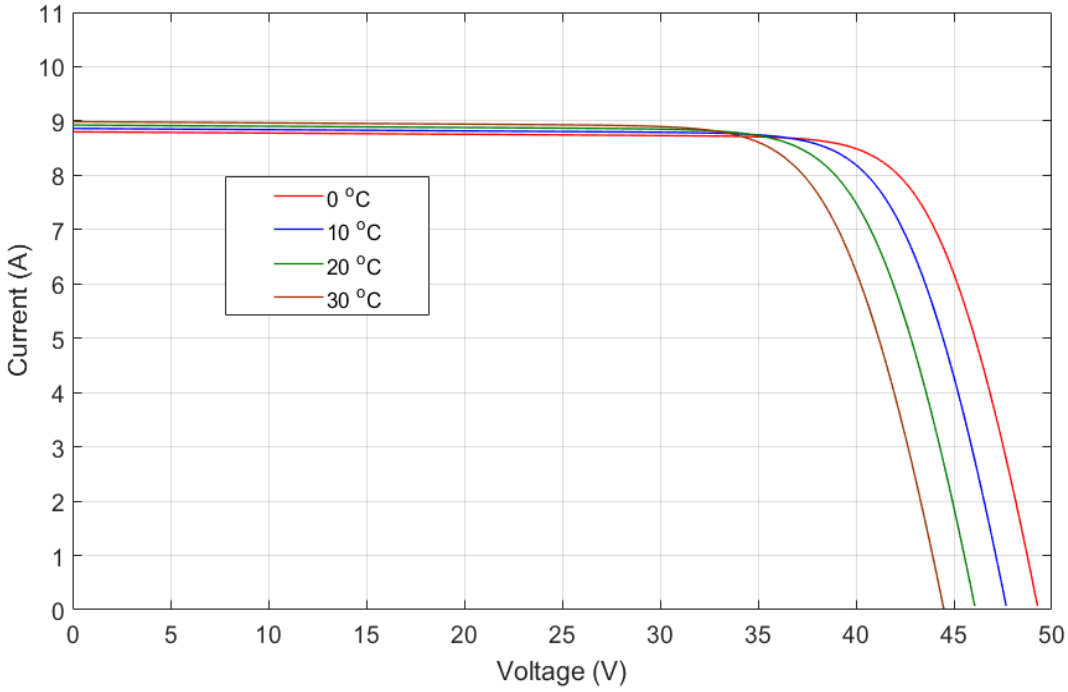

Figure 3.10: Effect of changing temperature on IV curve

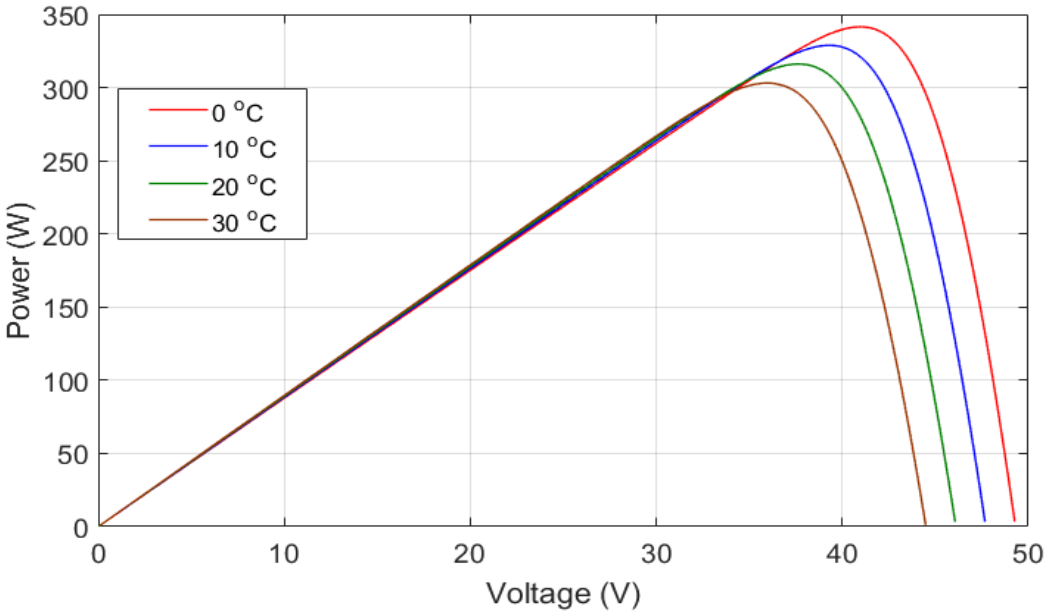

Figure 3.11: Effect of changing temperature on PV curve

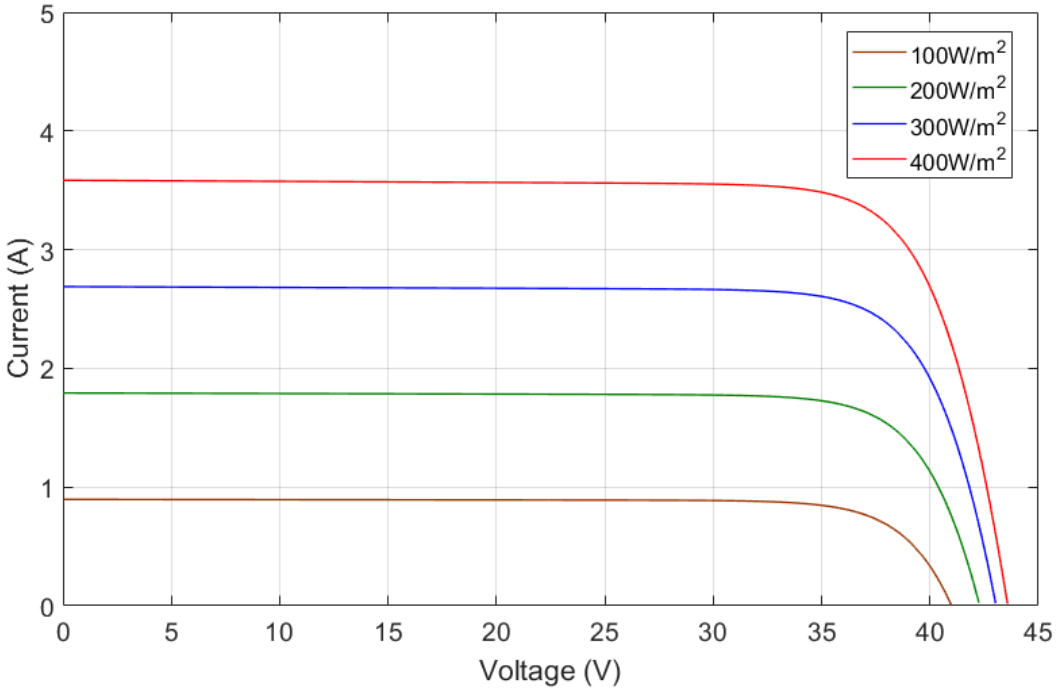

Figure 3.12: Effect of changing irradiance on IV curve

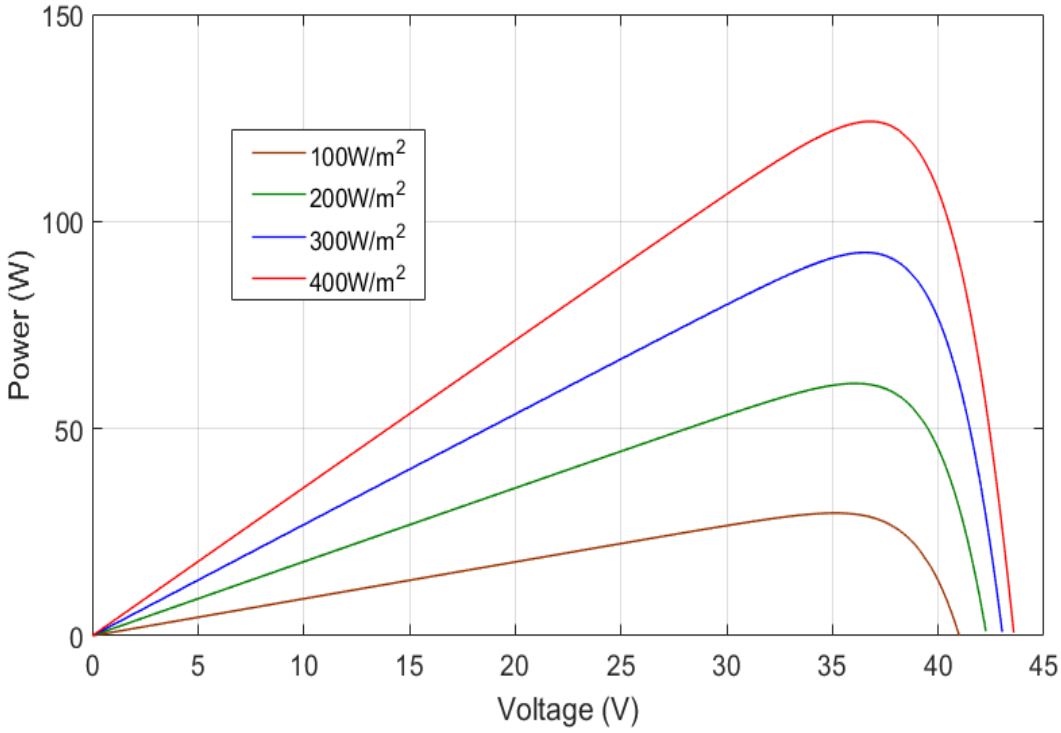

Figure 3.13: Effect of changing irradiance on PV curve

3.5.3. Calculating V_{OC}

If the short-circuit current known, the open-circuit voltage can be obtained using the diode equation without considering the effect of the parasitic resistances. While the parasitic resistances affect the position of the MPP in the IV curve, they do not a significant effect on the position of the V_{OC} and I_{SC}. The open-circuit voltage any combination of irradiance and temperature can be calculated using equation (3.7). Figure 3.14 gives the open-circuit voltage for a wide range of temperature and irradiance obtained using the temperature coefficient of the open-circuit voltage and short-circuit current. The value of the open-circuit voltage is needed to obtain the IV curve for a given irradiance and temperature condition.

$$V_{OC} = \frac{k \times 298}{q} \times \ln\left[\frac{I_{SC}}{I_0} + 1\right] + \alpha_{OC} \times (T - 25) \qquad (3.7)$$

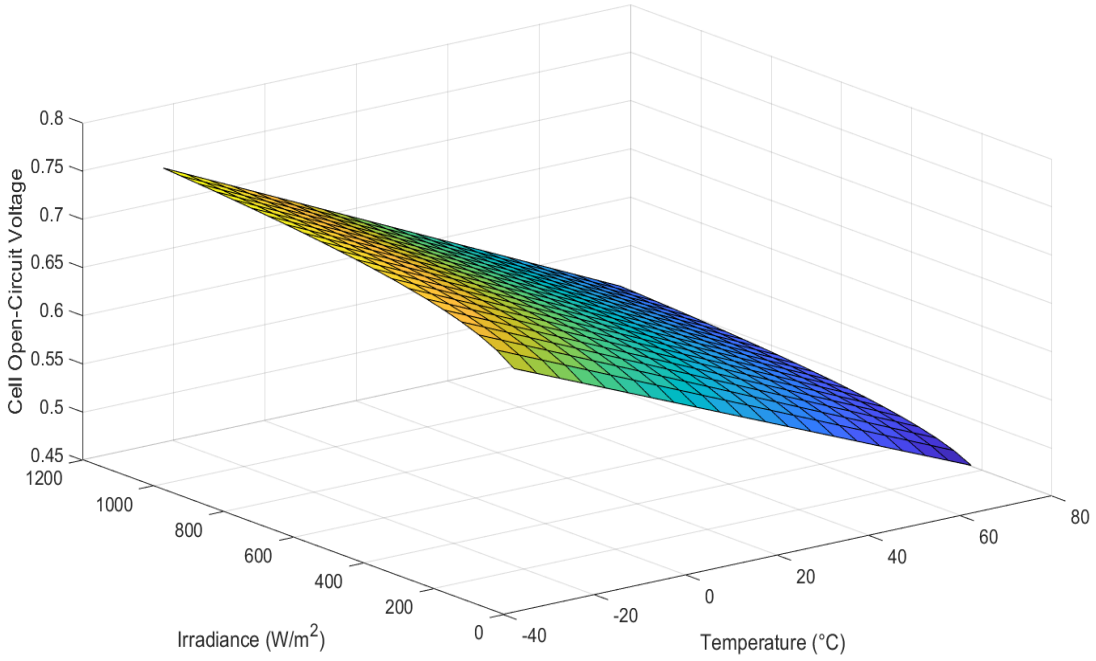

Figure 3.14: Open-circuit voltage for PV module

3.5.4. Calculating Maximum Power

With series and shunt resistances, and the saturation current known, the IV curve for any combination of irradiance and temperature can be obtained by solving equation (2.10). The current equation in (2.10) is an implicit equation due to the presence of current variable within the exponential term. As a result, a solution to (3.5) has to be obtained numerically. Equation (2.10) is solved by finding the value of current that satisfied a given voltage. The value of the current is solved for voltages from 0 to V_{OC}. Figures 3.15 and 3.16 gives the maximum power voltage and maximum power current respectively for some selected point.

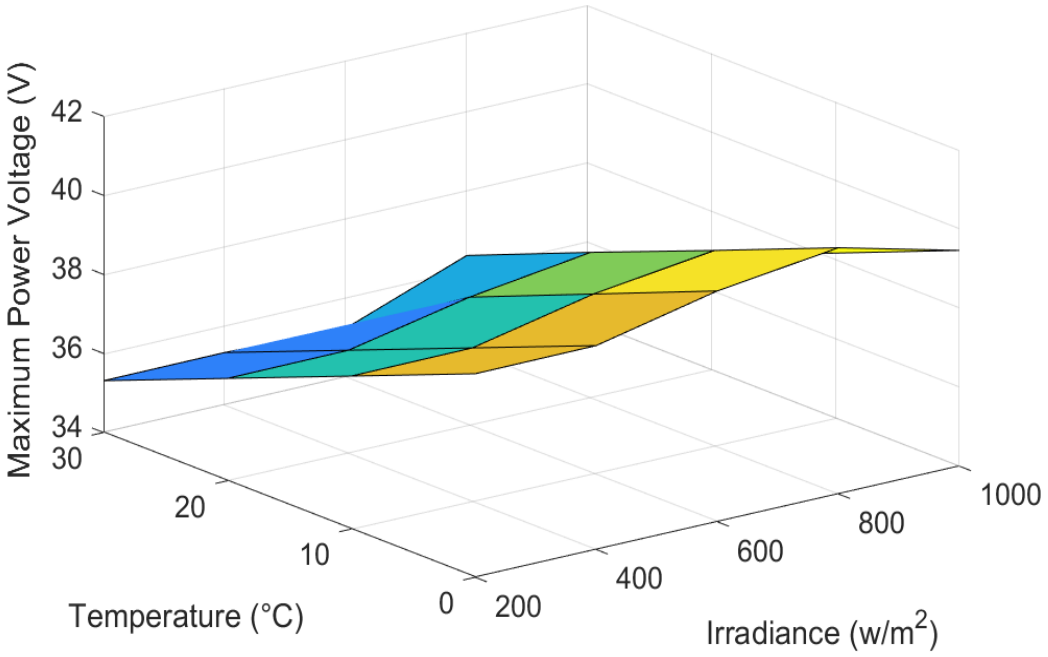

Figure 3.15: Module maximum power voltage

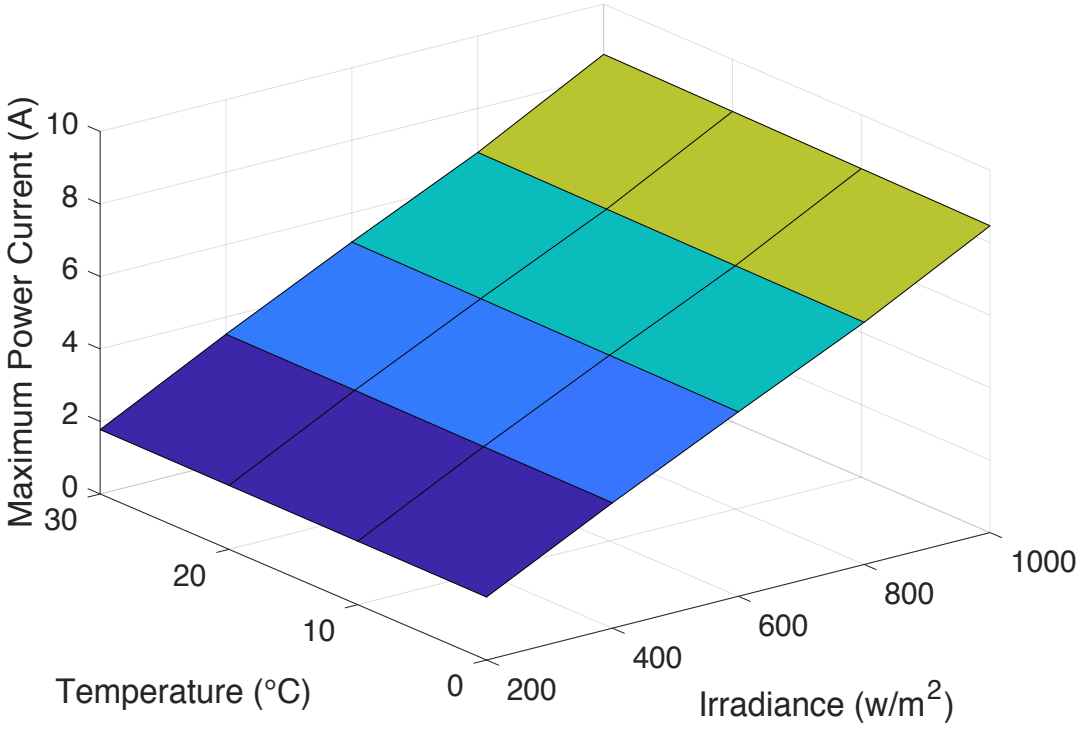

Figure 3.16: Module maximum power current

3.5.5. Maximum Power Point Operation

The calculated maximum power voltage or current is stored in a lookup table with temperature and irradiance as inputs. The output of the lookup table will be the reference voltage for the PI controller or will be used to obtain the duty cycle. Apart from the lookup table generating the reference parameter, rest of the MPPT operation is like the fractional open-circuit voltage or short-circuit current. The offline MPPT combines the simplicity of the fractional open-circuit voltage with the high accuracy of offline MPP calculation. The efficiency of this method is also affected by the number of point calculated for. For increased efficiency, the step size for the irradiance and temperature should be as small as possible. Interpolation in Simulink is used to determine the value for point between stored values. A flowchart for obtaining lookup table date is given in Figure 3.17. The operation of the offline MPPT is shown in Figure 3.18.

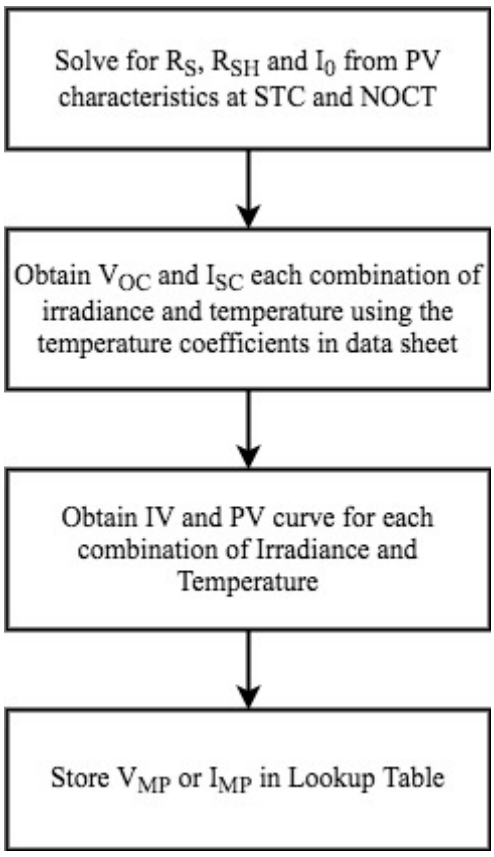

Figure 3.17: Flowchart for lookup table data

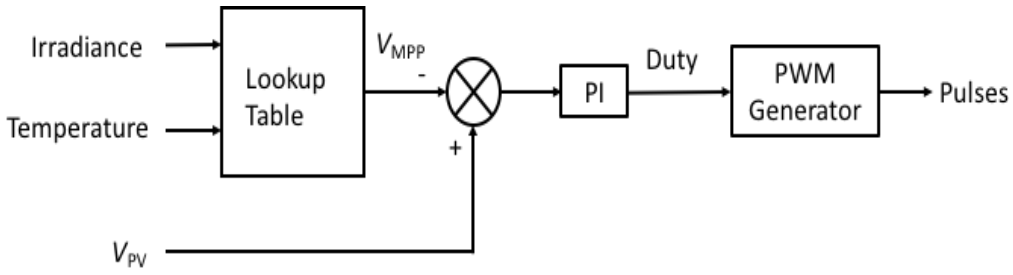

Figure 3.18: Maximum power operation

3.5.6. Creating Reserve (De-Loading)

PV systems can be de-loaded to operate at a percentage of maximum power (percentage de-loading) or at a percentage that guarantees a fixed amount of reserve power (constant power de-loading). Two methods can be used to achieve both types of de-loading.

Method 1:

In this method, a linear relationship is assumed between the PV voltage and the PV power. As shown in Figure 3.19, the voltage increases near linearly with power until it gets close to the maximum power point. The steepness of the PV curve decreases close to maximum power. From Figure 3.19, to a lesser extent, the PV power also has a negative linear relationship with the difference of the open-circuit voltage and maximum power voltage unit close to the maximum power voltage where there is a reduction in steepness. Assuming complete linearity, a 10% reserve can be achieved with at voltage given in equations (3.8) and (3.9).

$$V_{10\%} = V_{MP} \times 0.9 \tag{3.8}$$

$$V_{10\%} = (V_{OC} - V_{MP}) \times 0.1 + V_{MP} \tag{3.9}$$

It is preferable to use equation (3.8) as the right-hand side of the maximum power point is initially steeper and will lead to significantly less power than expected. The PV curve shown in Figure 3.19 shows the deviation expected from assuming a linear relationship.

In order to create a constant power reserve, the maximum power has to be calculated. The maximum power can be readily obtained as the maximum power voltage and current are known from the offline calculation. The output power of the PV system is then to be the difference between the maximum power and the reserve power. The constant power reserve is achieved by reducing the reference voltage by a factor of the ratio of the operation power to the maximum power. The control for fixed power de-loading is shown in Figure 3.20.

Method 2:

Method 1 assumes the PV curve is a triangle with vertexes at the zero, maximum power point, and open-circuit voltage. This assumption will lead to an approximate value of the expected reserve. This method will not result in the exact amount of reserve required. Another method to improve the accuracy of the reserve power is to use the calculation of the voltages or currents to give exact reserve values. Instead of storing only the maximum power point in the lookup table, the voltage or current that will result in a range of percentage of maximum power is stored in a lookup table. That is storing part of the PV curve. In this case, a 3-D lookup table is required. The inputs to the lookup table will include the irradiance, temperature and the de-loading factor. The operation of this method for achieving a percentage reserve is given in Figure 3.21. Three lookup tables are needed to achieve a fixed power reserve using this method. The first two are 2-D lookup tables that output the maximum power current and voltage. The third lookup table is a 3-D lookup table to be operated at the percentage necessary to maintain the required reserve. Figure 3.22 shows the operation for a fixed power reserve using method 2.

The two deloading methods are compared for percentage deloading and fixed-power deloading. Using irradiance in Figure 3.23 [108] (accelerated data from minutes-seconds), Figure 3.24, gives the 20% deloading using the irradiance in Figure 3.2. Method 2 results in an output value closer to the actual 20% point than method 1. Figure 3.25 gives the output power for a 10kW reserve and method 2 also gives closer output power to the actual value for a 10kW reserve. The difference is power output between Method 1 and Method 2 is because method 1 is based on assuming direct relationship between the voltage and current while method two depends on calculation

of the reserve voltage. Method 1 can be used with the most common MPPTs while method 2 is only applicable to the offline MPPT.

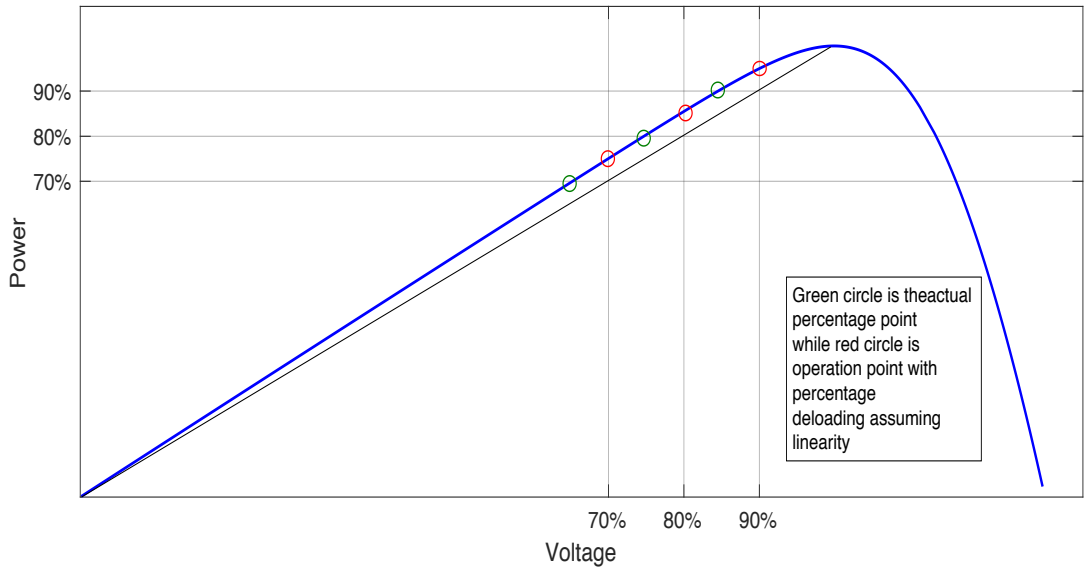

Figure 3.19: Method 1 Error in linear deloading

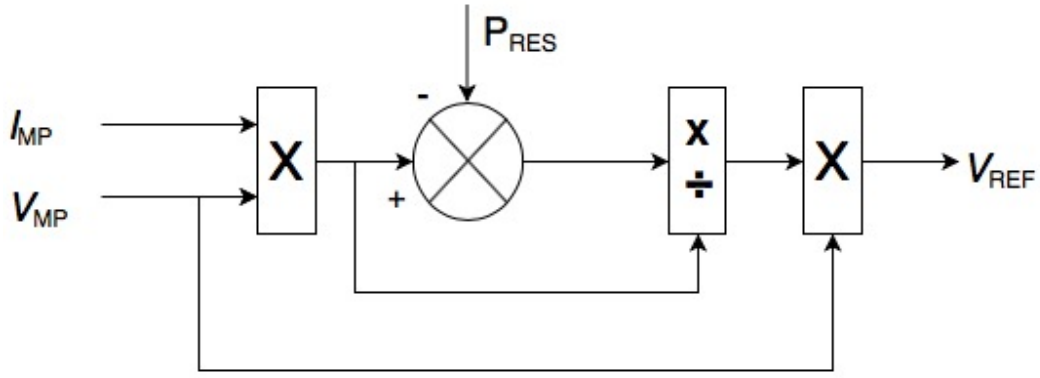

Figure 3.20: Fixed power deloading, method 1

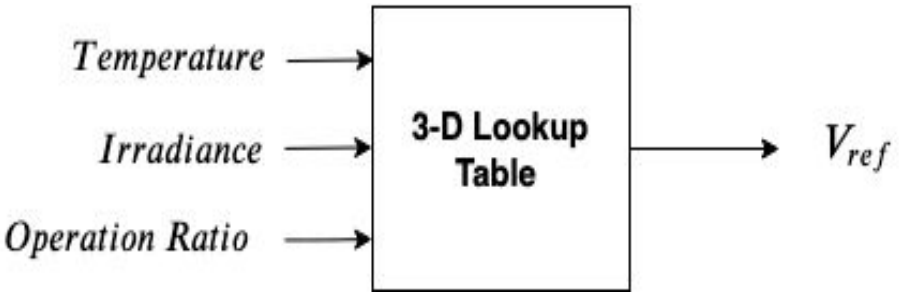

Figure 3.21: Percentage deloading, method 2

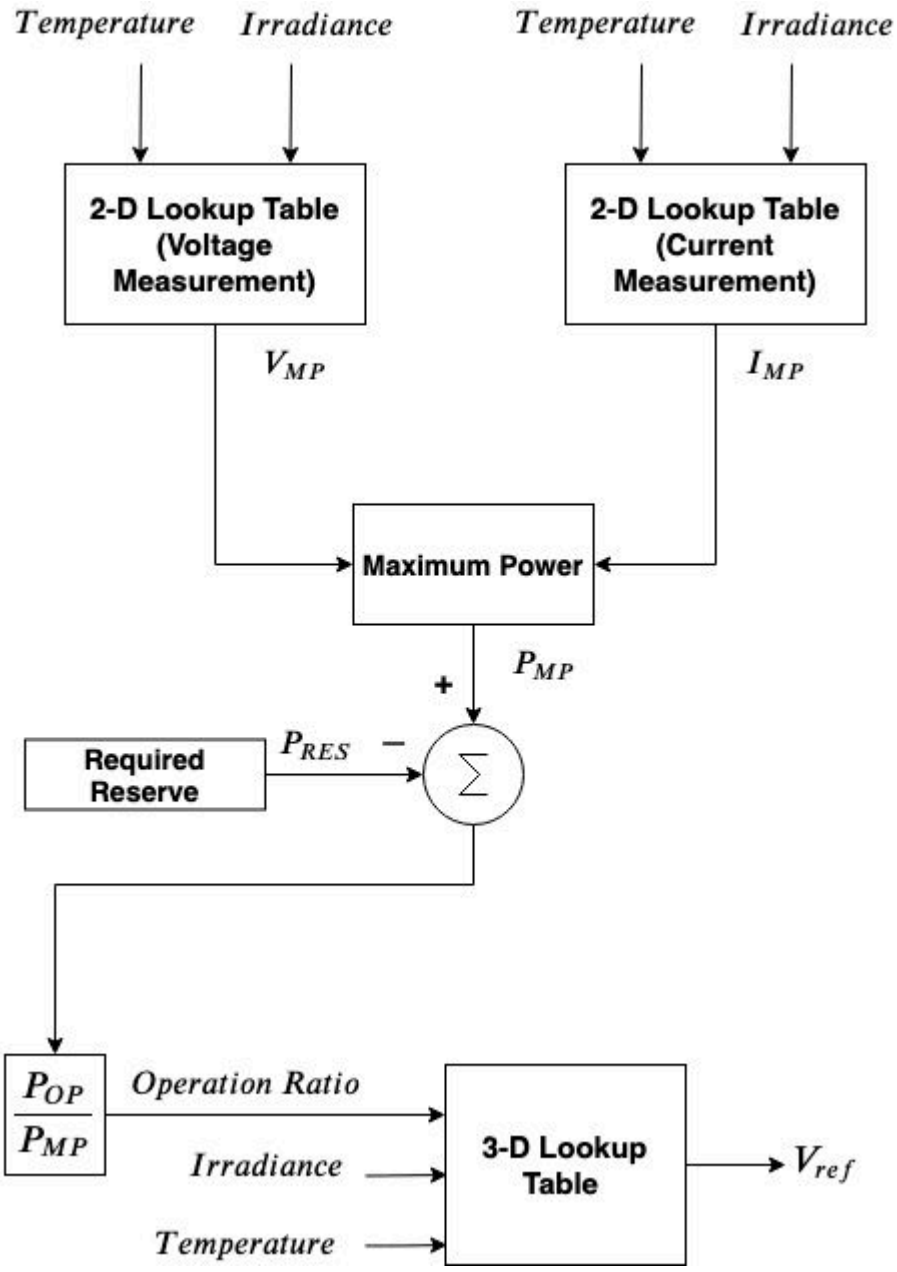

Figure 3.22: Fixed power deloading, method 2

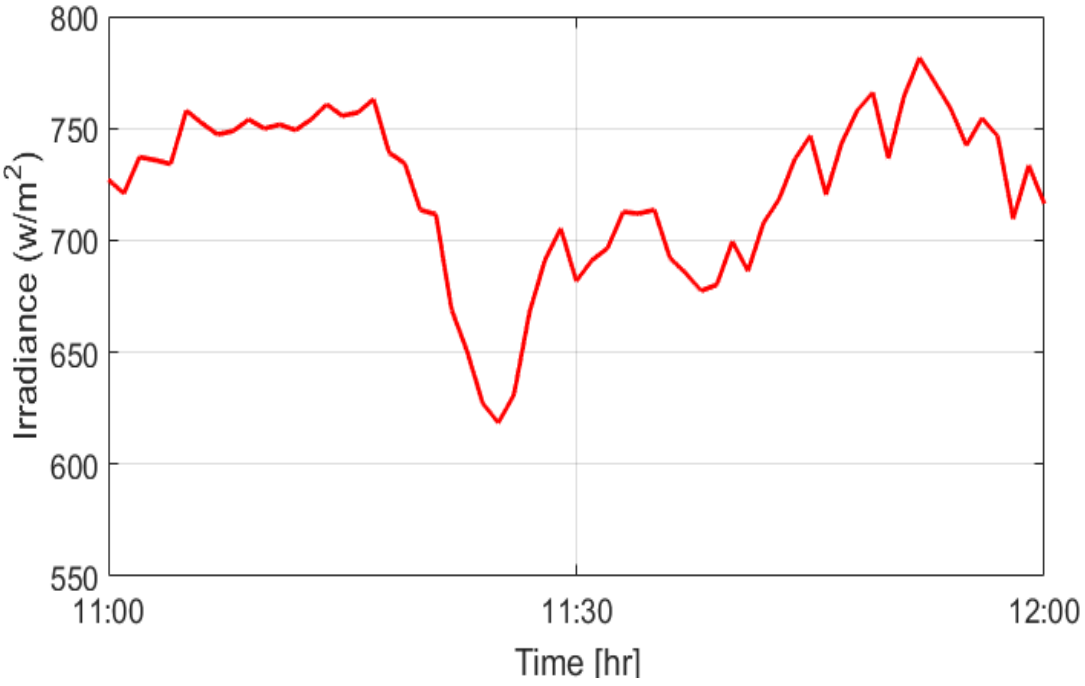

Figure 3.23: Real irradiance [108]

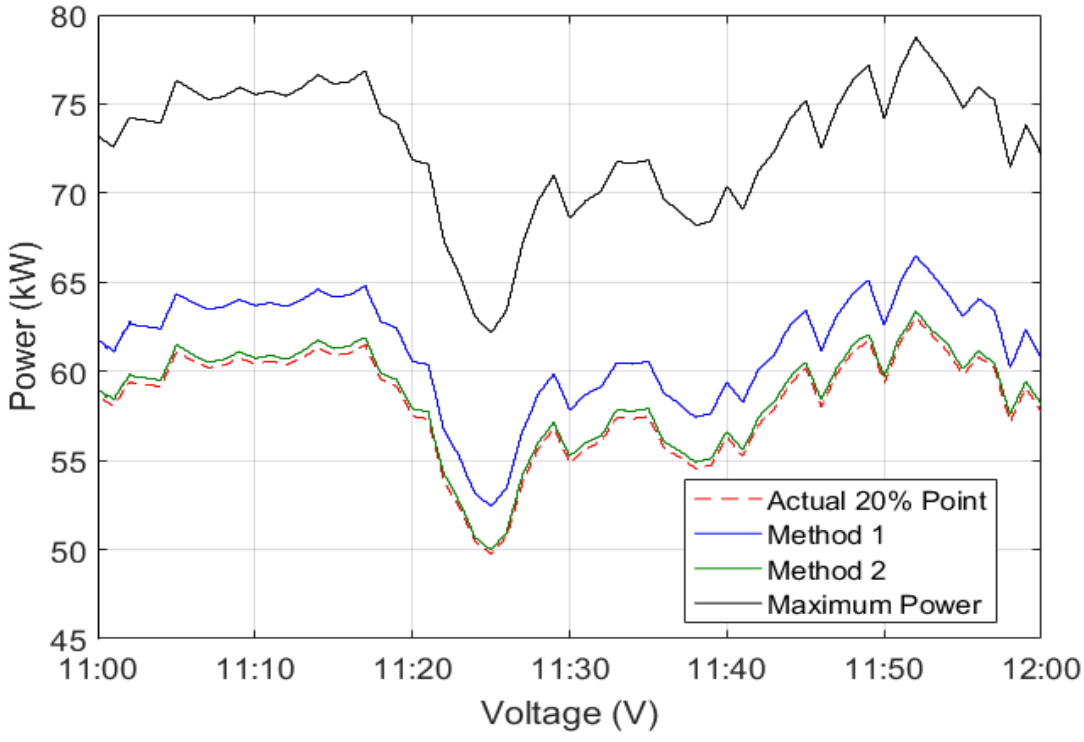

Figure 3.24: Comparison for percentage deloading

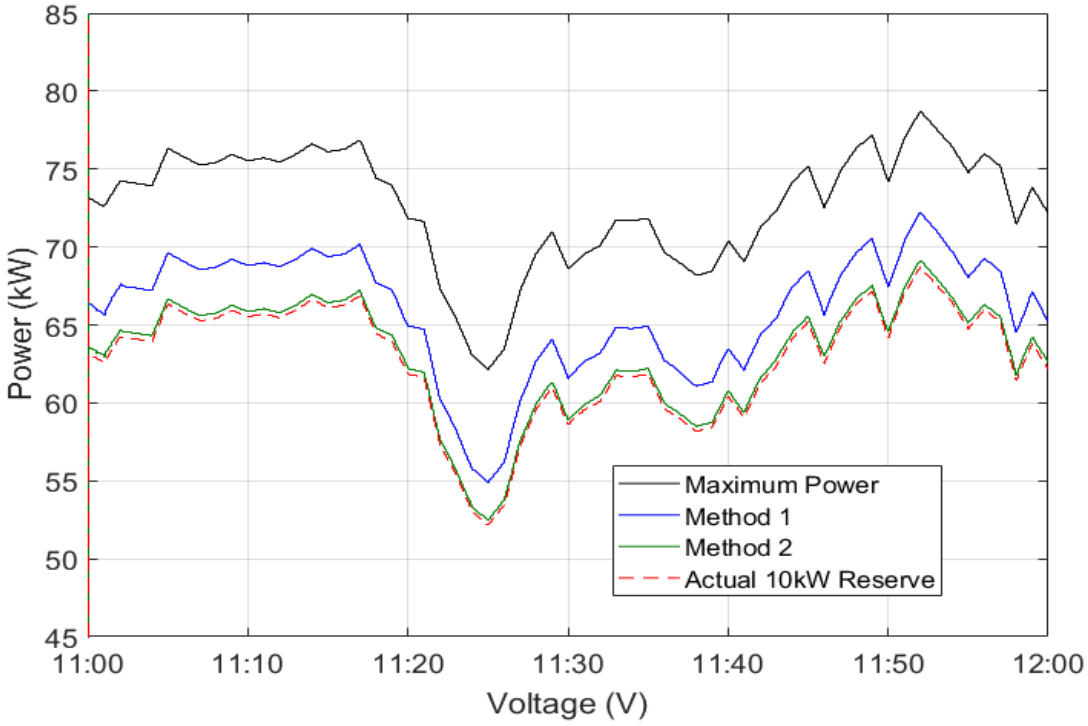

Figure 3.25: Comparison for fixed power deloading

3.6. Effect of MPPT on Reserve Maintenance

Authors in [107] explain that the ability of a PV system to maintain a given reserve is affected by the irradiance conditions and the parameters of MPPT technique. Some MPPT techniques could be challenged in fast-changing irradiance. This section investigates the effect of the MPPT technique only reserve maintenance. The deloading technique described in Method 1 of section 3.5 is used to operate the PV system at 80% of maximum power. The performance of the P&O, the constant voltage and Offline MPPT are compared.

Figure (3.26) gives the maximum power and the deloaded operation for the P&O with proposed modification, Offline MPPT, and constant voltage for irradiance increasing steadily from 200w/m^2 to 600w/m^2 in 10s. The offline MPPT resulted in the closest output to the expected output power while the P&O with additional loop gives the largest deviation. This is expected as the P&O is the only MPPT technique tested that performs an online computation. The available reserve for each of the MPPTs is given in figure (3.27). The most reserve and closed to the expected amount is from the offline MPPT, followed by the constant voltage. The reserve is available

at a particular time is also affected by the efficiency and tracking speed of the MPPT technique. It should be noted that the reference voltage used for the constant voltage MPPT is the maximum power voltage of the PV module.

Figure (3.28) gives the maximum power and reserve power for a sinusoidal irradiance. The P&O gives less output power than the other MPPTs. The difference in output power with the proposed P&O is larger when the irradiance is increasing and lesser when the irradiance is falling. The constant voltage and the offline MPPT gives very close output power. The slowness of the P&O causes it to have more reserve power when the irradiance is increasing. The reserve power available from sinusoidal irradiance with frequency of 1.5rad/s is shown in figure (3.29).

Figures (3.30) and (3.31) show the output power and available reserve for a sinusoidal irradiance of 2rad/s. Generally, the available reserve is affected by a combination of the de-loading technique, response speed and irradiance conditions. The predictability of the available reserve can be improved by improving the response speed and the accuracy of the de-loading technique. Accurate knowledge of the reserve available can be useful when PV systems are required to participate in active power control. The amount of reserve can inform on parameter selection for frequency support.

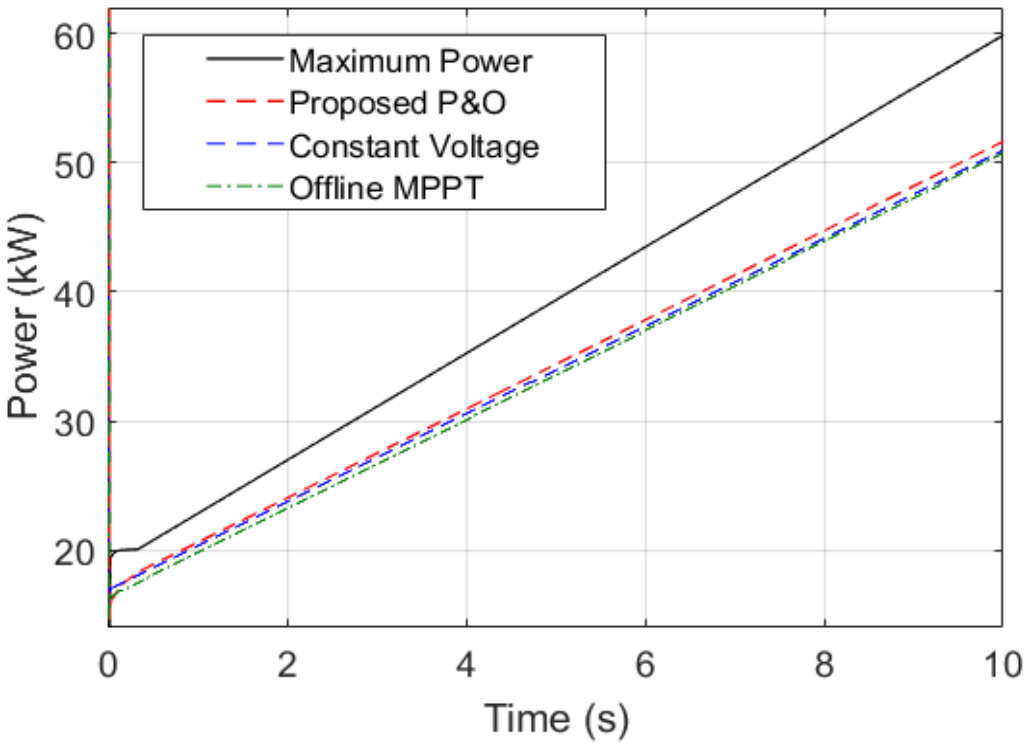

Figure 3.26: Deloading for increasing irradiance

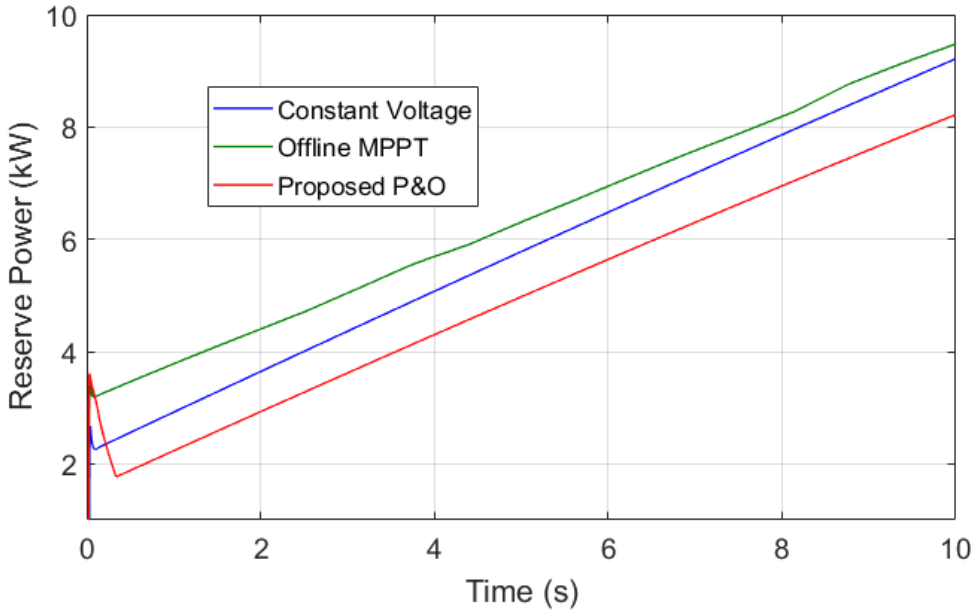

Figure 3.27: Available reserve for increasing irradiance

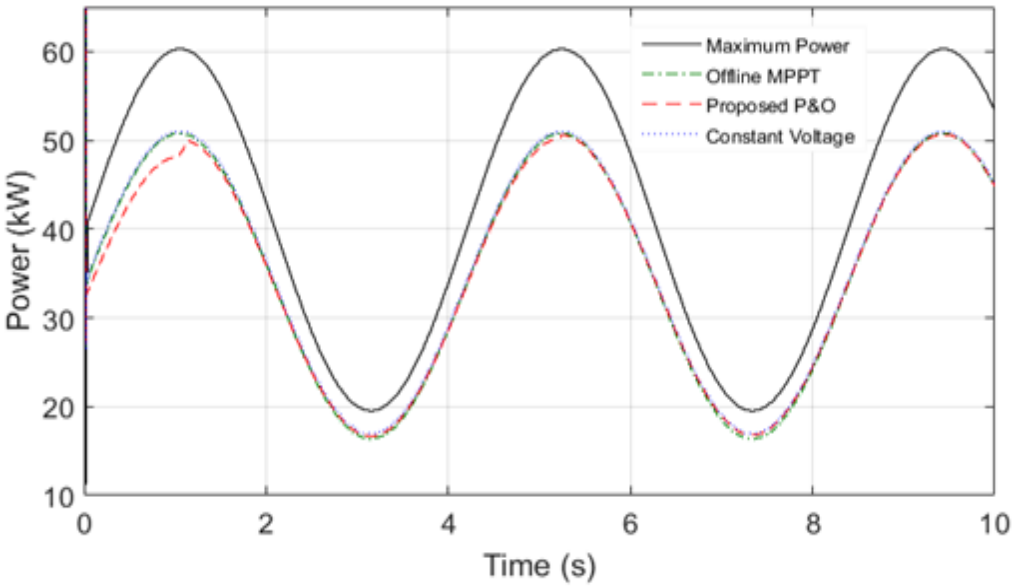

Figure 3.28: Deloading for sinusoidal irradiance (1.5rad/s)

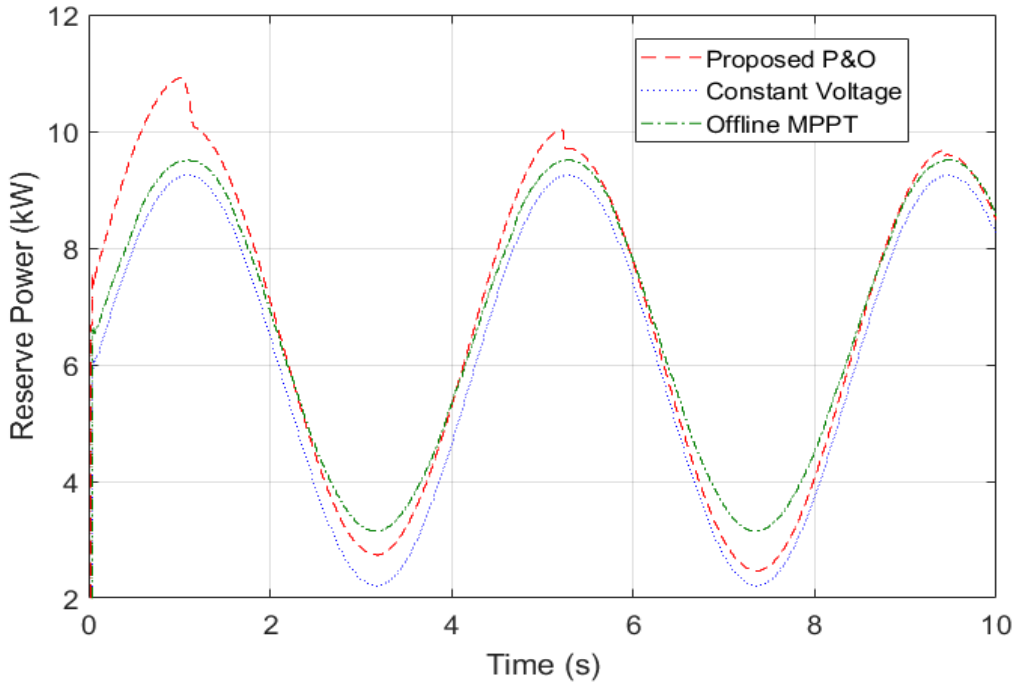

Figure 3.29: Available power for sinusoidal irradiance (1.5rad/s)

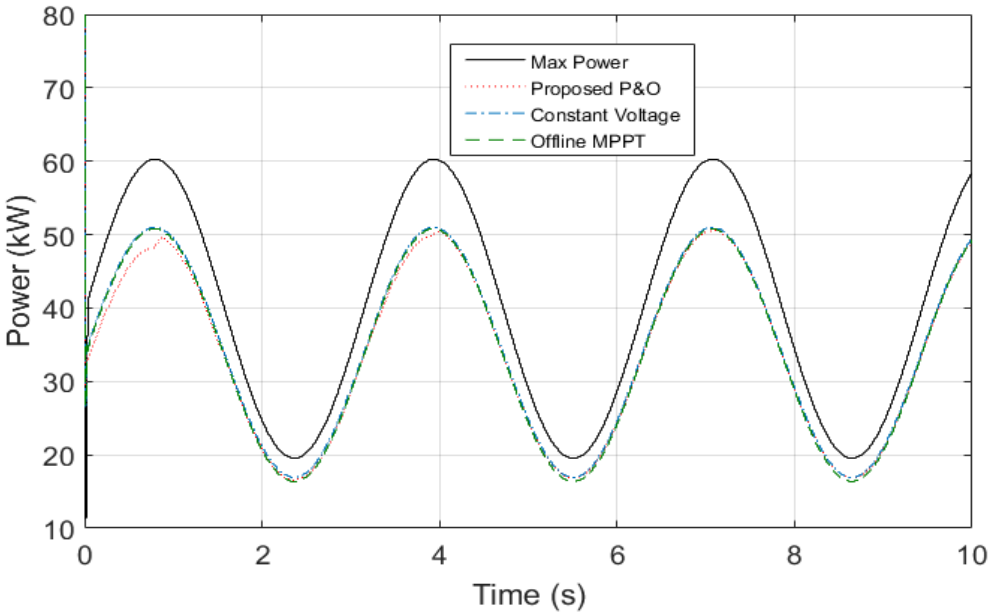

Figure 3.30: Deloading for sinusoidal irradiance (2rad/s)

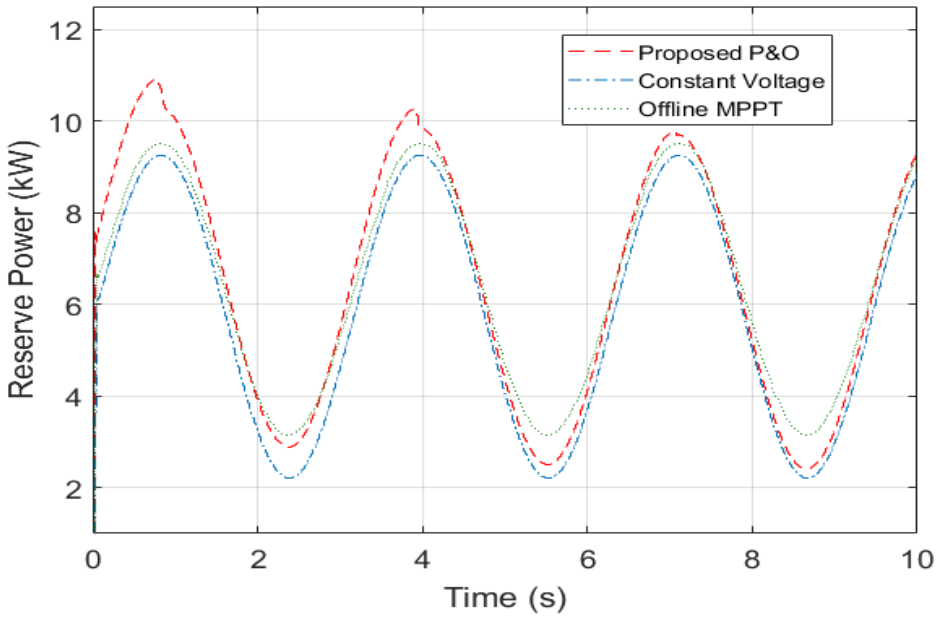

Figure 3.31: Available power for sinusoidal irradiance (2rad/s)

3.7 Summary

In this chapter, a review of various MPPT with respect to how deloaded operation can be achieved with each of them has been presented. A modification to the basic P&O algorithm has been proposed for avoidance of drift in any direction in fast increasing irradiance. This will enable PV system with the P&O to carry out APC

functions. An offline MPPT is proposed for fast response and high accuracy and is suitable for APC functions. Two methods for deloading the PV system is presented and compared for percentage deloading and fixed-power deloading. Lastly, the effect of MPPT in reserve maintenance evaluated. Three MPPT are compared in increasing and sinusoidal irradiance conditions for their ability to maintain reserve. The results showing that reserve is affected by a number of factors including the efficiency of the MPPT, the response speed and the deloading technique used.

Chapter 4 : Frequency Support from Photovoltaic Power Plant

4.1. Introduction

The commitment of various countries to reduce CO_2 emission will result in an increase in the percentage of generation from grid-connected photovoltaic systems. Due to the nature of photovoltaic generation, system inertia will decrease with increasing photovoltaic penetration. As discussed in chapter 2, reducing inertia will have an adverse effect on frequency stability. Addressing the effect of high photovoltaic generation in power system frequency is necessary for maintaining frequency stability in high renewable penetration systems.

Operation and control methods have been proposed for photovoltaic systems to contribute to frequency stability. In [58], the authors propose inertia support from a large PVPP but do not explain how a change in power from the inertia support can be achieved. Also, the authors do not explain how the reserve operation is achieved and the MPPT used. In [60], frequency support is provided by operating the PV system at a higher voltage than the maximum power voltage and adjusting the voltage based on changes in frequency. The de-loading technique used in [60] is not very accurate due to the higher degree of non-linearity between power and voltage from the maximum power point to the open-circuit voltage. Moreover, how the maximum power voltage is determined is not explained. The method in [59] requires knowledge

of the MPP parameters. However, this is not known as the MPP is searched for in real-time by most MPPTs, and there is a constant adjustment to MPPT. In [59], the authors used a value of voltage higher than maximum power voltage but also did not explain how a de-loaded value is obtained and deloading implemented. Reference [103] presents an APC method for frequency support that uses linear regression to determine maximum power.

The method by which a PV reserve operation is achieved is pertinent to its participation in frequency support. The de-loading method determines how a change in power is achieved. It also determines the accuracy of the change and the speed with which the change is implemented. This chapter explores the frequency support of a photovoltaic power plant. How frequency support can be achieved using the two de-loading techniques described in chapter 3 is explained for both percentage and fixed-power de-loading. Different support methods for PVPP to provide frequency support are tested. A variable droop support method is also proposed to reduce the reserve required for support. Case studies are carried out in different penetration scenarios and different support methods and parameters are used to evaluate the effect of penetration levels and support methods from PVPP. This chapter also evaluates the effect of MPPT technique of frequency response by comparing the resulting responses when the PV system employs the conventional perturb and observe, the P&O with modification in [102] and the offline MPPT proposed in chapter 3.

The rest of this chapter is structured as follows: Section 4.2 explains how a change in active power from support parameters is implemented for different reserve and de-loading methods. Section 4.3 explains different methods for PVPP to participate in frequency support. Section 4.4 presents case studies of responses in different penetrations and different support methods. Section 4.5 evaluates the effect of MPPT choice by comparing the response with different MPPT techniques. The conclusion is presented in Section 4.6.

4.2. Reserve and APC for Frequency Support

PVPPs need to operate with a reserve to participate in frequency support except when operated together with an energy storage system. Additional power requested by

the support methods and parameters have to be translated to change in PV output power to achieve the necessary frequency support. Translating requested support to change in power output requires some modification or coordination with the employed MPPT and de-loading technique. In this section, how to achieve a change in power with the two de-loading methods described in chapter 3 is explained.

For method 1, since a linear relationship is assumed between the voltage and the power up to MPP, any percentage change in voltage will result in the same percentage change in power. For a PV system using percentage de-loading, the steps to achieve change in power is given in figure (4.1). Because this de-loading technique assumes linearity slightly more power increase than requested will be added to the output of the PVPP. This will improve the response when there is a large negative difference between generation and load, and PVPP penetration is low but could negatively affect response when the PV penetration is high, and the generation-load imbalance is small. When the fixed-power reserve is used, the requested change in power has to be translated to a change in reserve power, or the percentage change in power can be added to the voltage like with percentage de-loading. Figure 4.2 gives the steps for APC with a system implementing fixed-power reserve using method 1.

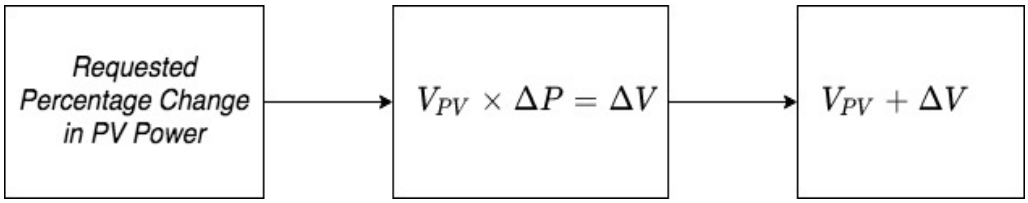

Figure 4.1: Method, APC for percentage deloading

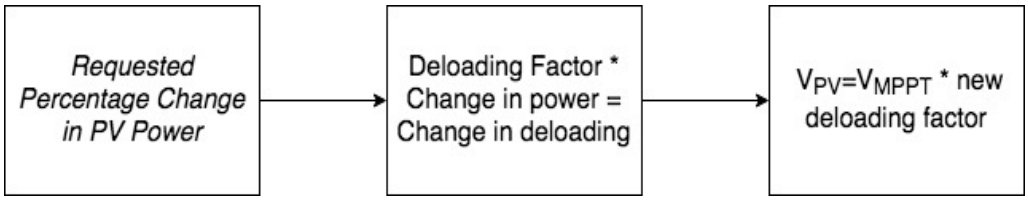

Figure 4.2: APC with fixed power deloading

A more accurate change in power can be obtained using method 2. This is because a very close approximation of the actual value is used. When a PVPP is using

method 2 for percentage de-loading, requested power is achieved by multiplying the percentage change in power by the de-loading percentage. The sum of the multiplication and the de-loading percentage becomes the percentage input to the lookup table. The steps for adding power requested by support parameters for percentage de-loading is given in Figure 4.3. When method 2 is used to achieve a fixed power reserve, power adjustment is achieved by converting the sum of the requested power and the PV power into a new percentage of MPPT which then becomes the input for the lookup table.

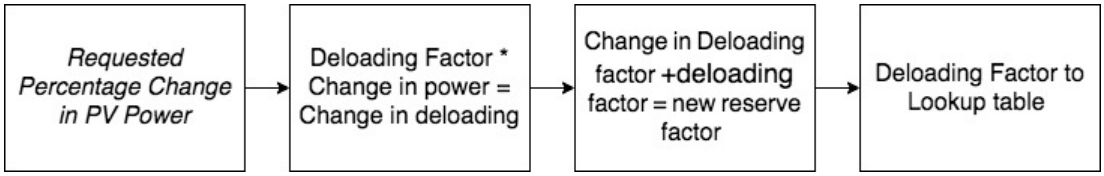

Figure 4.3: Method 2, APC for percentage reserve

4.3. Frequency Support Methods

4.3.1 Non-Dynamic Fast Frequency Response

In this support method, the output of the PVPP is increased by a fixed, predetermined amount when the frequency drops below a defined threshold. As a result of the speed of APC of PVPP, it is expected that a step increase in output power of the PVPP should affect the nadir and ROCOF. The support method can be implemented by using a switch to change reference voltages depending on change in frequency. Figure 4.4 gives the implementation of non-dynamic fast frequency response.

This frequency support method has some drawbacks. The support method gives a step increase in power without considering the change in frequency. This can result in varying and unpredictable degrees of support, depending on the severity of the generation-load imbalance. Although a significant reduction in the nadir can be achieved using this method since all support power is delivered once, it is not an efficient use of reserve power. Since the increase in power is permanent as it does not change after it has occurred, this results in a reduction in reserve and thus reducing the ability of the PVPP to support subsequent frequency response to generation-load imbalance.

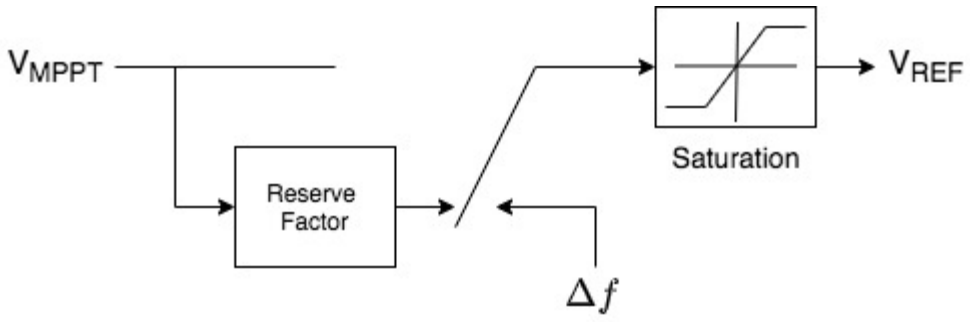

Figure 4.4: Fast Frequency Response

4.3.2 Droop Support

PV systems can also implement droop support which is the method by which synchronous generators provide primary frequency support. Because of the speed of response from PV systems, it is expected that droop support from PV system will have more effect in reducing the nadir than droop support from synchronous generators.

This support is implemented by adjusting the voltage by on the product of a droop gain (D_G) and the change in frequency. The implementation of this support method is given in Figure 4.5. The main advantage of the droop support over the non-dynamic FFR is that it is proportional to change in frequency. The reference voltage is limited to the maximum power voltage. The maximum power voltage is the operating voltage for the PV system that will result in maximum output power. The maximum power voltage changes with irradiance and temperature. The PV system will experience a drop in power if operating voltage exceeds maximum power voltage.

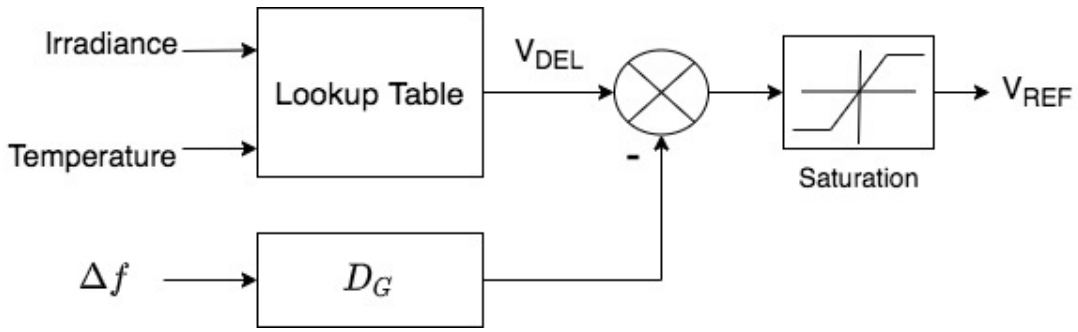

Figure 4.5: Droop Support

4.3.3 Inertia Support

Although solar PV systems do not have any stored kinetic energy, the reserve created by deloading can be released in a manner similar to the release of kinetic energy from rotating masses of synchronous generators. This method is expected to be effective in reducing the overall ROCOF due to the fast response of the PV system. The power added by inertia response of synchronous generators is given by [34]:

$$\Delta P = 2H \times \frac{d(\Delta f)}{dt} \tag{4.1}$$

The value of *2H* in equation (4.1) will be replaced with the inertia gain *K*. The measurement of the ROCOF usually results in a noisy signal, and a low-pass filter is needed to filter the noise [43]. The change in power is also implemented by directly adjusting the voltage by the same value as the change in power. The inertia support and droop support can be combined to give a similar response as synchronous generators. The control loops for combined inertia and droop support is given in figure (4.6).

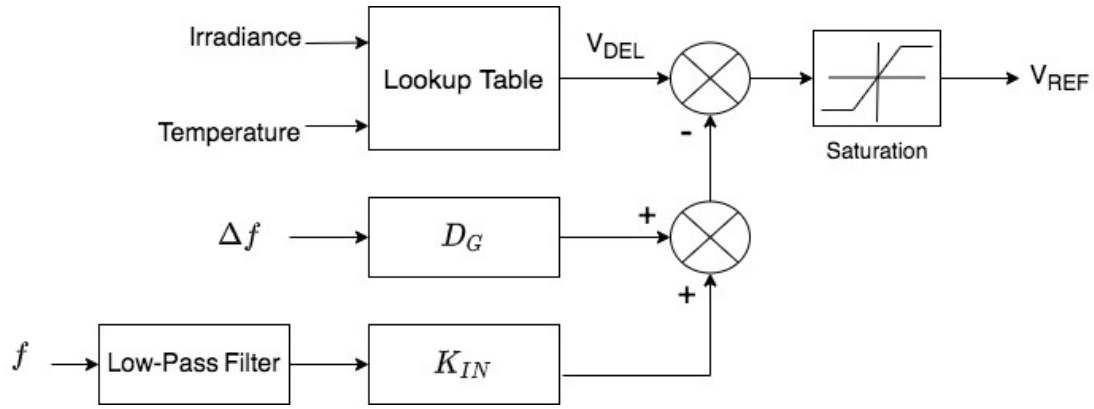

Figure 4.6: Combined Droop and Inertia Support

4.3.4 Variable Droop Support

Because the fast frequency response increases the output of the PV system by a step when the frequency drops below a defined threshold, it will arrest falling frequency with the most power at an early stage of the frequency evolution. The non-dynamic FFR has two drawbacks as a result. First, because the FFR is non-dynamic, the output power of the PV system does not return to its pre-event value after system frequency has been stabilized. This will effectively reduce the reserve and increase the share of PV in the power system. A smaller reserve will also reduce the ability of the PV system to respond to future frequency events. Second, is that it can overcompensate for the power imbalance if the step value if not properly chosen.

The droop support, although proportional to the change in frequency, does not fully exploit the fast response of the PV system. The output power from droop control is highest close to the time the frequency evolution is at the nadir. The fast response of the PV system can be exploited to deliver more support at the moment immediately after the frequency event. This can be used to obtain a more effective response.

The aim of the variable droop control is to take advantage of the large initial step in power from the FFR and the proportionality of the droop control to for a more effective response. Two variable droop control methods are proposed.

Variable Drop Method 1:

In the first variable droop method, the output power of the PVPP is increased by a step immediately after a generation-load imbalance the same way with the FFR. The step increase in power is then maintained for some time (step support time), which should cover the inertia time frame. After the selected time has passed, the droop gain then returns to an original set value. Because of the initial step increase in power, the ROCOF will be improved. At steady state, the output of the PVPP would have been reduced from the initial step value.

The value of the step increase in power following the frequency event has to be converted to a droop gain. This is determined by dividing the required change in power by the change in frequency. For example, if the required increase in PV power

is 0.05pu, and the imbalance occurs at 1s. The power increase from the PV system is defined by the following equation:

$$P_{inc} = 0.05pu \quad 1 \leq t \leq 4 \tag{4.2}$$

$$P_{inc} = \Delta P_{set\ droop} \quad 4 < t < t_{sup} \tag{4.3}$$

Equation 4.2 indicates that the step increase in power is maintained for 3s, while t_{sup} is the support time. The droop gains for both time frames (i.e. FFR and droop) is given by the following equations:

$$D_g = \frac{0.05}{\Delta f} \quad 1 \leq t \leq 4 \tag{4.4}$$

$$D_g = D_{set} \quad t < t < t_{sup} \tag{4.5}$$

Variable Droop Method 2:

In the second variable droop control method, the droop gain used to maintain a step increase in power for the first few seconds after the frequency event is gradually returned through straight line relation of a predetermined negative slope (K). This is the main difference between the two methods as the gain is instantly dropped to set value after step support. The gradual reduction of the droop after step support will prevent a secondary frequency droop. The droop has to be reduced by a predefined function. The droop after the step support time frame is given as:

$$D_g = D_{t=4} + (t-4) \times K \quad 4 < t < t_{sup} \tag{4.6}$$

K is the rate at which the droop is reduced. A lower droop limit should be set at the required final droop gain. Like in method 1, the PVPP reserve is also regained using this method. The main difference is that the value of *K* determines how fast the reserve is regained.

4.4. Case Studies – Effect of penetration and support methods

4.4.1 Test System

In order to test the frequency support methods, the output of a PVPP is connected to a Load frequency control (LFC) system. The solar module used is the TSM310PD14, and the parameters are in Table 4.1. The PV system is made up of 66 parallel strings with each string containing five series-connected modules. The system produces 100kW at STC. The PV uses the offline MPPT proposed in chapters 3. The entire synchronous generation is lumped into a single machine [38] and is represented by a steam turbine with time constant of 0.5s and governor with time constant of 0.2s model with an equivalent inertia and system droop. The equivalent inertia is given by equation (2.8). Schematic of the test system used is given in Figure 4.7.

Frequency support from PVPP is implemented by adding the change in PVPP output in response to frequency deviation to the power balance of the LFC system. The change in frequency from the LFC system and implemented support method determine the change in power from the PVPP. The requested change in power is then transformed into a change in the operating voltage of the PVPP. The change in voltage is then summed to the reference voltage of the MPPT.

The effect of varying penetration is simulated by adjusting the total inertia constant based on equation (2.8). The change in PV power is also multiplied by a penetration factor before addition to the LFC system. For example, a system with synchronous generators with inertia constant of 5s with no PV penetration will have inertia constant of 4s with 20% PV penetration. The change in PVPP output power will be multiplied by 0.2 for a 20% penetration before addition to the LFC system. The change in synchronous generator power is also reduced by a penetration factor to account for PV penetration.

Table 4.1: Module Data for TSM310PD14

Parameter	STC	NOCT
Open-Circuit Voltage	45.5V	42.2V
Short-Circuit Current	8.85A	7.15A
Maximum Power Voltage	8.38A	6.72A
Maximum Power Current	37.0V	34.4V

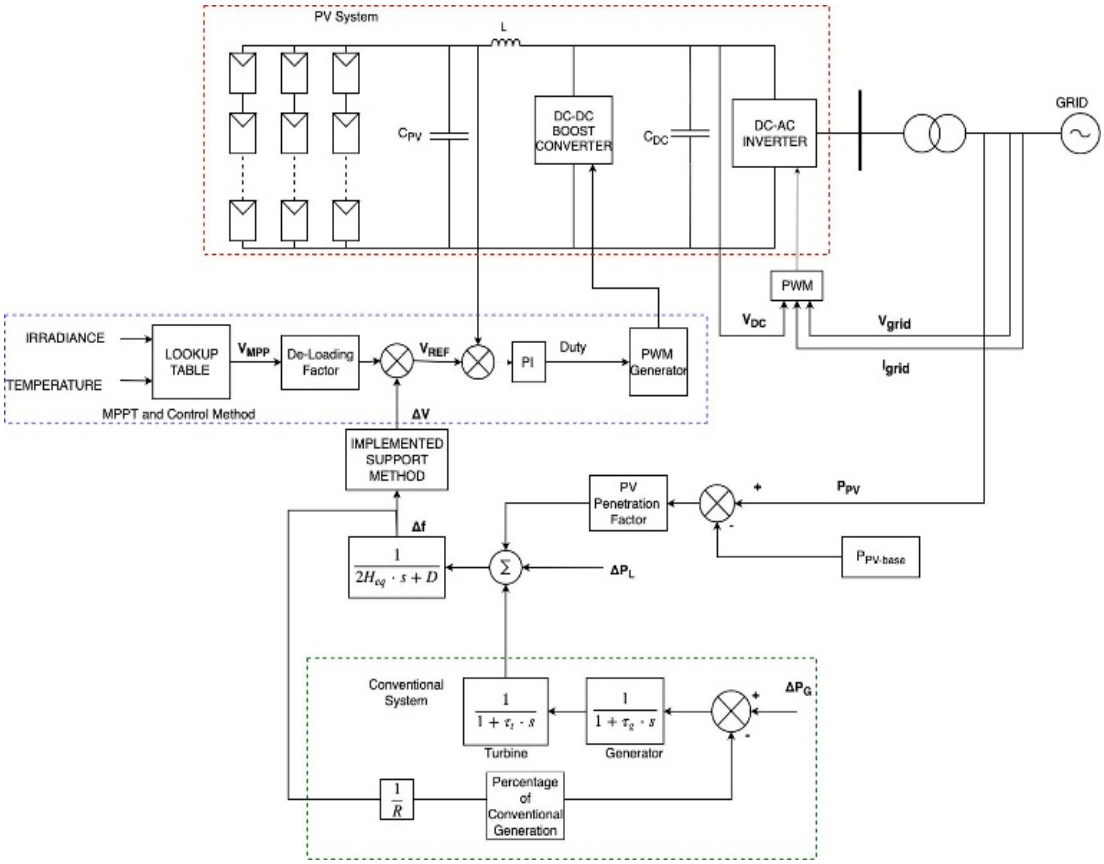

Figure 4.7: LFC system with PVPP

4.4.2 Increasing PV Penetration

The frequency methods described in section 4.3 are implemented for a system at different levels of penetration to evaluate their effectiveness in frequency response and the effect in systems with reducing inertia. Figures 4.8, 4.9 and 4.10 gives the responses for a 0.1pu load increase when inertia, droop and combined inertia and droop support are implemented respectively. Figures 4.8, 4.9 and 4.10 each gives the responses in 10%, 20% and 30% PVPP penetration with the PVPP operating with a 20% reserve. Penetration scenarios are achieved by multiplying the output from the PV and synchronous generators by a penetration factor. Both the droop support and the combined inertia and droop support resulted in a smaller nadir slower overall ROCOF with increasing penetration. This indicates that the support from the droop (droop gain =20) and the combined inertia and droop (droop =20, K=10) adequately replaces the lost inertia due to increasing penetration. The combined droop and inertia support resulted in the smallest nadir and slowest ROCOF when compared to the droop and inertia only support. This is due to the fact that the combined inertia and droop will release more power at the onset of the frequency event than the droop and inertia support. Additional responses for combined droop and inertia support are given in Appendix A.

The inertia only, however, resulted in a larger nadir and faster ROCOF with increasing PVPP penetration. This is due to the fact the inertia only cannot replace both the inertia and droop support from the synchronous generation. The inertia only support also resulted in a larger steady-state frequency deviation than the droop and combined droop and inertia with increasing penetration.

Figure 4.11 presents responses from the non-dynamic fast frequency response. All the reserve from the PVPP was released following a generation load imbalance. The responses Figure 4.11 show the smallest nadir and slowest ROCOF when compared to the responses in Figures 4.8, 4.9 and 4.10. However, an over frequency event can occur if the increase in power is very high. Practically, this is unlikely if only a small percentage of source provides this support and only increase their output power by a small percentage.

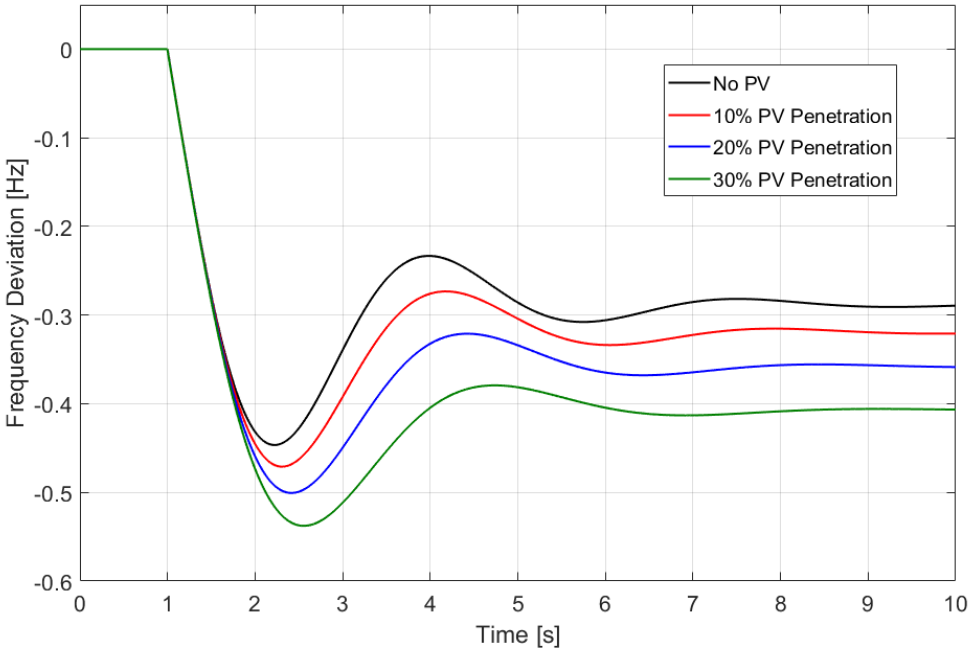

Figure 4.8: Inertia Support (K_{in}=10)

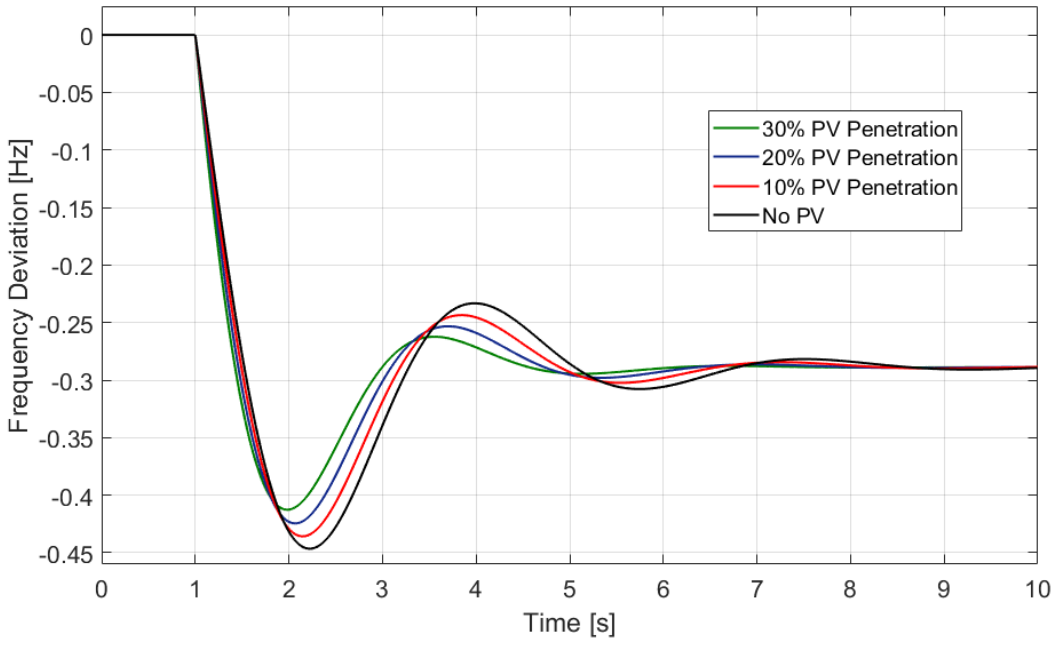

Figure 4.9: Droop Support (D_g=20)

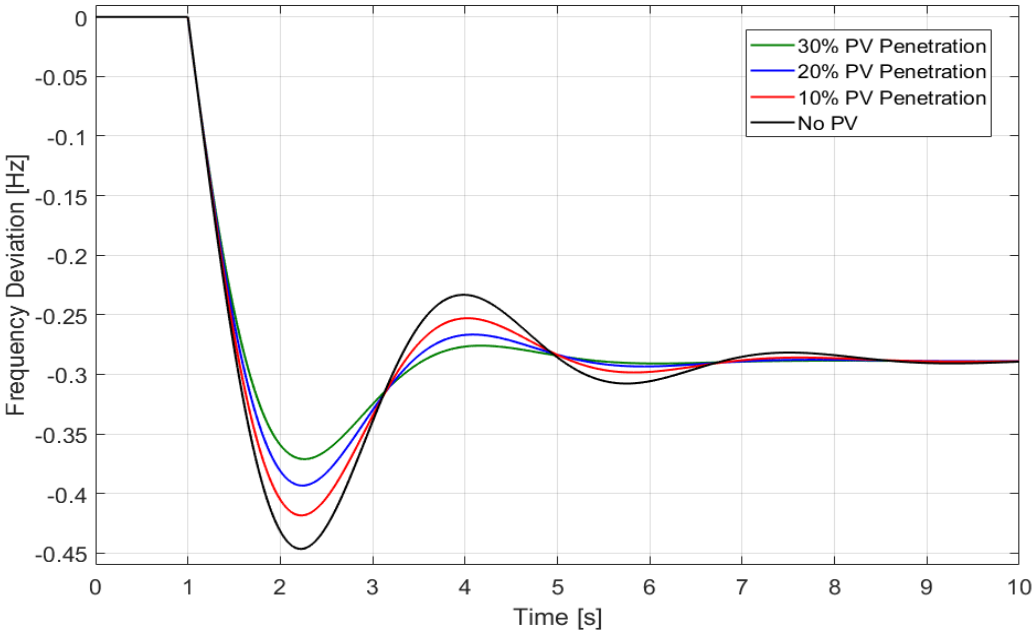

Figure 4.10: Combined inertia (K_{in}=10) and Droop (D_g=20)

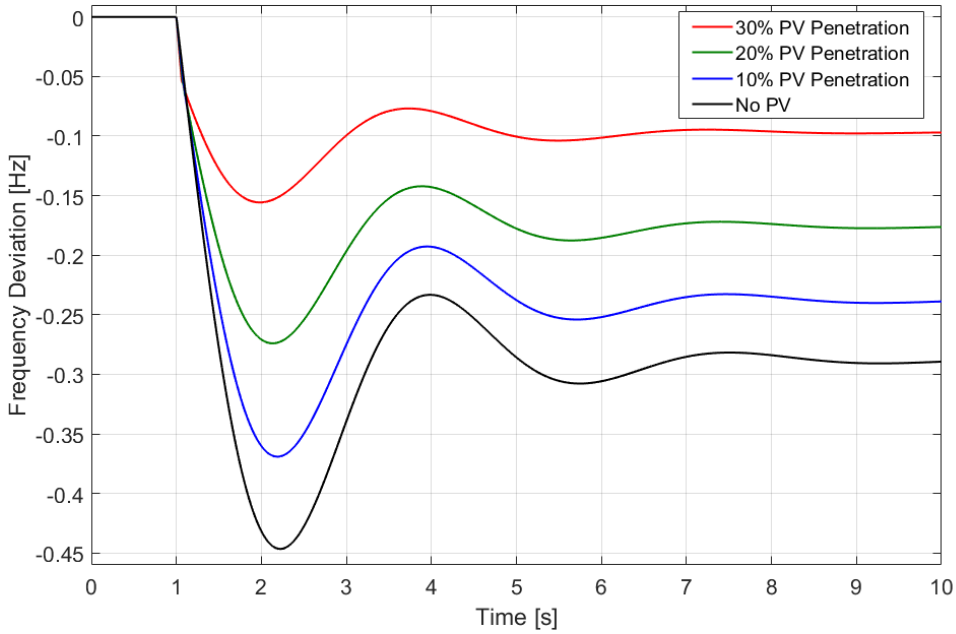

Figure 4.11: Fast Frequency Support

4.4.3 Synchronous Generator Support VS PVPP

In order to compare PVPP support to synchronous power plant support, responses to a 0.1pu increase in load are evaluated. Figure 4.12 give the responses to a system with 20% PV penetration with combined droop and inertia support, the system with no PV penetration and system with only droop support. The droop gain for the generator and the PVPP was both 20, and the inertia gain for the PVPP is 10. The response of the LFC system with no PV penetration resulted in a larger nadir and slower ROCOF than with 20% PV penetration with droop only and combined droop and inertia. This indicates that for a system with 20% PVPP penetration, with droop and combined droop and inertia support, there is no detrimental effect on the frequency response.

Figure 4.13 show the change in the PVPP power (with droop support) and change in the generator power for the responses in Figure 4.12. The per-unit increase in PV power is higher than the per unit increase in the generator power. This is an indication of the faster response of the PVPP since they both have the same droop gain.

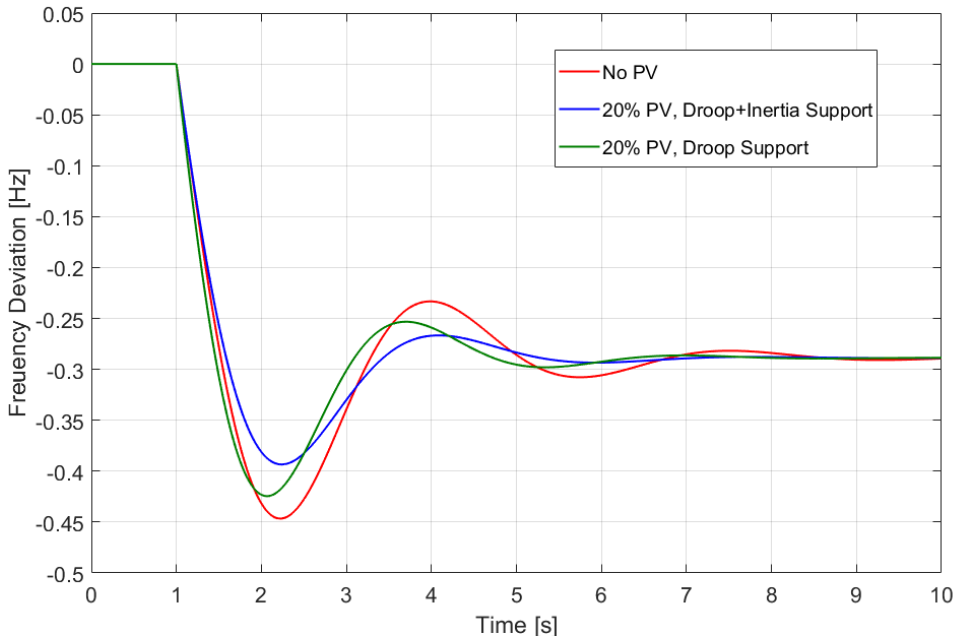

Figure 4.12: Synchronous generator vs PVPP

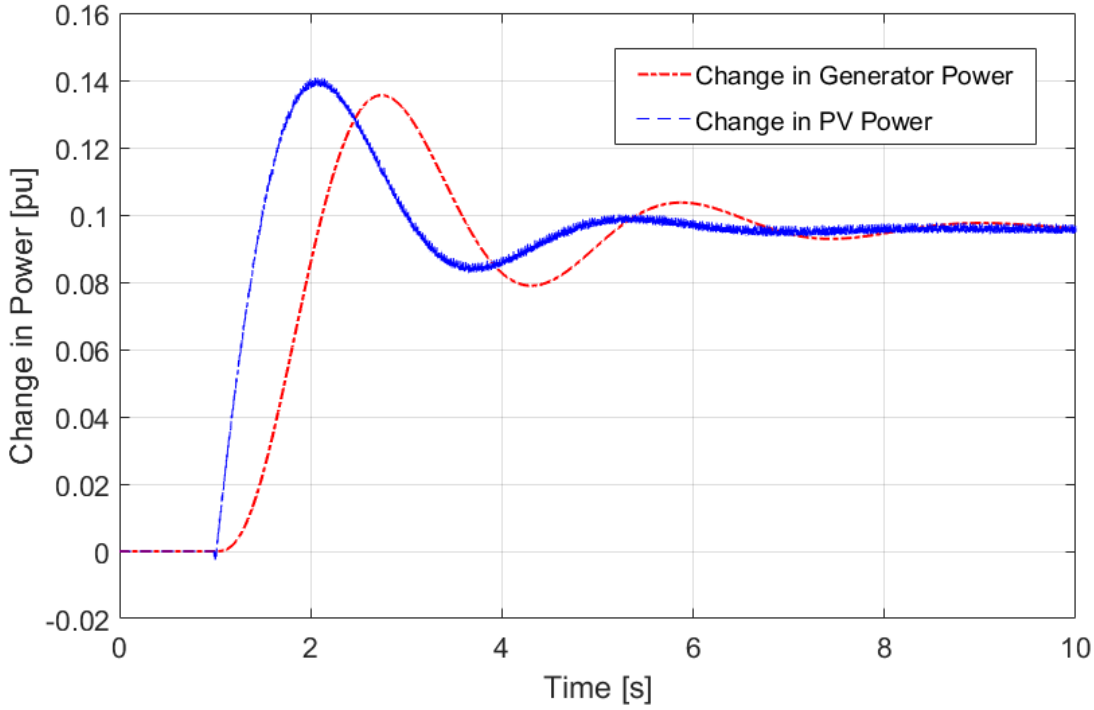

Figure 4.13: Change in power (PVPP vs Synchronous)

4.4.4 Variable Droop Support

The variable droop support methods described in Section 4.3.4 are implemented on LFC system with 30% PVPP penetration and 20% reserve. Figure 4.14 shows the response when method 1 variable droop is used. In Figure 4.14, the power is increased such that all the reserve is used in response to a 0.1pu load increase. The step increase in power is maintained for 3s, and then the droop gain returns to 20. The sudden drop in droop gain results in the second dip. The nadir of the second dip is lower than the first dip but still smaller than the nadir for droop support (droop gain = 20) and very close to the nadir for combined droop and inertia support with 30% PVPP penetration (See Figures 4.9 and 4.10). Figure 4.14 however has the same steady-state deviation as droop only and combined droop and inertia with 30% PVPP penetration. The change in PV power when method 1 variable droop is used is given in figure 4.15.

Figure 4.14 also shows the response when method 2 of the variable droop control is implemented. The first nadir in both variable droop methods are the same value but the second drop from method 2 has a significantly slower ROCOF and a

nadir value much closer to the first nadir. The second nadir from method two is smaller than the nadir in the droop and combined droop and inertia responses with 30% PVPP penetration. The gradual reduction of the droop gain to set value resulted in steady-state deviation as the conventional droop. The response speed of other synchronous generators in the power system could affect the severity of the second drop. The second droop will be larger for a slower response from other generators in the system because there will be less power from their droop support. The change in power from the PVPP for the method 2 is given in Figure 4.17.

The variable droop method has effectively combined the advantages of both the faster frequency support and the droop control to deliver response with the smaller nadir and still maintain some reserve. This method could be useful in optimising the use of a reserve to deliver the most effective response which available reserve and still maintain the ability to respond to subsequent frequency events.

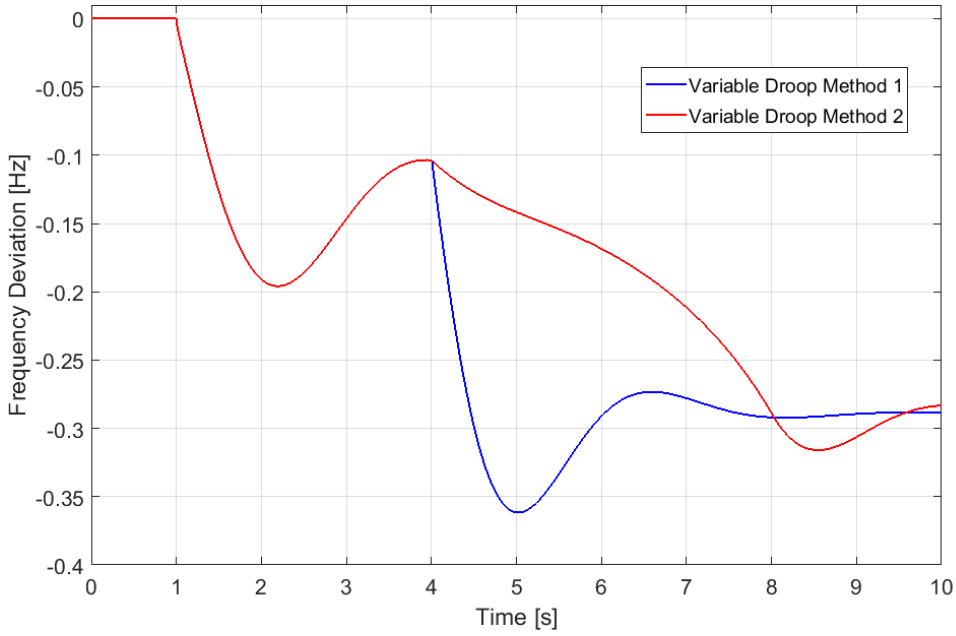

Figure 4.14: Variable Droop Response

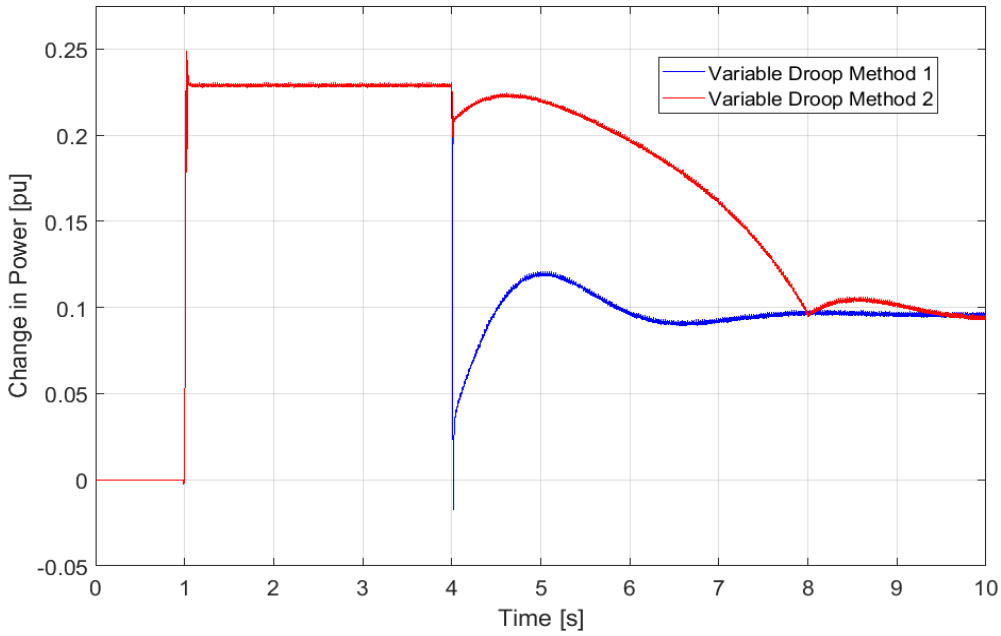

Figure 4.15: Change in PVPP for variable droop

4.4.5 Effect of Available Reserve

PVPPs need to maintain a reserve to provide an under-frequency response. The amount of reserve available can affect the ability of the PVPP to execute implemented support method. Also, the performance of various support methods in utilizing available reserve can make an important factor for consideration in designing frequency support scheme for PV systems. Figure 4.16 gives the maximum power increase to a response to a 0.1pu increase in load with the combined inertia and droop (D_g=20, K_{in}=10), implemented for 10%, 20% and 30% PV penetration. The maximum increase in power is 16.25% for 10% penetration, 15.27% for 20% penetration and 14.36% for 30% penetration. The maximum power increase for the various penetration levels translates to a reserve of at least 13.98%, 13.25% and 12.5% of maximum PV power for 10%, 20% and 30% penetration levels. Because the PVPP had a 20% reserve for the response in Figure 4.16, the implemented support method was fully executed.

Figure 4.17 gives the responses when the reserve is limited to 10% of maximum power, which is less than all the reserve needed for the penetration levels considered. The nadir for all three penetration levels increased. The worst affected is

the response in the 30% PVPP penetration case followed by the 20% PVPP penetration case. This is likely because of higher penetration. Figure 4.18 shows the change in PVPP power for the response in Figure 4.17. The flat peak is an indication that for some time, the power required was greater than the maximum available power from the PVPP. The responses in Figure 4.17 however, still have a smaller nadir and slower ROCOF than the response from the system with no PVPP penetration.

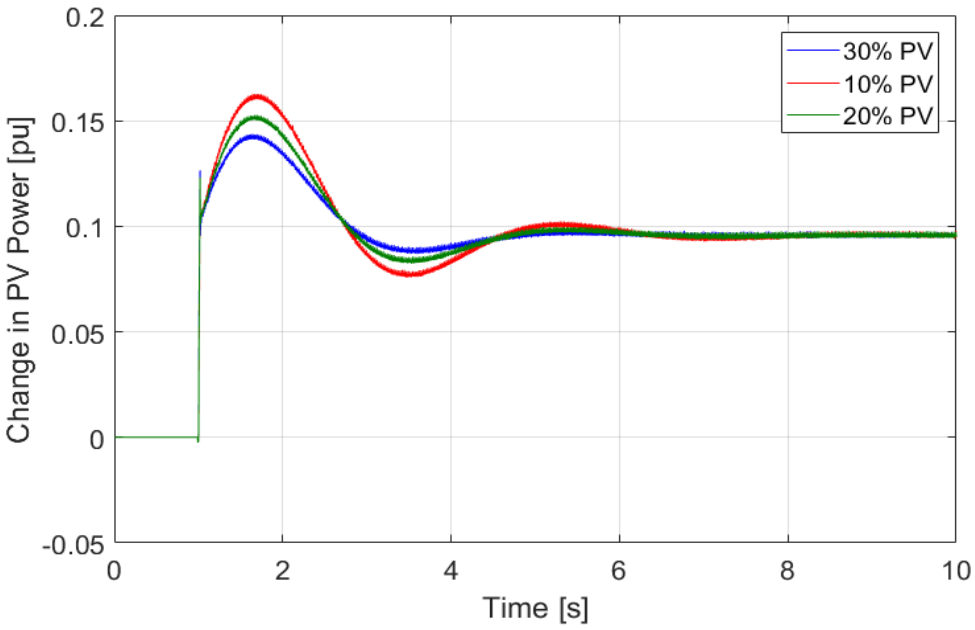

Figure 4.16: Change in PVPP power for combined droop and inertia with 20% reserve

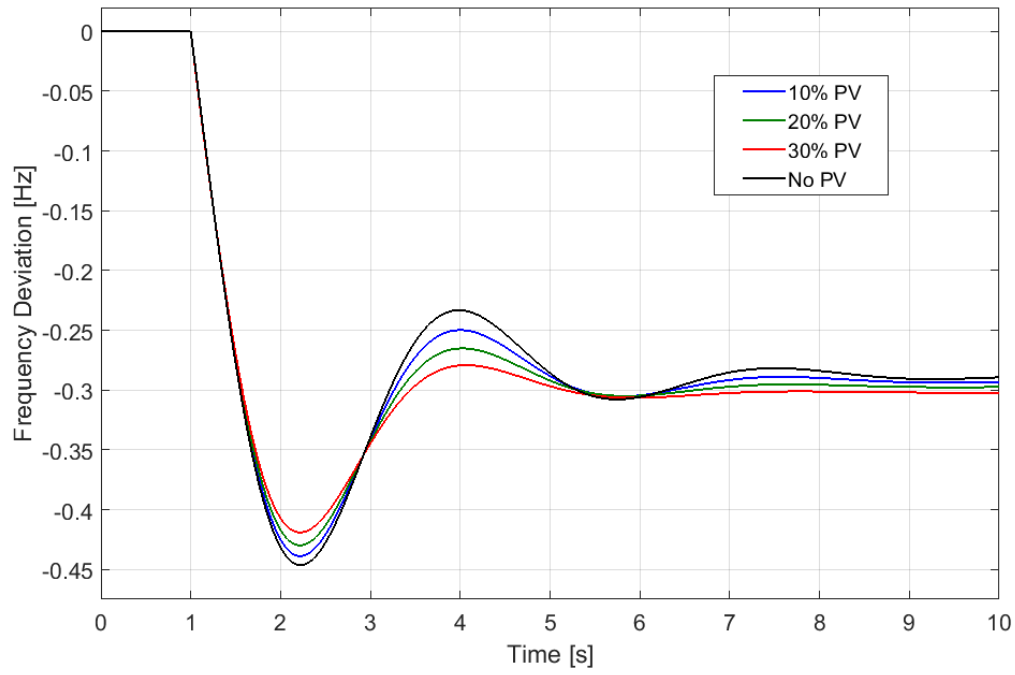

Figure 4.17: Combined droop and inertia with 10% reserve

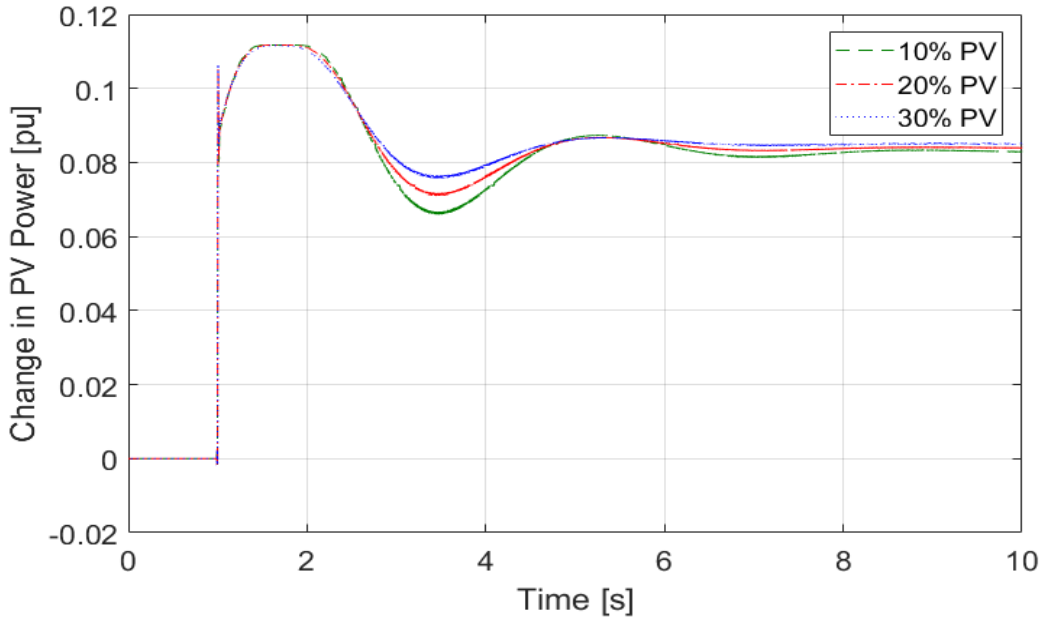

Figure 4.18: Change in PV power for responses in Figure 4.17

4.5. Effect of MPPT choice on Frequency Support

As discussed in chapter 3, the various MPPT techniques have different responses speeds, accuracy and deloading methods. These difference could have implications on the performance of a PV system participating in frequency support. This is because the quality of response is affected by speed. Also, some MPPT techniques oscillate around MPPT or can significantly increase step size to find MPP during operation. Increasing the step size during a frequency response could negatively affect response if the power swing is large enough. The offline MPPT proposed in chapter 3 is designed particularly to have a fast response speed and high accuracy to be suitable for frequency support from PVPP. The proposed modification to the P&O for drift avoidance is developed to enable comparison to the offline MPPT performance in frequency response. In this section, the response of the P&O with proposed modification, the constant voltage MPPT and the offline MPPT to a frequency deviation will be compared and evaluated. The responses are obtained in constant irradiance, rapidly increasing irradiance and sinusoidal irradiance. In all responses in the section, the PVPP is implemented with droop support with a droop gain of 20.

Figure 4.19 gives the response to a constant irradiance. The differences in the nadir are small. The proposed P&O has the smallest nadir while the offline MPPT has the largest nadir. The constant voltage is operated at maximum power voltage at STC. Because the irradiance is fixed, the difference in tracking speed does not affect the response hence the speed advantage of the offline MPPT is not reflected in the responses. The responses at constant irradiance are only determined by the accuracy of the MPPT.

In the responses in Figure 4.20, the PVPP is subjected to rapidly increasing irradiance. The irradiance used increases from 200w/m^2 to 600w/m^2 in 10 seconds. In this case, the offline MPPT resulted in the smallest nadir followed by the constant voltage and then the P&O. This is expected as the offline MPPT, and the constant voltage performs no online calculation while the P&O is constantly searching for maximum power. The increase in power which triggers the event occurs at 1s. It is likely that if the event is triggered at a later time, the performance of the P&O will be

worse as its slower response speed would have resulted in more significant power different from other MPPTs.

In Figures 4.21 and 4.22, the PVPP is subjected to sinusoidal irradiance of 1.5rad/s and 2rad/s respectively. In Figure 4.21, the proposed P&O gives the smallest nadir followed by the offline MPPT. In Figure 4.22, the offline MPPT gives the smallest nadir, followed by the proposed P&O.

The offline MPPT performs best in increasing irradiance conditions because it combines high tracking speed and accuracy. In rapidly increasing and decreasing irradiance, the offline MPPT give very similar result while more variation in nadir size occurs with the P&O and constant voltage. This indicates that their performance is to a larger extend affected by environmental conditions than the offline MPPT.

The difference in the nadir for the different MPPTs in Figures 4.19, 4.20. 4.21 and 4.22 are negligible and vary depending on the MPPT design and irradiance conditions.

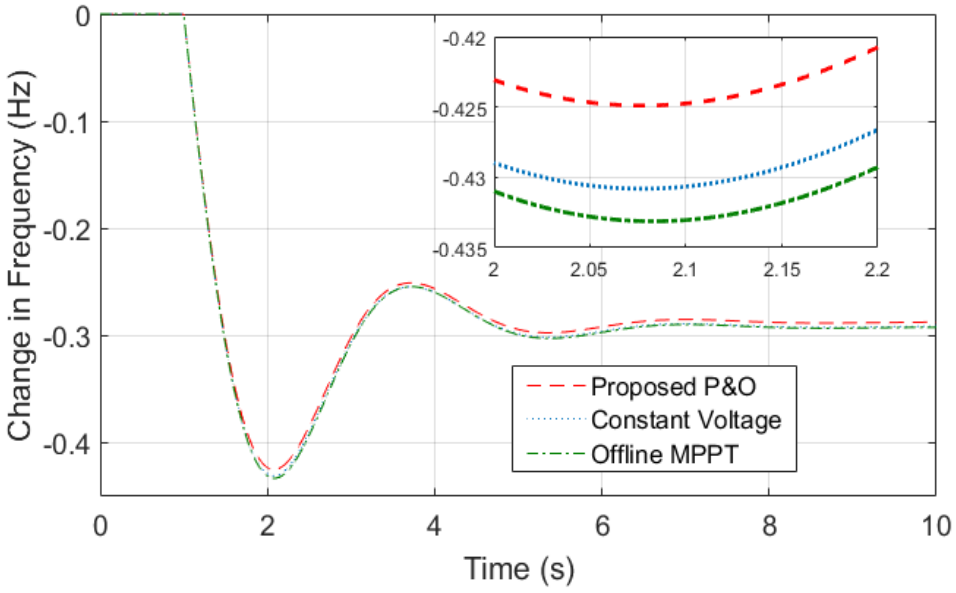

Figure 4.19: Response for constant irradiance

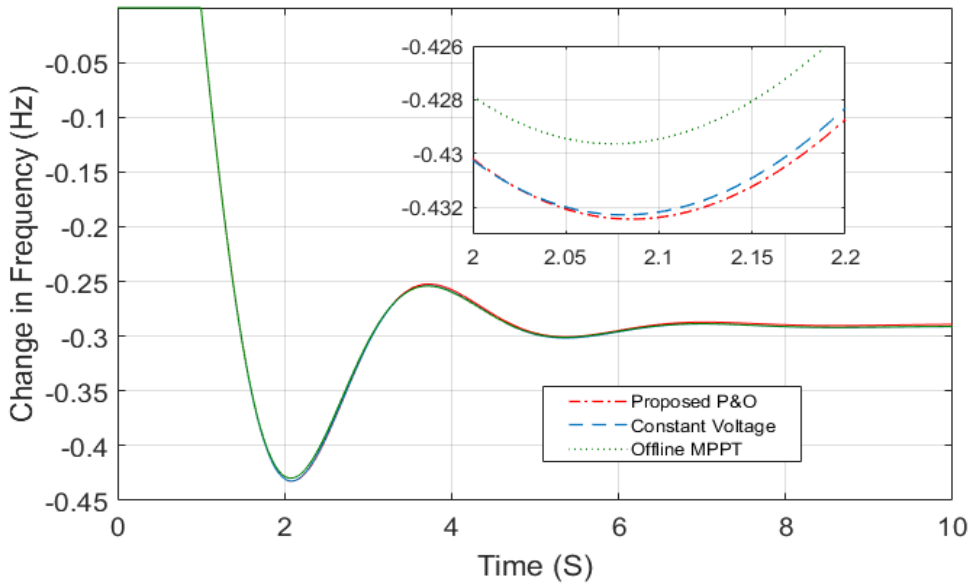

Figure 4.20: Response for increasing irradiance

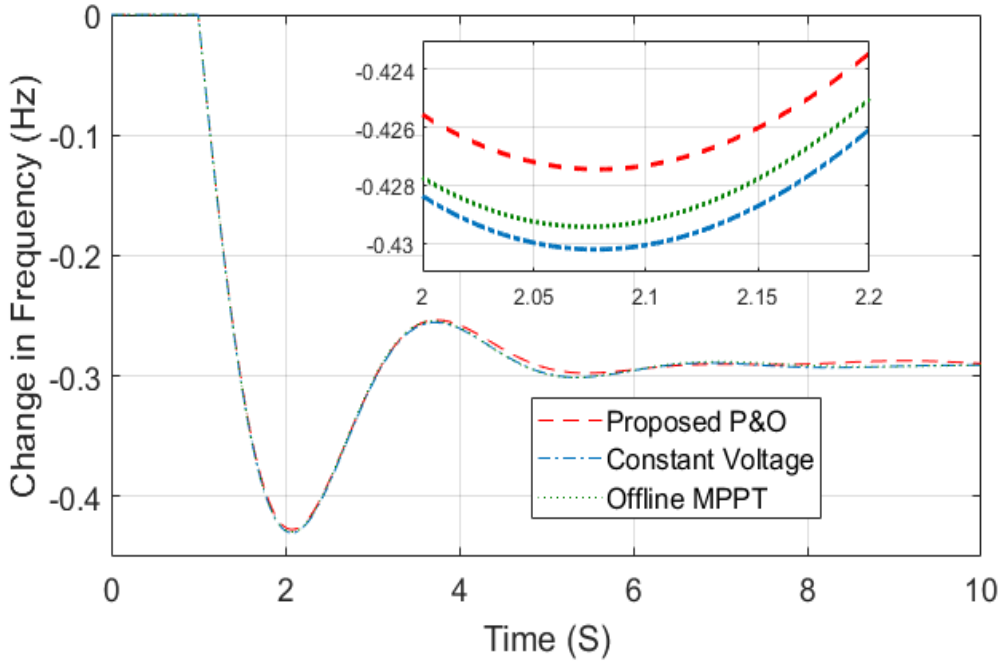

Figure 4.21: Response for sinusoidal irradiance (1.5rad/s)

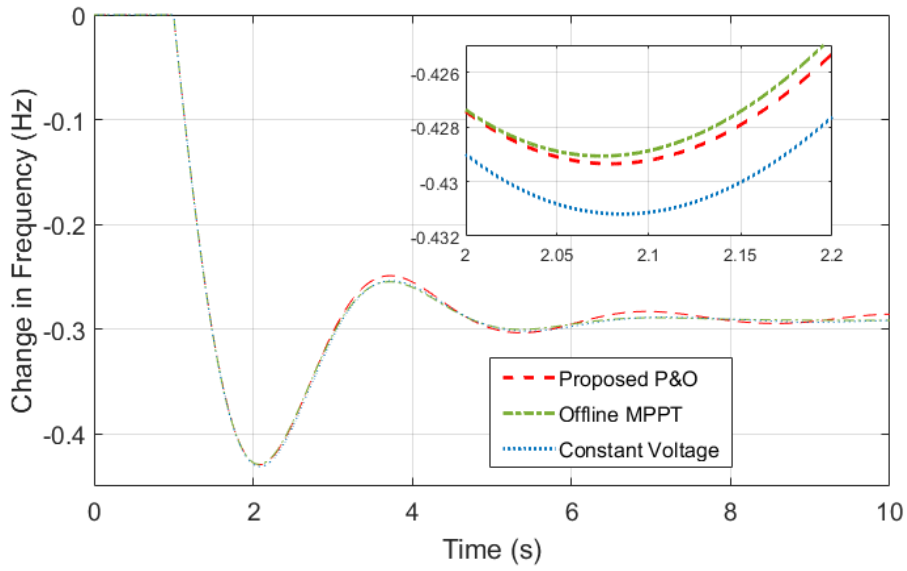

Figure 4.22: Response for sinusoidal irradiance (2rad/s)

4.6. Summary

In this chapter, the ability of PVPP to contribute to frequency support is evaluated. The effectiveness of PVPP support at different penetration levels using different support methods has been demonstrated. The frequency responses indicate that with adequate reserve, PVPP can eliminate the adverse effect of low inertia in power systems. However, the skilful reserve management is essential to obtain the best response with least reserve. The proposed variable droop method improves the performance and maintains the PVPP's ability to participate in future frequency events.

From comparison with other MPPTs, the offline MPPT used for frequency support in this chapter gives consistent performance for varying environmental conditions.

Chapter 5 : Framework for Quantifying and Comparing Frequency Support Ability

5.1 Introduction

As stated in previous chapters, control and operation strategies for various forms of generation to participate in frequency support has been the focus of some recent research. Strategies for frequency support from wind power plants, photovoltaic power plants, battery storage systems, flywheel storage systems, and pumped hydro are well-known [13, 29, 109, 110]. Authors in [111] have proposed frequency support from dynamic demand control. Some renewable energy systems do not have inertia, and some are interfaced with converters and decoupled from system frequency. The resource in most renewable generation are variable and hence result in variable output power. Variable power generation could lead to a high occurrence rate of generation-load imbalance. However, the need for clean and sustainable power generation has resulted in a drive for higher renewable energy integration. Increasing renewable energy penetration could have a deteriorating effect on frequency response due to lower system inertia. Hence, the proposal of new support methods for renewable sources to contribute to frequency support.

While frequency support from non-conventional generation sources has proven to be effective in ameliorating the effect of low inertia in power system [13], little attention has been given to quantifying and comparing the amount of support

obtainable from different generating units. Because of the inherent differences in generation response characteristics, different generation forms will usually result in different performance in providing frequency support, even if they have the same support parameters. These differences in response characteristics imply that an understanding of the factors that affect frequency support performance is useful in understanding the degree to which generating units will contribute to frequency support. The main effect of the differences in governor/turbine models of generating units is the resulting response speed. The quality of frequency support from a generating unit can be assessed by the response speed [112]. The response speed and support parameters together determine the frequency response performance of a power system.

Future power systems are expected to have a diverse generation of sources participating in frequency support. These sources will include PV, Wind, BESS, which are capable of providing frequency support. However, some sources, such as centrally controlled DSR scheme or BESS may have a response delay, which affects its frequency support performance [113]. Frequency support can also be obtained by demand response which involves the adjustment of power consumption based on changes in frequency [46, 112, 114, and 115]. Some of these methods require a communication channel to measure the change in frequency and transmit the change in power [116]. This will lead to the introduction of a time delay in the system. The effect of time delay should be considered in measuring the ability of a unit providing frequency support.

Because frequency response varies for different generating units, there is a need for a general method to compare the economic cost and benefit of frequency support from diverse generating units. In [117], a method is proposed for determining the payments for frequency support from wind turbines based on compliance with grid code. In [118], the effect of frequency support from wind power plants on the overall economic performance of power plants is assessed but does not give a basis for comparing different plants.

This chapter proposes a framework for comparing the frequency support from diverse generating sources considering the effect of response speed, support

parameters, support methodology, and time delay. A Second-order system used to represent generating units of different response speeds. Different generating units are represented by changing one of the time constants of the system. The response of the second-order system is analysed for different support methods and parameters, and the responses compared. The effect of delay on the frequency response is also analysed. A method for comparing support quality and extent of support is also presented. The method of comparison combines both response speed and support parameters, while the extent of support is determined using a combination of the available reserve, speed, and support parameters. A method for frequency support comparison based on economic consideration is also presented. The PV system used is chapter 3 and 4 is used to verify the effectiveness of comparison to a Second-order system.

The rest of the chapter is structured as follows: Section 5.2 presents the relationship between the response speed, support methods and parameters, the nadir and maximum power increase of a response. Section 5.3 describes a method for support comparison and measuring the extent of support obtainable from a generating unit. Section 5.4 describes the comparison of support with economic consideration. In section 5.5, a case study with a PV system and the conclusion is presented. 5.6 presents the conclusion.

5.2 Frequency Response and Response Speed

Governor and turbine models usually comprise of transfer functions that determine the frequency response characteristics of the generation unit [38]. A second-order system is used to represent the generating units. Generating units of varying speeds can be analysed by varying the time constant.

Figure 5.1 shows the LFC system with the governor/turbine represented by a Second-order transfer function. τ_1 and τ_2 are the time constants of the two transfer functions, H is the system inertia, R is the droop constant, D is the damping coefficient, ΔP_L is the change in load and ΔP_G is the change in power of the generating unit. The relationship between the change in power and the change in frequency is given as:

$$\Delta P_G(s) - \Delta P_L(s) = 2Hs\Delta f(s) + D\Delta f(s) \tag{5.1}$$

For a sudden change in load, $\Delta P_L(s) = \Delta P_L/s$ and, the droop gain, $K_D = 1/R$, the response becomes:

$$\frac{-\Delta f(s)K_D}{(\tau_1 s+1)(\tau_2 s+1)} - \frac{\Delta P_L}{s} = 2Hs\Delta f(s) + D\Delta f(s) \tag{5.2}$$

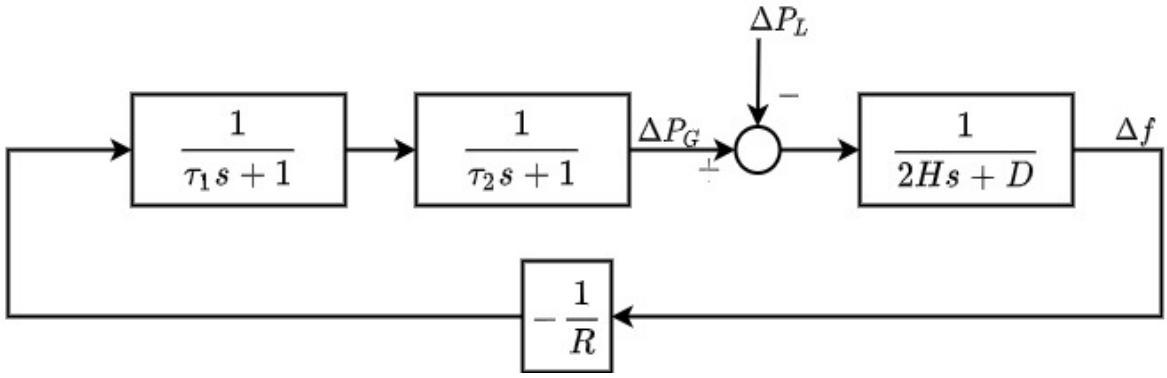

Figure 5.1: LFC with Second-order System

The change in frequency is expressed as:

$$\Delta f(s) = \frac{(-\Delta P_L\tau_1 s-\Delta P_L)(\tau_2 s+1)}{\big((2Hs+D)(\tau_1 s+1)(\tau_2 s+1)+K_D\big)s} \tag{5.3}$$

The effect of the response speed on the nadir is the focus of this chapter. The nadir occurs when the ROCOF is zero. The time at which the nadir occurs can be obtained by using the Laplace derivative property. The Laplace transform of a derivative is given as:

$$\mathcal{L}\{f'(t)\} = sF(s) - f(0^-) \tag{5.4}$$

Since $f(0^-) = 0$, the ROCOF in Laplace becomes:

$$\mathcal{L}\left\{\frac{\Delta f(t)}{dt}\right\} = \frac{(-\Delta P_L\tau_1 s-\Delta P_L)(\tau_2 s+1)}{(2Hs+D)(\tau_1 s+1)(\tau_2 s+1)} \tag{5.5}$$

In (5.3), for a set of parameters (H, K_D, D and τ_1 and τ_2), Δf and ΔP_L vary directly at a given time. The ratio of Δf and ΔP_L at the time nadir occurs will be referred to as the nadir coefficient in this chapter. Figure 5.2 gives the responses for a system with $H = 5$, $D = 1$, $K_D = 20$, $\tau_1 = 0.2$ $\tau_2 = 0.4$ when ΔP_L is 0.1pu, 0.2pu

and 0.3pu. The ratio of Δf and ΔP_L at the nadir in Figure 5.2 is -0.06916. The nadir coefficient is useful for determining the nadir for any change in load. The nadir is given as:

$$nadir = nadir\ coefficient\ \times \Delta P_L \tag{5.6}$$

Figures 5.3 and 5.4 show the graph of the nadir coefficient against time constant (τ_2) for the response of a system with droop control while $\tau_1 = 0.1$. The Figures show that for a system with an instantaneous response (i.e., $\tau = 0$), the nadir is not affected by the inertia and is determined by K_D. The effect of inertia on the nadir increases as response speed decreases. This means that the difference in nadir between two systems with the same response speed and different inertia increases as response becomes slower. The results also show that a lower nadir is obtained with a lower value of K_D. The combination of K_D and τ and H can be used to gauge and compare the nadir from different systems. For example, from Figures 5.3 and 5.4, a system with $H = 4$, $K_D = 20$, $\tau_1 = 0.1$ and $\tau_2 = 2$ and system with $H = 4.5$, $K_D = 25$, $\tau = 0.1$ and $\tau_2 = 3$ will have the same nadir coefficient of -0.12.

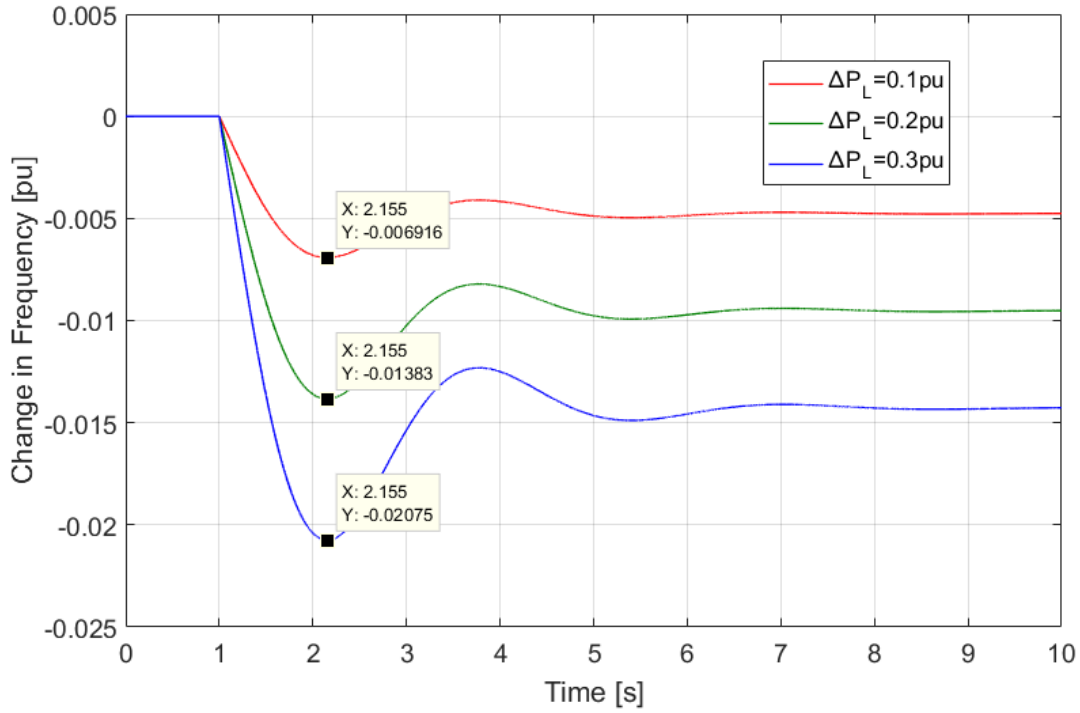

Figure 5.2: Effect of changing load on nadir

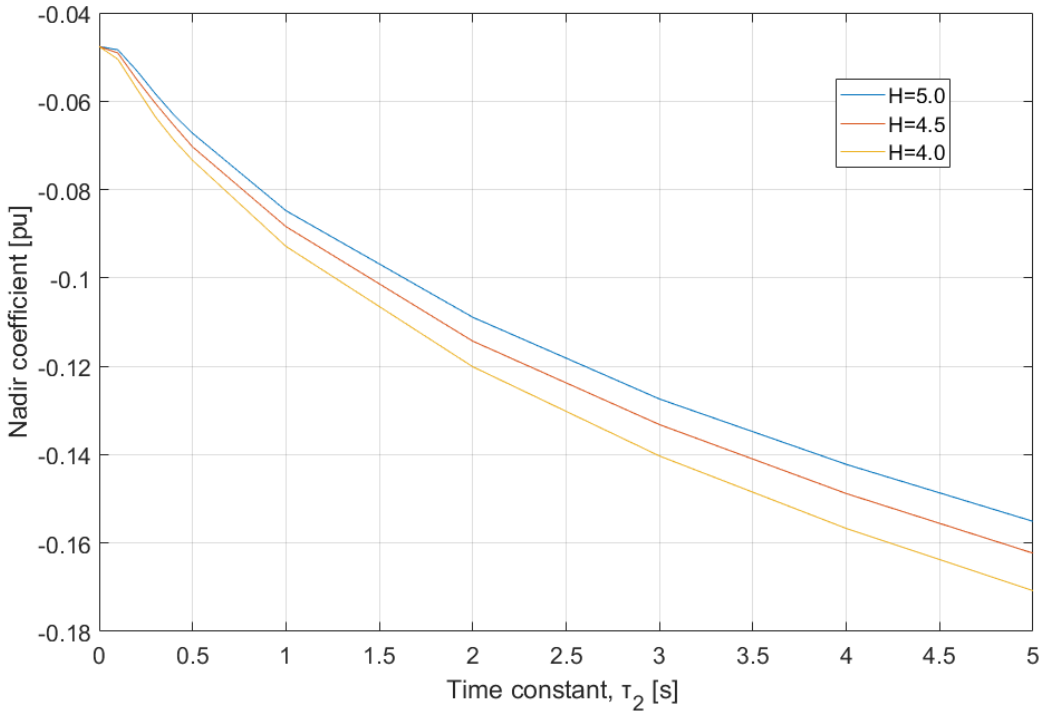

Figure 5.3: Nadir coefficient when K_D is 20

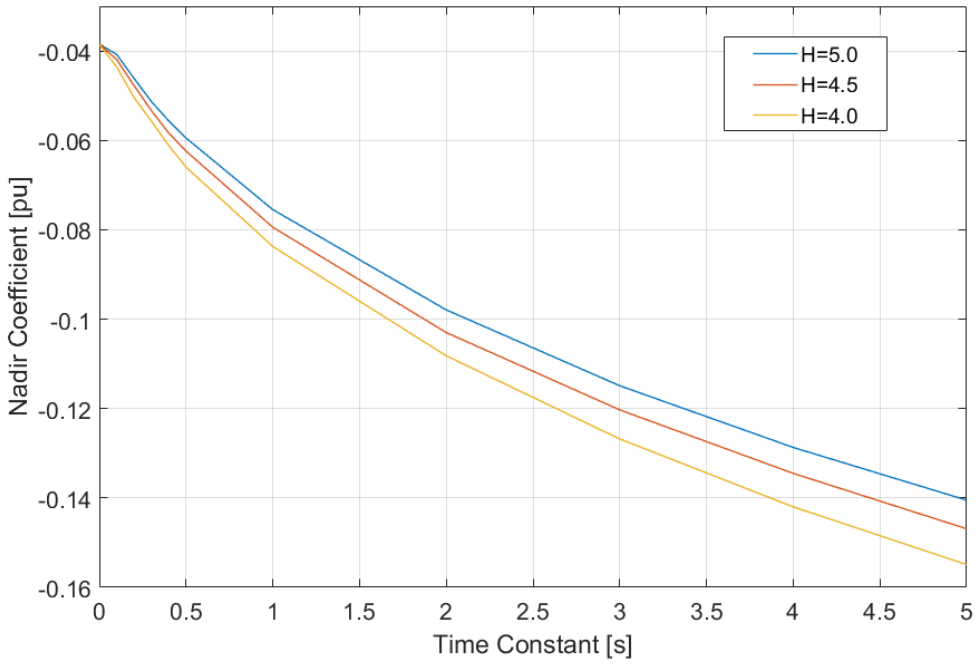

Figure 5.4: Nadir coefficient when K_D is 25

5.2.1 Maximum Power Increase

The maximum change in power by a generating unit is also affected by its response speed. For a step increase in load, the maximum power increase will occur at a later time than the nadir. The relationship between the response speed and the maximum change in power can be used in distributing support burden and selecting support parameters based on the available reserve. The frequency response is affected if the change in power required by the support parameters cannot be achieved. For a step change in load, the change in power coefficient is given as:

$$\Delta P_G(s) = \frac{K_D}{\left((2Hs+D)(\tau_1 s+1)(\tau_2 s+1)+K_D\right)s} \tag{5.7}$$

The rate of change of the change in power of the generating unit in Laplace can be given as:

$$s\Delta P_G(s) = \frac{K_D}{\left((2Hs+D)(\tau_1 s+1)(\tau_2 s+1)+K_D\right)} \tag{5.8}$$

The value of the maximum power change is readily obtained by solving the inverse of (5.7) at the time maximum power change occurs.

Figures 5.5 and 5.6 gives the graph of the maximum power increase coefficient and the time constant (τ_2) of the LFC system with droop control while $(\tau_1 = 0.1)$. The maximum power increase for a response to a step-change in load can be obtained by equation (5.9).

$$\Delta P_{max} = Max.Power\ Increase\ coefficient\ \times \Delta P_L \tag{5.9}$$

For generating units with an almost instant response, (i.e. $\tau = 0$), the maximum power increase is the same irrespective of inertia. The maximum power increase, as well as the nadir, is only affected by the value of K_D for instantaneous systems. From Figures 5.5 and 5.6, it is observed that the maximum change in power of the system in a step response increases with an increasing time constant. Although at higher time constants, the maximum power increase begins to drop for the same step-change load. Increasing K_D with will lead to a higher maximum power and smaller nadir. The

results in Figure 5.5, and 5.6 can be a guide in choosing parameters to achieved specific maximum power increase.

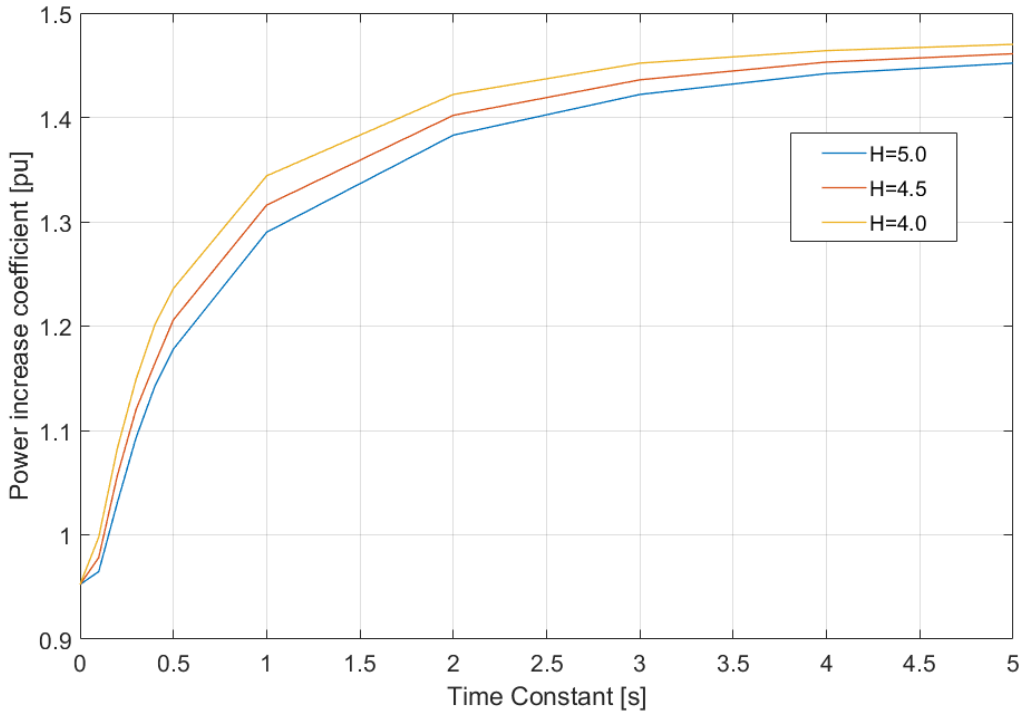

Figure 5.5: Power increase coefficient when K_D is 20

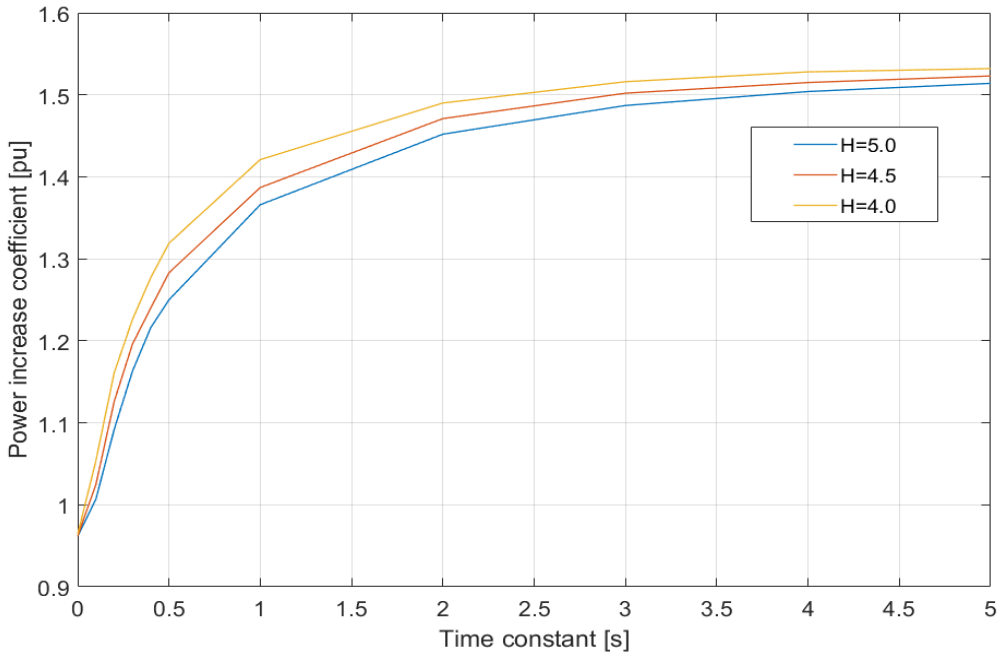

Figure 5.6: Power increase coefficient when K_D is 25

5.2.2 Response speed and synthetic inertia

The importance of inertia in power systems has been discussed in chapter 2 of this thesis. Some non-synchronous and inertialess sources can provide frequency support by releasing additional power based on the ROCOF. This frequency support method is usually called synthetic inertia in literature. Control for synthetic inertia contribution has been implemented in wind turbines [42] and photovoltaic power plants [109]. While inertia from synchronous power plants is inherent and will release power instantaneously based on the ROCOF, change in output power from synthetic inertia control is affected by the response speed of the generating unit. Unlike inertia from conventional generators, synthetic inertia cannot be summed into a single value in a system with generators with different response speeds. The effect of synthetic has to be analyzed for various response speed. The LFC with synthetic inertia is given in Figure 5.7.

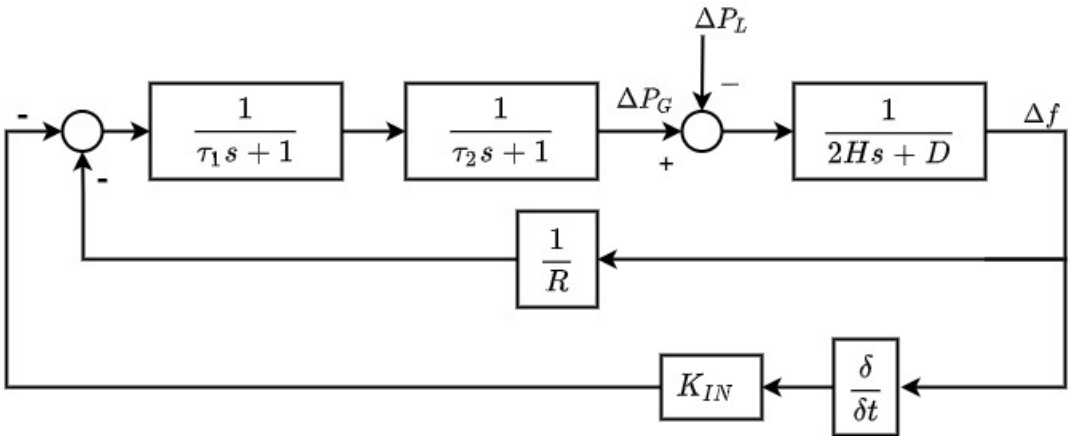

Figure 5.7: LFC with droop and inertia loop

This sub-section analyses the effect of response speed on the frequency response of a generating unit with both droop and synthetic inertia support. Unlike conventional inertia, synthetic inertia may require a reserve, for example, a PV power plant or may not require a reserve, as is the case in wind turbines. The effect of synthetic inertia provision on the change in output power of the generating unit, the relationship between the response speed and support parameter is important in the

distribution of support burden. The power balance for a system with synthetic inertia support is the same as Eq. (5.1). However, due to the synthetic inertia support loop, ΔP_G changes to become:

$$\Delta P_G(s) = \left[\frac{1}{(\tau_1 s+1)(\tau_2 s+1)}\right] \times \left[\frac{-\Delta f(s)}{R} - K_{in} s\Delta f(s)\right] \tag{5.10}$$

where K_{in} is the inertia gain. The response becomes:

$$\frac{-\Delta f(s)K_D - K_{in} s\Delta f(s)}{(\tau_1 s+1)(\tau_2 s+1)} - \frac{\Delta P_L}{s} = 2Hs\Delta f(s) + D\Delta f(s) \tag{5.11}$$

The change in frequency can then be expressed as:

$$\Delta f(s) = \frac{-(\tau_1 s+1)(\tau_2 s+1)}{[(2Hs+D)(\tau_1 s+1)(\tau_2 s+1)+K_D+sK_{in}]s} \tag{5.12}$$

Including synthetic inertia, the change in frequency in Laplace is:

$$\Delta f(s) = \frac{-(\tau_1 s+1)(\tau_2+1)}{K_D+K_{in}s} \times \Delta P_G \tag{5.13}$$

By substituting the value of change in frequency in (5.13) in the power balance equation, the power balance equation then becomes:

$$\Delta P_G - \Delta P_L = \frac{-(\tau_1 s+1)(\tau_2+1)(2Hs+D)}{K_D+K_{in}s} \times \Delta P_G \tag{5.14}$$

The maximum power increase coefficient when a generating unit combines both droop and inertia support can be given as:

$$\Delta P_G(s) = \frac{(K_D+K_{in}s)}{[(2Hs+D)(\tau_1 s+1)(\tau_2 s+1)+K_D+sK_{in}]s} \tag{5.15}$$

The maximum power change for generating units with droop and synthetic inertia can be obtained by solving the inverse Laplace of (5.15). The time maximum power change occurs can be obtained by finding the time $s\Delta P_G(s)$ for the droop + synthetic inertia system is zero.

Figure 5.8, and 5.9 give the graph of nadir coefficient and time constant for different values of K_{in} when K_D is 20. The nadir become smaller with increasing K_{in}. As expected, the effect of emulated inertia support diminishes with an increasing time constant. The effect of response speed is the main difference between emulated inertia and conventional inertia support. As seen in Figures 5.8 and 5.9, the effects of

emulated inertia correspond to an increase in conventional inertia when the time constant is between 0 and 0.2s. Another advantage of emulated inertia support is that the maximum increase in power required for the attainment of a nadir decreases with increasing K_{in}. This can be observed in Figure 5.10, as the value of K_{in} increases, the maximum power increase becomes smaller and the corresponding nadir also becomes smaller as seen in Figure 5.8. The effect of emulated inertia support can be used as a guide to set support parameters. The main drawback of this method is the measurement of df/dt with can have a lot of noise and lead to large changes in power from inertia support [43].

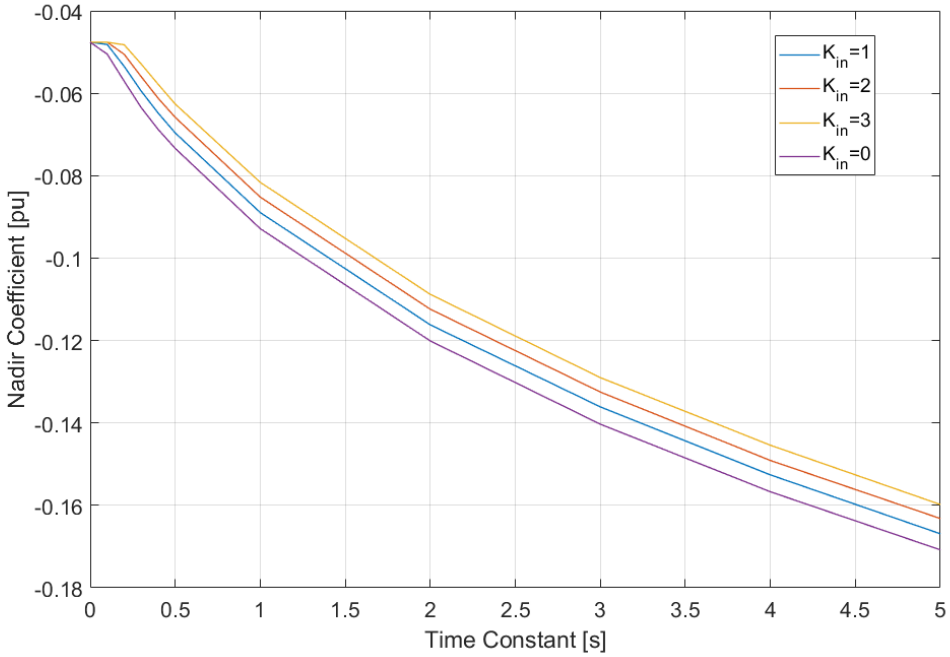

Figure 5.8: Nadir coefficient with K_D=20 and H=4

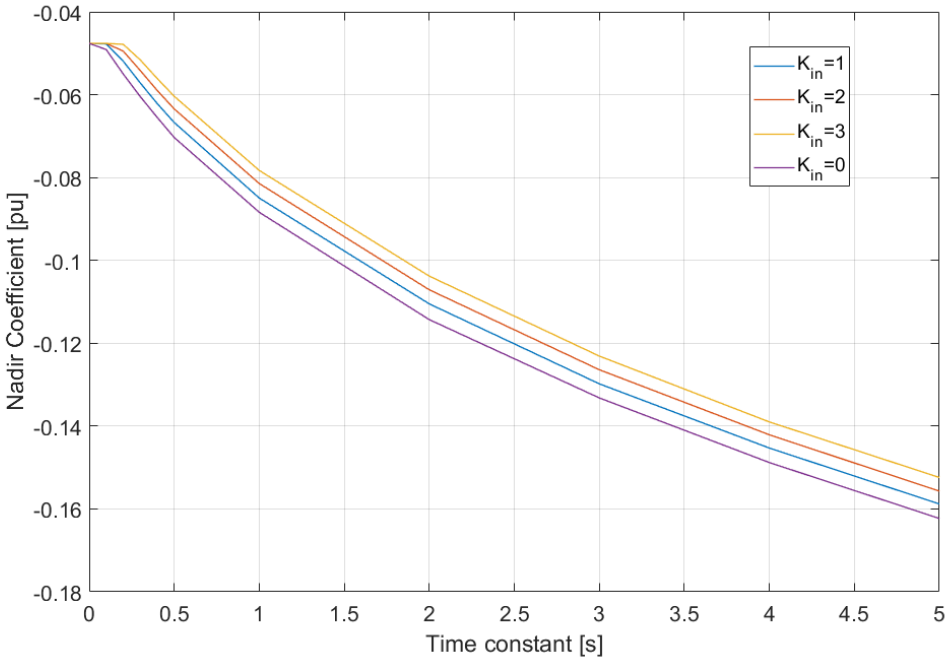

Figure 5.9: Nadir coefficient with K_D=20 and H=4.5

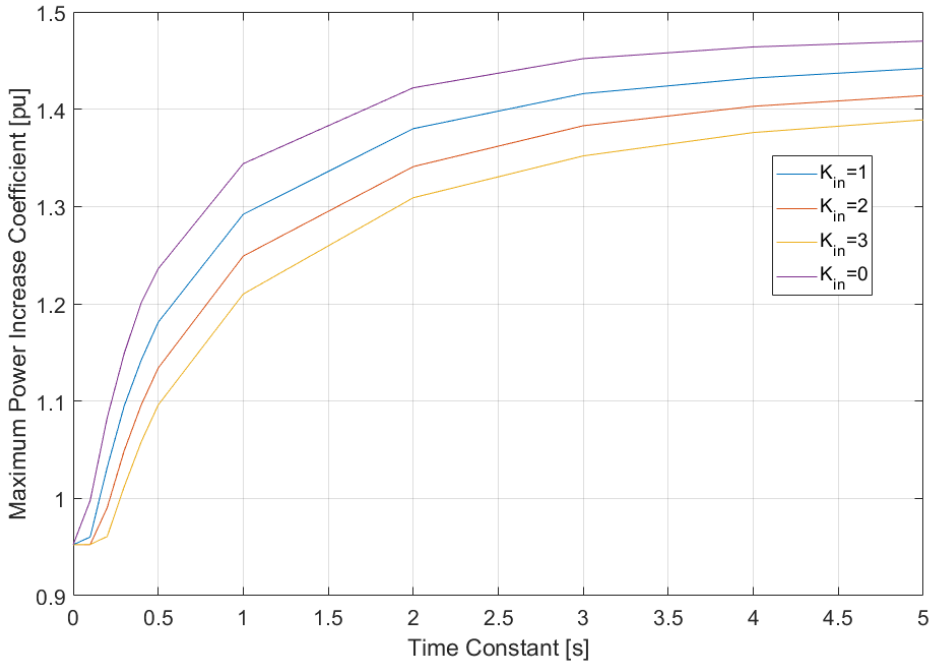

Figure 5.10: Power increase coefficient with K_D=20 and H=4

5.2.3 Effect of delay on Frequency Response

Smart grids with high renewable penetration will need frequency support from demand-side response to increasing system resilience [18]. Demand-side response includes the reduction of power consumption of controllable loads such as air conditioners and refrigerators in response to frequency changes. The charging and discharging of PEV can be used to support system frequency. The use of DSR for frequency support will require the transmission of control signals which will result in the introduction of a delay in the LFC system. These delays will have an effect on the overall instantaneous additional power from a generating unit and thus affecting the frequency response. The representation of delay in a system is given in Figure 5.11, where τ_D is the delay. The resulting change in frequency in Laplace for a system with delay and implementing droop control is given by (5.21).

$$\Delta f(s) = \frac{(-\Delta P_L \tau_1 s - \Delta P_L)(\tau_2 s + 1)}{\left((2Hs + D)(\tau_1 s + 1)(\tau_2 s + 1) + (K_D \times e^{-\tau_D})\right)s} \tag{5.16}$$

Because the denominator of (5.21) is not a polynomial, it is difficult to find the inverse Laplace and solve in the time domain. The effect of delay is observed in simulation by the use of a transport delay in Simulink.

The results in Figures 5.12 and 5.13 show that the frequency nadir worsens with increasing time delay. The results from the droop and inertia support show that for a very fast system, the nadir is not affected by a loss of inertia. Time delay, however, affects the resulting nadir for irrespective of the speed of the system.

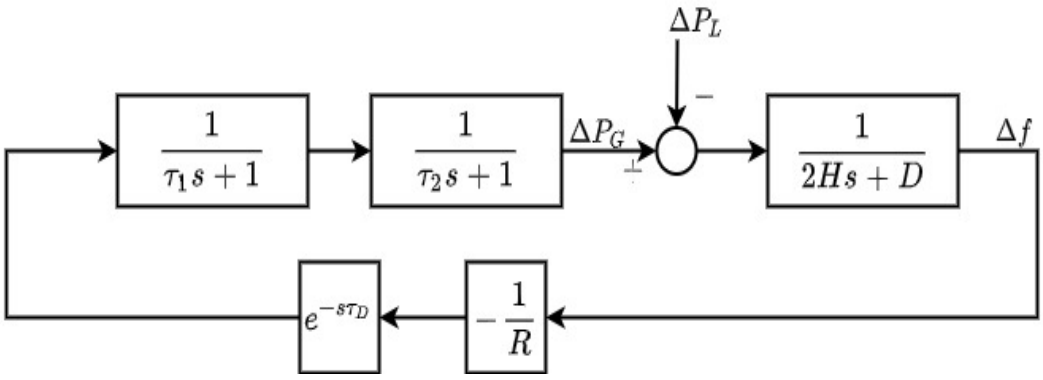

Figure 5.11: LFC with time delay

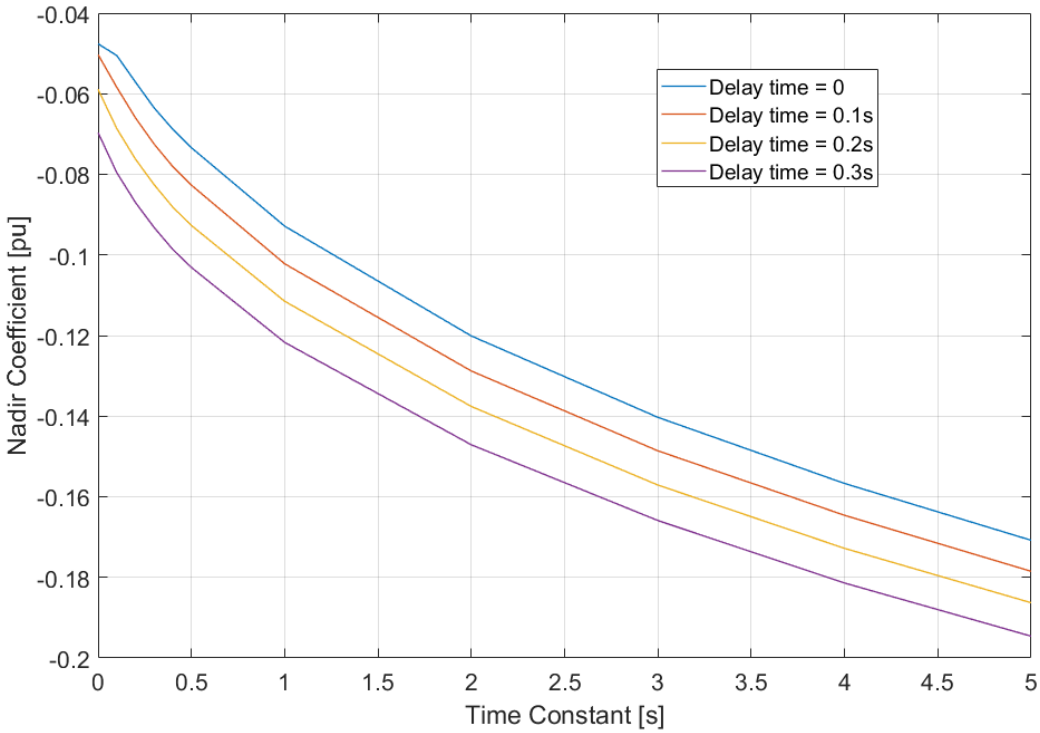

Figure 5.12: Effect of delay on nadir with K_D=20 and H=4

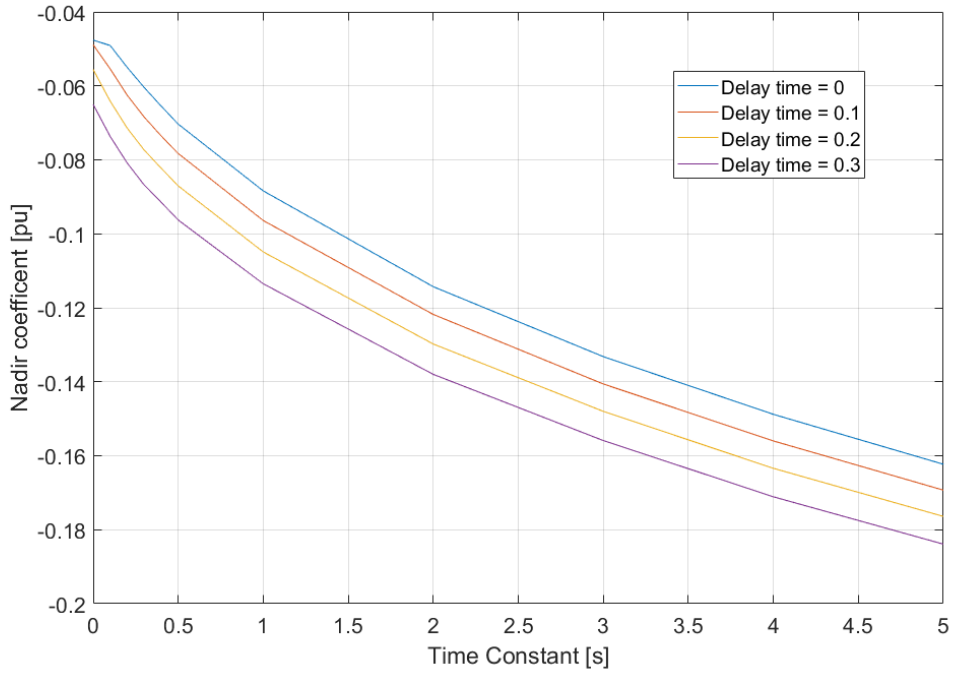

Figure 5.13: Effect of delay on nadir with K_D=20, H=4.5

5.4 Comparing Support Ability

While the response speed of a generating unit indicates its ability to provide support, the amount of support delivered during operation is a combination of the effects of the response speed and support parameters. This section describes how the performance of a generating unit can be assessed using the response speed and the support parameter. The response speed, support parameters, or both can be changed in some generating units and cannot be changed in other. The relationship between support parameters and speed is useful in comparing expected support and can be a guide in improving and comparing support obtained from a unit or the entire system.

The nadir of the frequency response of generating units can be compared by the change in output power of the units immediately after a generation-load imbalance. The units with a larger change in power will usually have lower nadir than units with a lesser change in power. A handy way to compare with generating units with different units and support parameters is to determine which unit will give more output power in a short period after the generation-load imbalance.

In the time domain, change in the power of the generating unit becomes (5.17)

$$\Delta P_G(t) = \left(1 - e^{-t/\tau}\right) \times K_D \times \Delta f \tag{5.17}$$

For a given change in frequency, $\left(1 - e^{-t/\tau}\right) \times K_D$ determines the output power. The value of $\left(1 - e^{-t/\tau}\right) \times K_D$ can be used to determine the generating unit that will result in a smaller nadir, assuming the unit has the same inertia. Let the comparison value (CV) be given as:

$$CV = \left(1 - e^{-t/\tau}\right) \times K_D \tag{5.18}$$

For systems with different inertia and droop gain, the inertia can be considered as an additional power with an instant response, i.e., not affected by response speed. The change in generator power then becomes:

$$\Delta P_G(t) = 2H \times \frac{d\Delta f}{dt} + \left(1 - e^{-t/\tau}\right) \times K_D \times \Delta f \tag{5.19}$$

For a given change in frequency and ROCOF, the system with a larger value of $2H + \left(1 - e^{-t/\tau}\right) \times K_D$ will result in the smaller nadir in frequency response.

When synthetic inertia is considered, the change in power becomes:

$$\Delta P_G(t) = 2H \times \frac{d\Delta f}{dt} + \left(1 - e^{-t/\tau}\right) \times K_D \times \Delta f + \left(1 - e^{-t/\tau}\right) \times K_{in} \times \frac{d\Delta f}{dt} \tag{5.20}$$

The expression for comparison value (CV) then becomes:

$$CV = 2H + (K_{in} + K_D)\left(1 - e^{-t/\tau}\right) \tag{5.21}$$

Generating units with different droop gain, emulated inertia gain, inertia and response speed can be compared by solving (5.21) at a small time after generation load imbalance.

Table (5.1) gives the value of CV for randomly selected values of pairs of a time constant, inertia, synthetic inertia, droop gain and the resulting nadir coefficient of a system with each set of parameters. Except for the set of parameters in no. 4 and no. 12 of table (5.1), for any sets of parameters compared, a higher value of CV usually corresponds to a smaller value of nadir in simulation. The frequency for parameters in no. 7 does not drop below the steady-state value so the nadir is the steady-state frequency deviation, which depends on the droop gain. Although the parameters in no. 13 have a smaller value of CV than the parameters in no. 12, parameters in no. 12 results in a smaller nadir. This is because no. 12 has significantly larger inertia than no. 13 and no. 13 has significantly larger droop gain than number 12. This makes it harder to determine if parameters in no. 12 will perform better by observing the output after 0.1s.

This method can be confused if a very small time is chosen and there is a large difference in inertia between the compared generating units. This can make a unit with larger inertia but lesser support parameter result in a higher value of CV. To avoid this, time chosen to solve (5.21) should not be too small and not too large. For example, between 0.2 and 0.5.

Frequency support in cases of a sudden increase in load or sudden loss of generation will require a power increase. This means that generating units will have to operate with some amount of reserve to participate in droop and emulated inertia support. As stated earlier, the maximum power increase for a unit participating in frequency support depends on the response speed and response parameter- including inertia. A way to measure the extent to which a system can provide frequency support is to measure how much support can be obtained considering the limit of the power reserve.

The extent to which a generating unit can provide support for a specific set of support parameters can be determined by calculating the power imbalance that results in the maximum reserve power as the maximum change in power of the generating unit. This can be achieved using (5.7) or (5.15) depending on support methods used and solving for ΔP_L. A larger ΔP_L for for maximum ΔP_G for a system with certain support parameters indicates that the system will be able to provide support for a larger generation-load imbalance. This can serve as both an indicator of the quality of support from the generating unit and the extent to which it can provide support.

Table 5.1: Comparison Value Table

NO	Time Constant (s)	2H	K_D	K_{in}	CV	Nadir Coefficient (10^{-2})
1	0.2	7	18	0.5	14.2792	-5.525
2	1	7.6	17	1	9.3129	-9.097
3	0.7	9	21	1.2	11.9553	-6.6611
4	2	10	23	1.7	11.2046	-9.144
5	0.8	8.4	20	0.9	10.8558	-7.411
6	0.9	7.9	19	0.8	9.9822	-8.187
7	0	9.4	17	2	28.4	-5.556
8	1.7	8.7	18	2.7	9.8825	-9.826
9	0.3	8.1	25	3	16.0371	-4.22
10	1	8.8	23	2.1	11.1886	-7.052
11	1.8	9.3	19	0.9	10.3754	-10.14
12	0.6	10	16	1.5	12.6866	-7.046
13	0.9	7	25	2.5	9.8919	-6.867
14	1.1	7.5	24	2.7	9.8202	-7.421
15	0.6	9.2	17	2.2	12.1476	-6.744
16	1.8	7.8	18	1.1	8.8322	-11.05
17	1.2	8.3	23	2.9	10.3708	-7.555
18	0.7	8.9	21	0.7	11.7887	-6.779
19	0.5	8.5	20	0.6	12.2341	-6.303
20	1.5	8	20	2.8	9.4704	-9.066

5.5 Quantifying support value with Economic Consideration

Apart from support from conventional inertia, generating units will usually have to operate below maximum capacity to be able to provide upward regulation. The cost of maintaining a power reserve is a factor that affects the overall quality of a generating unit in providing frequency support. In this section, a framework for

comparing frequency support ability by considering the economics of providing support together with the technical factors that affect support performance.

The maximum power increase from a generating unit in frequency response is used as a measure of its performance. The ability of the generating unit to provide required maximum power is affected by the amount of reserve available. Maintaining power reserve affects the cost of power generation and requires some economic consideration. For the attainment of a given nadir, different generating units will result in different maximum power increase. The cost of the maximum power increase for different nadir value is a basis for comparing the economic performance of the generating unit, which is a result of response speed and support parameters. The total cost of attaining a maximum power increase then becomes:

$$C_T = Cost\ per\ watt\ of\ Increase\ \times Max.Power\ Increase \tag{5.22}$$

The value of C_T gives the cost of obtaining a particular nadir. The control parameters and factors that affect response can be selected to obtain a particular value of C_T for a range of generation-load imbalance.

Another way to measure the economic value is to consider the payment for the provision of a particular response – that is the nadir in this work. Factoring the payment enable comparison based on net gain for providing frequency response. The economic value in attaining a particular nadir is given as:

$$EV = Payment - C_T \tag{5.23}$$

A higher value of EV for a particular value of nadir means more economic benefit for generating units with parameters that result in such value.

To demonstrate the effect of cost and payment on the economic value of support from generating units, responses from two generating units represented with time constants of 0.6 and 0.8 are compared. The generating units provide support with droop control. Table (5.2) shows the parameters for the compared units. The parameters have been set to give the units the same nadir coefficient, but different power increase coefficient. The same nadir coefficient implies that both systems will result in the same nadir for the same generation-load imbalance. The two systems will also differ in the maximum power increase by the same percentage for the same generation-load imbalance. Figure 5.14 shows the plot of the ratio of the unit cost of

the two units (G1: G2) against the ratio of the resulting overall cost of the maximum power increase in frequency response. The data point (0.9005, 1) shows that for the generating units, G1 and G2 to have the same overall cost of power increase, the cost of G1 will be 90.05% of the cost of G2. The data point (1, 1.111) shows that when the unit cost of G1 and G2 are the same, the overall cost of the power increase of G1 will be 111.1% of the cost of G2. For equal payment for support from G1 and G2, only the total cost of is sufficient for economic comparison. When payment for G1 and G2 are different, the value of EV should be used for comparison.

Table 5.2: Parameters of units for cost comparison

	H(s)	τ(s)	K_D	Power Increase Coefficient	Nadir Coefficient
G1	4	1	21	1.2162	-8.333×10^{-2}
G2	5	0.7392	15	1.095	-8.333×10^{-2}

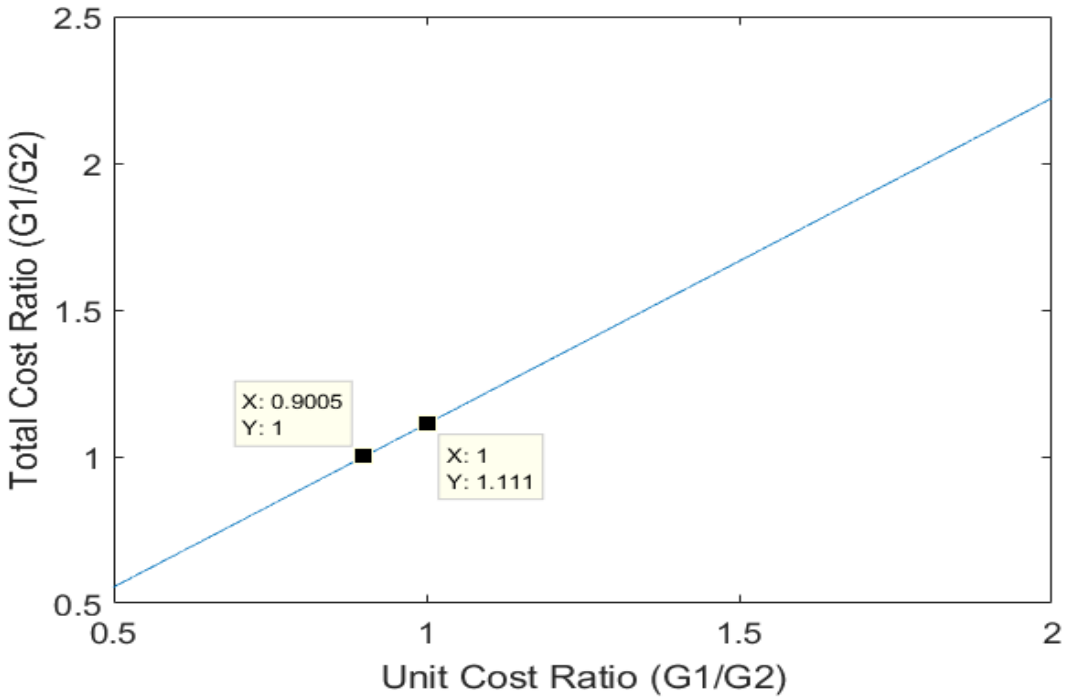

Figure 5.14: Cost ratio comparison

5.6 Discussion

The PV system is subjected to a step increase of 10W to obtain its response speed. From Figure 5.15, the PV power increases by 5.96W after 0.1s. The equivalent time constant for the PV system is estimated to be 0.01s. When the PVPP is replaced with a Second-order system with its equivalent time constant, the resulting change in power for frequency response to a 0.1 increase in load with droop response ($K_D = 20$) is given in Figure 5.16. The change in PV power from the equivalent Second-order system in Figure 5.16 is very similar to the change in power from the PV model given in Figure 4.13). Figure 5.17 shows the frequency response of the system with the PVPP represented by second-order system equivalent system with 20% penetration. The resulting frequency response in the equivalent Second-order system has very close nadir to the response for droop control in Figure 4.12.

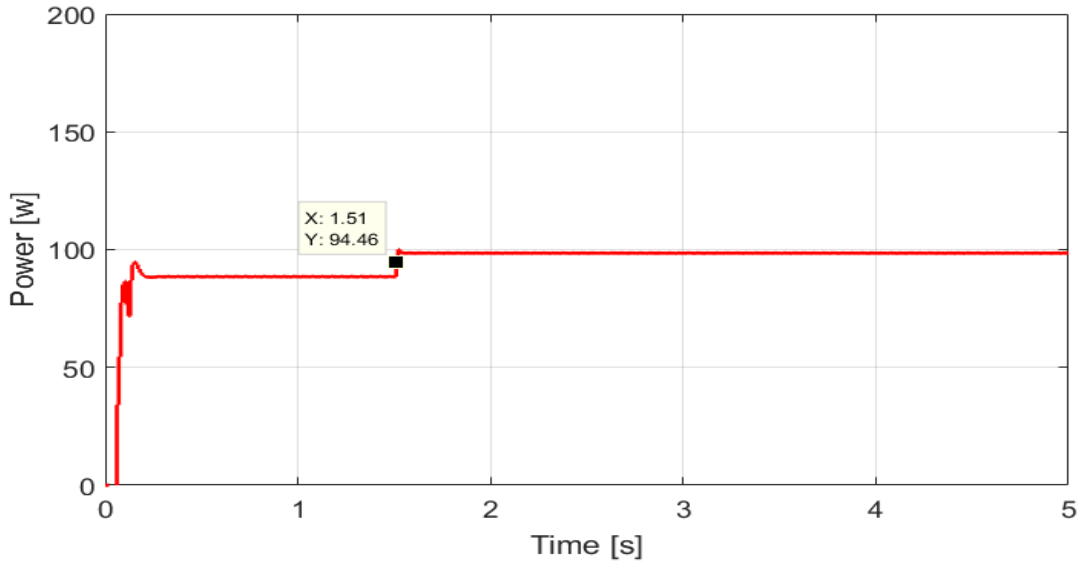

Figure 5.15: Step increase in PV power

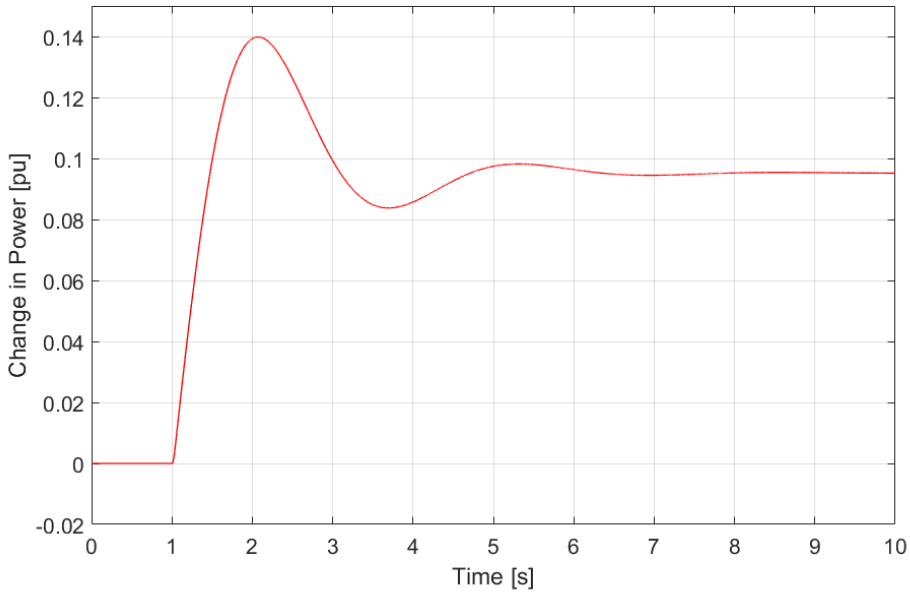

Figure 5.16: Change in PV power from representative Second-order system

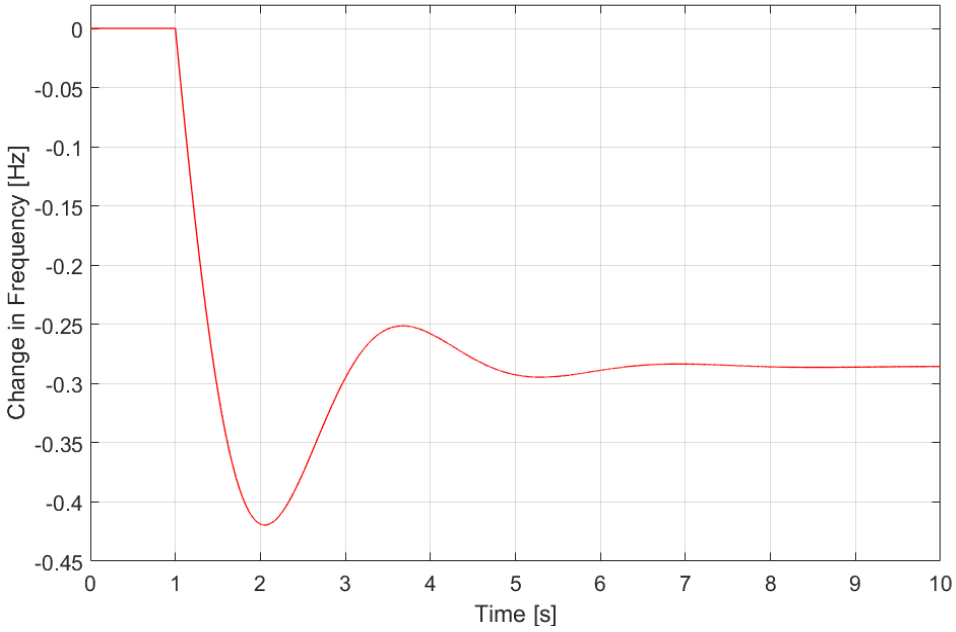

Figure 5.17: Frequency response from Second-order representative system

5.7 Summary

This chapter has shown that the response speed of generators, together with the implemented support methods and parameters, determines the quality of frequency

response when judged by the frequency nadir. The resulting nadir for generating units with droop and droop plus synthetic inertia for different values of K_{in}, K_D and inertia, for a range of response speeds, confirm the effect of response speed on nadir. The results form a basis for the selection of parameters to obtain particular nadir from frequency response. Although the response speed for some generating units (mostly conventional plants) cannot be changed, as they depend on the plant type [16] and manufacturing, the response speed of some can be improved. For example, the response speed of PVPP can be improved by selecting a fast responding MPPT and an active power control method.

Different combinations of support parameters can be chosen to obtain a particular frequency nadir. But for a given nadir, the different combinations will require different maximum-power-increase and result in different steady-state deviation. Results from this chapter present the increase in power for different combinations of K_{in} and K_D for units implementing droop support. It is advantageous for a nadir to be obtained with the smallest maximum increase in power possible. Results show that while increasing the K_D for a system or unit will result in a smaller nadir, increasing K_D will also increase the maximum change in power. However, combining droop and synthetic inertia support will result in smaller nadir and a smaller increase in maximum power. This means a combination of droop and synthetic inertia can be used to obtain optimal maximum power increase for frequency response. Considerate selecting support methods and parameters can increase the extent to which a generating unit or system can provide frequency support.

A framework for comparing frequency support based on support parameters and economic consideration is also presented. This is useful in distributing support burden based on economic cost and benefit of providing support from different generating units.

Chapter 6 : Conclusion and Recommendations for Future Work

6.1 Conclusions

This thesis has demonstrated that APC can be carried out by a PVPP with appropriate control. The results indicate that a PVPP can contribute to the frequency stability of a power system and offset the impact of reducing inertia of a power system on a frequency response. An offline MPPT is first proposed for fast performance. This is because conventional MPPTs are not designed for frequency support where both speed and efficiency are important. The offline MPPT works by storing the maximum power voltage in a 2-D lookup table. The maximum power voltage is the output for any combination of irradiance and temperature. The maximum power point is obtained by numerically solving the diode IV curve equation for a wide operation range of the PV module. The characteristics of the module from the datasheet is used to determine the open-circuit voltage and short-circuit current for different irradiance and temperature combination. Unlike with the conventional P&O and incremental conductance, reserve can be maintained by directly changing the reference voltage and the maximum power value is known. However the effect of module ageing on the efficiency of the offline MPPT is not evaluated in this thesis. The output power of PV modules reduce with age and this may affect the accuracy of the offline MPPT

calculation over time. Also, the offline MPPT needs to be practically evaluated in diverse irradiance conditions and its performance in shading condition evaluated.

A PV system implementing the proposed offline MPPT and operating with a reserve is controlled to provide frequency response. FFR, emulated inertia, droop control and combined droop + inertia are implemented. The results show that PV systems implementing FFR, droop control and combined droop + inertia results in smaller nadir with increasing penetration when appropriate parameters are selected. This is owed to the fast response of the PV system. The amount of available reserve is identified as the main factor that determines the effectiveness of frequency support from PVPP. A variable droop control is proposed to increase the effectiveness of frequency support and utilize available reserve. The variable droop combines the FFR and droop support. The FFR is used to deliver support for the first few seconds immediately after a frequency event then the support switches to droop control. A comprehensive description of how a PVPP can participate in frequency response has been presented in this thesis. The different aspects such as MPPT and APC has been described. This is useful in evaluating the role of PV systems in future power systems and designing frequency support schemes for power systems with significant PV penetration. Frequency support by PVPP require that they are operated below maximum power point. Operating PVPP below maximum power point will have economic implications which need to be assessed. PVPP can also provide frequency support by operating at maximum power with a storage system. The different merits and demerits of these two methods need to be analyzed.

The basic P&O algorithm fails to track maximum power in fast-increasing irradiance and several modifications have been proposed to drift-free operation. Most solutions to the drift of the basic P&O requires changing the perturbation size of the voltage or duty cycle when an increasing irradiance is detected. This method is effective in preventing a drift. However, changing the perturbation size can lead to large swing in power. In this thesis, drift-free operation is achieved by keeping the PV voltage oscillating around its value just before the irradiance begins to increase. By maintaining drift-free operation, PV systems with P&O algorithm can participate in APC in dynamic irradiance conditions. Results from this thesis show that the performance of a PV system providing frequency support can be affected by the speed

and the efficiency of the MPPT. The performance can also be affected the accuracy of the APC method. However, the proposed modification to the P&O leads to slight deviation from MPP when the irradiance is increasing and it is necessary to evaluate its overall performance with a field test.

Another major contribution of this thesis is the designing of a framework for quantifying and comparing frequency support. A Second-order system is used to represent different generators and their response speeds are represented by the time constants. Derivation of the relationship between the change in frequency and support parameters is presented. The nadir and maximum power increase coefficient for any generation-load imbalance are obtained for different support parameters. Inertia emulation, droop control and droop + inertia support methods are considered. The effect of response delay on the maximum power increase and nadir coefficients is analyzed. The results obtained provides guidance to selecting frequency support methods and parameters to obtain a particular nadir or maximum power increase coefficient in a frequency event.

Frequency support burden can also be distributed with economic consideration. The cost of de-loading generating units will differ among units and should be considered in designing frequency support schemes. Technically, the best frequency support schemes should deliver the smallest nadir and the least maximum power increase.

6.2 Recommendations for Further Work

- Results from this thesis show that the MPPT used in a PV system can affect its performance in some APC functions. Future work can examine the role of the MPPT parameters such as the sampling rate, voltage step size, duty cycle step size and dynamic tracking ability in APC performance for different MPPT techniques.
- Field testing and verification of the efficiency of the proposed offline MPPT. The proposed MPPT was implemented using simulation. However, a field testing is essential to validate the performance of the proposed offline MPPT in practical PV systems. Partial shading is another condition that can affect the output power of a PV system. The performance of a PV system with the offline

MPPT should be evaluated in partial shading conditions. This can be done by subjecting the module to non-uniform irradiance. If required modifications should be developed for improved performance in partial shading conditions. Testing the P&O with additional loops in a small size PV system and comparison to other complex P&O MPPT methods.

- The efficiency of PV systems reduces as the modules degrade. Conventional MPPTs using real-time perturbations can still track MPP. The offline MPPT uses a one-time calculation of the maximum power voltage and current. Further work can evaluate the effect of aging of the PV modules on the IV curve. The long-term efficiency of the proposed module can be improved by the continuous adjustment of the calculated MPP values as the module age. Machine learning could be used to adjust the MPP values over time.
- Future work can evaluate the effect on the cost power from PVPP providing frequency support.
- The effect of the proposed modification to the overall efficiency of the PV system can be evaluated using a small-scale PV system and compared to other P&O modifications for drift avoidance.
- Results from this thesis show that the available reserve affects the ability of PV system to provide frequency support. Future work can optimize the use of reserve to provide frequency support.
- Further testing of Frequency support from a PV power plant can be done with the use of a PV simulator or small-scale PV system and a grid simulator. The different support techniques can be implemented in simulated fault conditions. A comprehensive comparison of different MPPT for different APC functions can be carried out in a PV system connected to a grid simulator.
- Future work can evaluate the efficiency of the proposed P&O with proposed additional loop. The proposed P&O with other drift-avoiding MPPTs for efficiency, simplicity and cost of implementation.

References

[1] GISTEMP Team, 2020, 'GISS Surface Temperature Analysis (GISTEMP), version 4', NASA Goddard Institute for Space Studies. Dataset accessed: 17 April 17, 2020 at https://data.giss.nasa.gov/gistemp/.

[2] N. G. Lenssen, J. Schmidt, M. Hansen, et al., 'Improvements in the GISTEMP uncertainty model' in Journal of Geophysical Research: Atmospheres, vol 124, no. 12, pp. 6307-6326, 2019, http://doi.org/10.1029/2018JD029522.

[3] IPCC, 2018: Summary for Policymakers. In: Global Warming of 1.5°C. An IPCC Special Report on the impacts of global warming of 1.5°C above pre-industrial levels and related global greenhouse gas emission pathways, in the context of strengthening the global response to the threat of climate change, sustainable development, and efforts to eradicate poverty. World meteorological organization, Geneva, Switzerland, 32 pp.

[4] B. D. Santer, K. E. Taylor, T. M. L. Wigley, et al. 'A search for human influences on the thermal structure of the atmosphere', Nature 382, pp. 39-46. https://doi.org.10.1038/382039a0

[5] IPCC, 2014, 'Climate Change 2014: Synthesis report. Contribution of working groups I, II, an III to the Fifth Assessment Report on the intergovernmental panel on Climate change. IPCC, Geneva, Switzerland.

[6] E. Dlugokencky and P. Tans, 'NOAA/ESRL,' www.esrl.noaa.gov/gmd/ccgg/trends, accessed May 2020.

[7] D.M. Etheridge, L.P. Steele, R.L. Langenfelds, R.J. Francey, J.-M. Barnola and V.I. Morgan. 1998. Historical CO_2 records from the Law Dome DE08, DE08-2, and D.S.S. ice cores. In Trends: A Compendium of Data on Global Change. Carbon Dioxide Information Analysis Center, Oak Ridge National Laboratory, U.S. Department of Energy, Oak Ridge, Tenn., U.S.A.

[8] EU, 'Directive (EU) 2018/2001 of the European Parliament and of the Council of 11 December 2018 on the promotion of the use of energy from renewable sources (Text with EEA relevance). http://data.europa.eu/eli/dir/2018/2001/oj, Accessed: 2 May 2020.

[9] Ofgem, 'Electricity generation mix by quarter and fuel source (GB),' https://www.ofgem.gov.uk/data-portal/electricity-generation-mix-quarter-and-fuel-source-gb, Accessed: May 2, 2020.

[10] Department for Business, Energy & Industrial Strategy, 'UK Renewable electricity capacity and generation, October to December 2019,' Section 6, Available: https://www.gov.uk/government/statistics/energy-trends-section-6-renewables, Accessed: May 2, 2020.

[11] Q. Shi, F. Li, Q. Hu, et al. 'Dynamic demand control for system frequency regulation: Concept review, algorithm comparison, and future vision,' in Electric Power Systems Research, vol. 154, pp. 75-87, 2018.

[12] U. Akram, M. Nadarajah, R. Shah, et al. 'A review on rapid responsive energy storage technologies for frequency regulation in modern power system,' in Renewable and Sustainable Energy Reviews, vol. 120, 109626, 2020.

[13] M. Dreidy, H. Mokhlis and S. Mekhilef, 'Inertia response and frequency control techniuqes for renewable energy sources: A review,' in Renewable and Sustainable Energy Reviews, vol. 69, pp. 144-155, 2017.

[14] IEA, 'Solar PV power generation in the Sustainable Development Scenario, 2000-2030,' IEA, Paris https://www.iea.org/data-and-statistics/charts/solar-pv-power-generation-in-the-sustainable-development-scenario-2000-2030

[15] P. Kundur, J. Paserba, V. Ajjarapu, et al. 'Definition and Classsification of Power System Stability,' in IEEE Transactions on Power Systems, vol. 19, no. 2, pp. 1387-1401, May 2004.

[16] R. Yan, N. -Masood, T. K. Saha, et al. 'The Anatomy of the 2016 south Australia Blackout: A Catastrophic Event in a High Renewable Network,' in IEEE Transactions on Power Systems, vol. 22, no. 5, pp. 5374-5388, September 2018.

[17] L. Wu, 'Provision of Power System Frequency Response in the Context of High Wind Penetration,' PhD Thesis, Department of Electrical and Electronics Engineering, University of Strathclyde, 2014.

[18] National Grid Plc, 'Frequency Response Services,' Accessed: May 2020, Available: https://www.nationalgrideso.com/industry-information/balancing-services/frequency-response-services.

[19] National Grid Plc, 'Frequency Response Services,' Accessed: May 2020, Available: https://www.nationalgrideso.com/industry-information/balancing-services/frequency-response-services.

[20] National Grid Plc, 'Frequency Response Services,' Accessed: May 2020, Available: https://www.nationalgrideso.com/industry-information/balancing-services/frequency-response-services

[21] National Grid Plc, 'Firm Frequency Response,' Accessed: May 2020, Available: https://www.nationalgrideso.com/balancing-services/frequency-response-services/firm-frequency-response-ffr.

[22] National Grid Plc, 'Dynamic Containment,' Accessed: May 2020, Available: https://www.nationalgrideso.com/industry-information/balancing-services/frequency-response-services/dynamic-containment

[23] National Grid Plc, 'Phase 2 Auction Trial,' Accessed: May 2020, Available: https://www.nationalgrideso.com/balancing-services/frequency-response-services/frequency-auction-trial.

[24] National Grid Plc, 'Mandatory Response Services,' Accessed: May 2020, Available: https://www.nationalgrideso.com/balancing-services/frequency-response-services/mandatory-response-services.

[25] IEA (2019), Electricity Information 2019, IEA, Paris https://www.iea.org/reports/electricity-information-2019

[26] Department of Business, Energy and Industrial Strategy (2020), 'UK electricity generation, trade and consumption, October to December 2019.' https://www.gov.uk/government/statistics/electricity-section-5-energy-trends

[27] IEA (2019), 'Renewables 2019, IEA, Paris.' https://www.iea.org/reports/renewables-2019

[28] P. Du and J. Matevosyan, "Forecast System Inertia Condition and Its Impact to Integrate More Renewables,' in *IEEE Transactions on Smart Grid*, vol. 9, no. 2, pp. 1531-1533, March 2018.

[29] A. B. Attya, J. L. Dominguez-Garcia and O. Anaya-Lara, 'A review of requency support provision by wind power plants: Current and future challenges,' in Renewable and sustainable Energy Reviews, vol. 81, pp. 2071-2087, 2018.

[30] X. Yingcheng, T. Nengling, ‘Review of contribution to frequency control through variable speed wind turbine,’ in Renewable Energy, vol. 36, no. 6, pp. 1671-1677, 2011.

[31] M. T. Muhssin, L. M. Cipcigan, S. S. Sami, Z. A. Obaid, ‘Potential of demand side response aggregation for the stabilization of the grids frequency,’ in Applied Energy, vol. 220, pp. 643-656, 2018.

[32] J. Fang, H. Li, Y. Tang and F. Blaabjerg, ‘On the Inertia of Future More-Electronics Power Systems,’ in IEEE Journal of Emerging and Selected Topics in Power Electronics, vol. 7, no. 4, pp. 2130-2146, December 2019.

[33] C. Li, Y. Wu, Y. Sun, et.al, ‘Continous Under-Frequency Load Shedding Scheme for Power System Adaptive Frequency Control,’ in IEEE Transactions on Power Systems, vol. 35, no. 2, pp. 950-961, March 2020.

[34] P. Tielens, D.V. Hertem, ‘The relevance of inertia in power system,’ in Renewable and sustainable Energy Review, vol. 55, pp. 999-1009, 2016

[35] Y. Bian, H. Wyman-Pain, F. Li, et al. ‘Demand Side Contributions for System Inertia in the GB Power System,’ in IEEE Transactions on Power Systems, vol. 33, no. 4, pp. 3521-3530, July 2018.

[36] J. Morren, J. Pierik and S.W.H. de Haan, ‘Inertia response of variable speed wind turbines,’ in Electric Power Systems Research, vol. 76, pp. 980-987, 2006.

[37] A. Fernandez-Guillamon, E. Gomez-Lazaro, E. Muljadi, et al. ‘Power systems with high renewable energy sources: A review of inertia and frequency control strategies over time,’ in Renewable and Sustainable Energy Review, vol. 115, 2019

[38] P. Kundur, ‘Power system stability and control,’ USA, New York, McGraw Hill, 1994.

[39] E. Muljadi, M. Singh and V. Gevorgian, ‘Doubly Fed Induction Generatro in an Offshore Wind Power Plant Operated at Rated V/Hz,’ in IEEE Transactions on Industry Applications, vol. 49, no. 5, pp. 2197-2205, Sept.-Oct. 2013.

[40] O. Anaya-Lara, N. Jenkins, J. Ekanayake, et al., ‘Wind Energy Generation,Modelling and Control,’ John Wiley and Sons, 2009.

[41] N. R. Ullah, T. Thiringer and D. Karlsson, 'Temporary Primary Frequency Control Support by Variable Speed Wind Turbines – Potential and Application' in IEEE Transactions on Power Systems, vol. 23, no. 2, May 2008.

[42] J. Morren, S. W. H. Haan, W. L. Kling, J. A. Ferreira, "Wind turbines emulating inertia and supporting primary frequency control", in IEEE Transactions on Power Systems, vol. 21, no. 1, pp. 433-434, Feb. 2006.

[43] J. V. de Vyer, J. D. M. de Kooning, B. Meersman, et al. 'Droop control as an alternative Inertial Response Strategy for Synthetic Inertia on Wind Turbines,' in IEEE Transactions on Power Systems, vol. 31, no. 2, pp. 1129-1138, March 2016.

[44] P. Keung, P. Li, H. Banakar, et al. 'Kinetic Energy of Wind-Turbine Generators for System Frequency Support,' in IEEE Transaction on Power Systems, vol. 24, no. 1, pp. 279-287, February 2009.

[45] M. Garmroodi, G. Verbic and D. J. Hill, 'Frequency Support From Wind Turbine Generators With a Time-Variable Droop Characteristics,' in IEEE Transactions Sustainable Energy, vol. 9, no. 2, pp. 676-684, April 2020.

[46] S. Wang and K. Tomsovic, 'Fast Frequency Support From Wind Turbine Generators With Auxillary Dynamic Demand Control,' in IEEE Transactions on Power Systems, vol. 34, no. 5, pp. 3340-3348, September 2019.

[47] A. B. Attya and T. Hartkopf, 'Wind turbine support techniques during frequency drop – energy utilization comparison,' AIMS Energy Journal, vol. 2, no. 3, pp. 260-275, 2014.

[48] J. Zhang, M. Cheng, Z. Chen, et al. 'Pitch angle control for variable speed wind turbines,' Third International Conference on Electric Utility Deregulation and Restructuring and Power Technologies, Nanjing, pp. 2691-2696, 2008.

[49] R. G. de Almeida and J. A. Pecas Lopes, 'Participation of Doubly Fed Induction Wind Generators in System Frequency Regulation,' in IEEE Transaction on Power Systems, vol. 22, no. 3, pp. 944-950, August 2007.

[50] L. Wu, 'Provision of Power System Response in the context of High Wind Penetration,' PhD Thesis, Department of Electronic and Electrical Engineering, University of Strathclyde, UK, 2004

[51] G. Ramtharan, J. B. Ekanayake and N. Jenkings, ‘Frequency support from doubly fed induction generator wind turbines,’ in IET Renewable Power Generatioin, vol. 2, no. 1, pp. 3-9, March 2007.

[52] H. Luo, Z. Hu, H. Zhang, et al., ‘Coordinated Active Power Control Strategy for Deloaded wind turbines to Improve Regulation Performance in AGC,’ in IEEE Transactions on Power Systems, vol. 34, no. 1, January 2019.

[53] J. Nelson, ‘The Physics of Solar Cells,’ Imperial College Press, London, UK, 2003.

[54] National Renewable Energy Laboratory, ‘Best Research-Cell Efficiency Chart,’ Accessed: April 2020 Available: https://www.nrel.gov/pv/cell-efficiency.html

[55] A. R. Reisi, M. H. Moradi and S. Jamasb, ‘Classification and comparison of maximum power point tracking techniques for photovoltaic system: A review,’ in Renewable and Sustainable Energy Reviews, vol. 19, pp. 433-443, Marh 2012.

[56] V. Gevorgian and S. Booth, ‘Review of PREPA technical requirements for interconnecting wind and solar generation,’ National Renewable Energy Laboratory (NREL), Technical Report, 2013.

[57] A. Cabrera-Tobar, E. Bullich-Massague, M. Aragues-Penalba, et al. ‘Review of advanced grid requirements for the integration of large scale photovoltiaic power plants in the transmission system,’ in Renewable and Sustainable Energy Reviews, vol. 62, pp. 971-987, 2016.

[58] B. Cracium, T. Kerekes, D. Sera, et al. ‘Frequency Support Functions in Large PV Power Plants With Active Power Reserves,’ in IEEE Journal of Emerging and Selected Topics in Power Electronics, vol. 2, no. 4, pp. 849-858, December 2014.

[59] C. Rahmann and A. Castillo, ‘Fast Frequency Response Capability of Photovoltaic Power Plants: The Necessity of New Grid Requirements and Definitions,’ in Energies, vol. 7, pp. 6306-6322, 2014.

[60] P. P. Zarina, S. Mishra and P. C. Sekhar, ‘Exploring frequency control capabilities of a PV system in a hybrid PV-rotating machine – without storage system,’ vol. 60, pp. 258-267, September 2014.

[61] A. Evans, V. Strezov and T. J. Evans, ‘Assessment of utility energy storage options for increased renewable energy penetration,’ in Renewable and Sustainable Energy Reviews, vol. 14, pp. 4141-4147, 2012.

[62] X. Luo, J. Wang, M. Dooner, et al. ‘Overview of current development in electrical energy storage technologies and the application potential in power system operation,’ in Applied Energy, vol. 137, pp. 511-536, 2015.

[63] O. Palizban and K. Kauhaniemi, ‘Energy storage systems in modern grids – Matix of technologies and applications,’ in Journal of Energy Storage, vol. 6, pp. 248-259, May 2016.

[64] L. Lu, X. Han, J. Li, et al. ‘A review on the key issues for lithium-ion battery management,’ in electric vehicles,’ vol. 226, pp. 272-288, 2013.

[65] S. Adhikari and F. Li, ‘Coordinated V-f and P-Q Control of Solar Photovoltaic Generators with MPPT and Battery Storage in Microgrids,’ in IEEE Tansactions on Smart Grid, vol. 5, no. 3, pp. 1270-1281, May 2014.

[66] S. Zhang, Y. Mishra and M. Shahidehpour, ‘Fuzzy-Logic Based Frequency Controller for Wind Farms Augumented With Energy Storage Systems,’ in IEEE Transactions on Power Systems, vol. 31, no. 2, pp. 1595-1603, March 2016.

[67] J. Tan and Y. Zhang, ‘Coordinated Control Strategy of a Battery Energy Storgage System to Support a Wind Power Plant Providing Multi-Timescale Frequency Ancillary Services,’ in IEEE Transactions on Sustainable Energy, vol. 8. No. 3, July 2017.

[68] H. Silva-Saravia, H. Pulgar-Painemal and J. M. Mauricio, ‘Flywheel Energy Storage Model, Control and Location for Improving Stability: The Chilean Case,’ in IEEE Transactions on Power Systems, vol. 32, no. 4, July 2017.

[69] A. A. K. Arani, H. Karami, G. B. Gharehpetian, et al. ‘Review of Flywheel Energy Storage systems structure and application in power systems and microgrids,’ in Renewable and Sustainable Energy Review, vol. 69, pp. 9-18, 2017.

[70] F. Diaz-Gonzalez, M. Hau, A. Sumper, et al. ‘Corodinated operation of wind turbines and flywheel storage for primary frequency control support,’ in Electrical Power and Energy Systems, vol. 68, pp. 313-326, 2015.

[71] X. Wu, Y. Zhang, A. Arulampalam, et al. ‘Electrical Stability of Large Scale Integration of Micro Generation Into Low Voltage Grids,’ in International Journal of Electronics, pp. 1-23, 2005.

[72] S. Rehman, L. M. Al-Hadhrami and M. M. Alam, ‘Pumped hydro energy storage system: A technological review,’ in Renewable and Sustainable Energy Reviews, vol. 44, pp. 586-598, 2015

[73] Quident Energy, http://www.quidnetenergy.com/solution/?section=homeSection#homeSection Accessed: April 2020.

[74] A. B. T. Attya and T. Hartkopf, ‘Utilising stored wind energy by hydro-pumped storage to provide frequency support at high levels of wind energy penetration,’ in IET Generation, Transmission and Distribution, vol. 9, no.12, pp. 1485-1497, 2015.

[75] Scottish Renewables, ‘The Benefits of Pumped Storage Hydro to the UK,’ Report DNV GL 2016.

[76] F. Diaz-Gonzalez, A. Sumper, O. Gomis-Bellmunt, et al. ‘A review of energy storage technologies for wind power applications,’ in Renewable and Sustaiable Energy Reviews, vol. 16, pp. 2154-2171.

[77] K. Sahay and B Dwivedi, ‘Supercapacitors Energy Storage System for Power Quality Improvement: An Overview,’ in Journal of Electrical Systems, 2009.

[78] G. Venkataramani, P. Parankusam, V. Ramanlingam, et al. ‘A review of compressed air energy storage – A pathway for smart grid and polygeneration,’ in Renewable and Sustainable Energy Review, vol. 62, pp. 895-907, 2016.

[79] S. Koohi-Fayegh and M. A. Rosen, ‘A review of energy storage types, application and recent developments,’ in Journal of Energy Storage, vol. 27, (101047), 2017.

[80] J. Kim, V. Gevorgian, Y. Luo, et al. ‘Supercapacitor to Provide Ancillary Services With Control Coordination,’ in IEEE Transactions on Industry Applications, vol. 55, no. 5, September/Octorber 2019.

[81] Y. Tan, K. M. Muttaqi, P. Ciufo, et al. ‘Enhanced Frequency Regulation Using Multilevel Energy Storage in Remove Area Power Supply Systems,’ in IEEE Transactions on Power Systems, vol. 34, no. 1, January 2019.

[82] M. T. Muhssin, L. M. Cipigan, S. S. Sami, et al. ‘Potential of demand side response aggregation for the stabilization of the grids frequency,’ in Applied Energy, vol. 220, pp. 643-656, 2018.

[83] K. Dehghanpour and S. Afsharnia, ‘Electrical demand side contribution to frequency control in power systems: a review on technical aspects,’ in Renewable and Sustainable Energy Review, vol. 41, pp. 1267-1276, 2015.

[84] J. Kondoh, N. Lu and J. Hammerstrom, ‘An Evaluation of the Water Heater Load Potential for Providing Regulation Service,’ in IEEE Transactions on Power Systems, vol. 26, no. 3, pp. 1309-1316, 2011.

[85] S. A. Pourmousavi, and M. H. Nehrir, ‘Real-Time Central Demand Response for Primary Frequency Regulation in Microgrids,’ in IEEE Transactions on Smart Grid, vol. 3, no. 4, pp. 1988-1996, 2012.

[86] A. Molina-Garcia, F. Bouffard and D. S. Kirschen, ‘Decentralized Demand-Side Contribution to Primary Frequency Control,’ in IEEE Transactions on Power Systems, vol. 26. No. 1, February 2011.

[87] H. W. Qazi and D. Flynn, ‘Analysing the impact of large -scale decentralized demand side response on frequency stability,’ in Electrical Power and Energy Systems, vol. 80, pp. 1-9, 2016.

[88] C. Peng, J. Zou, L. Lian, et al. ‘An optimal dispatching strategy for V@G aggregator participating in supplementary frequency regulation considering EV driving demand and aggregator’s benefit,’ in Applied Energy, vol. 190, pp. 591-599, 2017.

[89] A. Mill et al., "Understanding variability and uncertainty of photovoltaics for integration with the electric power system," Lawrence Berkeley Nat. Lab., 2010

[90] X. Chen, Y. Du, H. Wen, L. Jiang, and W. Xiao, "Forecasting-Based Power Ramp-Rate Control Strategies for Utility-Scale PV Systems," in IEEE Transactions on Industrial Electronics, vol. 66, no. 3, pp. 1862-1871, March 2019

[91] J. Martins, S. Spataru, D. Sera et al. "Comparative Study of Ramp-Rate Control Algorithms for PV with Energy Storage Systems," Energies, 12, 1342.

[92] V. T. Tran, M. R. Islam, D. Sutanto, and K. M. Muttaqi, "Mitigation of Solar PV Intermittency Using Ramp-Rate Control of Energy Buffer Unit," in *IEEE Transactions on Energy Conversion,* vol. 34, no. 1, pp. 435-445, March 2019

[93] A. Sangwongwanich, Y. Yang and F. Blaabjerg, "Development of flexible active power control strategies for grid-connected photovoltaic inverters by modifying MPPT algorithms," 2017 IEEE 3rd International Future Energy Electronics Conference and ECCE Asia (IFEEC 2017 - ECCE Asia), Kaohsiung, 2017, pp. 87-92.

[94] A. Hoke, E. Muljadi and D. Maksimovic, "Real-time photovoltaic plant maximum power point estimation for use in grid frequency stabilization," 2015 IEEE 16th Workshop on Control and Modeling for Power Electronics (COMPEL), Vancouver, BC, 2015, pp. 1-7

[95] H. Beltran, E. Bilbao, E. Belenguer, I. Etxeberria-Otadui, and P. Rodriguez, "Evaluation of Storage Energy Requirements for Constant Production in PV Power Plants," in IEEE Transactions on Industrial Electronics, vol. 60, no. 3, pp. 1225-1234, March 2013

[96] A. Hoke and D. Maksimović, "Active power control of photovoltaic power systems," 2013 1st IEEE Conference on Technologies for Sustainability (SusTech), Portland, OR, 2013, pp. 70-77.

[97] J. Ahmed, and Z. Salam, "An improved perturb and observe (P&O) maximum power point tracking (MPPT) algorithm for higher efficiency, " in Applied Energy, Vol. 150, pp. 97-108, 2015

[98] M. Abdel-Salam, M.T El-Mohandes, and M. Goda, "An improved perturb-and-observe based MPPT method for PV systems under varying irradiation levels," in Solar Energy, Vol. 171, pp. 547-561, 2018

[99] S. Saravanan, N. Ramesh Babu, "Maximum power point tracking algorithms for photovoltaic system – A review," in Renewable and Sustainable Energy Reviews, Vol. 57, pp. 192-204, 2016.

[100] N. A. Kamarzaman, C. W. Tan, "A comprehensive review of maximum power point tracking algorithms for photovoltaic systems, " in Renewable and Sustainable Energy Reviews, vol. 37, pp. 585-598, 2014.

[101] M. A. Elgendy, B. Zahawi, and D. J. Atkinson, "Comparison of Directly Connected and Constant Voltage Controlled Photovoltaic Pumping Systems," in IEEE Transactions on Sustainable Energy, vol. 1, no. 3, pp. 184-192, Oct. 2010.

[102] M. Killi and S. Samanta, "Modified Perturb and Observe MPPT Algorithm for Drift Avoidance in Photovoltaic Systems," *in* IEEE Transactions on Industrial Electronics, vol. 62, no. 9, pp. 5549-5559, Sept. 2015.

[103] A. F. Hoke, M. Shirazi, S. Chakraborty, E. Muljadi, and D. Maksimovic, "Rapid Active Power Control of Photovoltaic Systems for Grid Frequency Support," in IEEE Journal of Emerging and Selected Topics in Power Electronics, vol. 5, no. 3, pp. 1154-1163, Sept. 2017

[104] L. M. Elobaid, A. K. Abdelsalam and E. E. Zakzouk, "Artificial neural network-based photovoltaic maximum power point tracking techniques: a survey," in IET Renewable Power Generation, vol. 9, no. 8, pp. 1043-1063, 11 2015

[105] D. Sera, R. Teodorescu, J. Hantschel and M. Knoll, "Optimized Maximum Power Point Tracker for fast changing environmental conditions," 2008 IEEE International Symposium on Industrial Electronics, Cambridge, 2008, pp. 2401-2407

[106] K. Yan, Y. Du and Z. Ren, "MPPT Perturbation Optimization of Photovoltaic Power Systems Based on Solar Irradiance Data Classification," in IEEE Transactions on Sustainable Energy, vol. 10, no. 2, pp. 514-521, April 2019.

[107] A. Sangwongwanich, Y. Yang, F. Blaabjerg, et al., 'Delta Power Control Strategy for Multistring Grid-Connected PV Inverters,' in IEEE Transactions on Industry Applications, vol. 53, no. 4, pp. 3863-3870, July/August 2017.

[108] F. Vignola, A. Andreas, "University of Oregon: GPS-based Precipitable water vapour (Data), " NREL Report No. DA-5500-64452, 2013. Available at http://dx.doi.org/10.7799/1183467

[109] F. Jibji-Bukar and O. Anaya-Lara, "Frequency support from photovoltaic power plants using offline maximum power point tracking and variable droop control," in IET Renewable Power Generation, vol. 13, no. 13, pp. 2278-2286, 7 10 2019.

[110] S. S. Sami (2017), 'Virtual energy storage for frequency and voltage control,' PhD Thesis, Cardiff University. Available at https://ethos.bl.uk/OrderDetails.do?did=1&uin=uk.bl.ethos.723587. (Accessed: January 29, 2020)

[111] J. A. Short, D. G. Infield and L. L. Freris, "Stabilization of Grid Frequency Through Dynamic Demand Control," in IEEE Transactions on Power Systems, vol. 22, no. 3, pp. 1284-1293, Aug. 2007.

[112] W. Yang, J. Yang, W. Guo, and P. Norrlund, Response time for primary frequency control of hydroelectric generating unit, International Journal of Electrical Power & Energy Systems, Volume 74, 2016, Pages 16-24

[113] P. V. Brogan, R. J. Best, D. J. Morrow, K. McKinley and M. L. Kubik, "Effect of BESS Response on Frequency and RoCoF During Underfrequency Transients," in IEEE Transactions on Power Systems, vol. 34, no. 1, pp. 575-583, Jan. 2019.

[114] I. Beil, I. Hiskens and S. Backhaus, "Frequency Regulation From Commercial Building HVAC Demand Response," in Proceedings of the IEEE, vol. 104, no. 4, pp. 745-757, April 2016.

[115] V. Trovato, I. M. Sanz, B. Chaudhuri and G. Strbac, "Advanced Control of Thermostatic Loads for Rapid Frequency Response in Great Britain," in *IEEE Transactions on Power Systems*, vol. 32, no. 3, pp. 2106-2117, May 2017.

[116] Zhu, Q (2017) *Frequency Supporting of Smart Grid with Wind Power via Demand Side Response.* PhD thesis, University of Liverpool. Available at: https://livrepository.liverpool.ac.uk/3005582/. Accessed: January 29, 2020.

[117] A. B. T. Attya and J. L. Domínguez-García, "A Novel Method to Valorize Frequency Support Procurement by Wind Power Plants," in *IEEE Transactions on Sustainable Energy*, vol. 11, no. 1, pp. 239-249, Jan. 2020.

[118] F. Teng and G. Strbac, "Assessment of the Role and Value of Frequency Response Support From Wind Plants," in IEEE Transactions on Sustainable Energy, vol. 7, no. 2, pp. 586-595, April 2016.

APPENDIX A

Figures A-1 and A-2 give the responses to a 0.1pu change in load for system with PVPP providing combined droop and inertia support. The responses show smaller nadir when K_{in} is 8 than when K_{in} is 6.

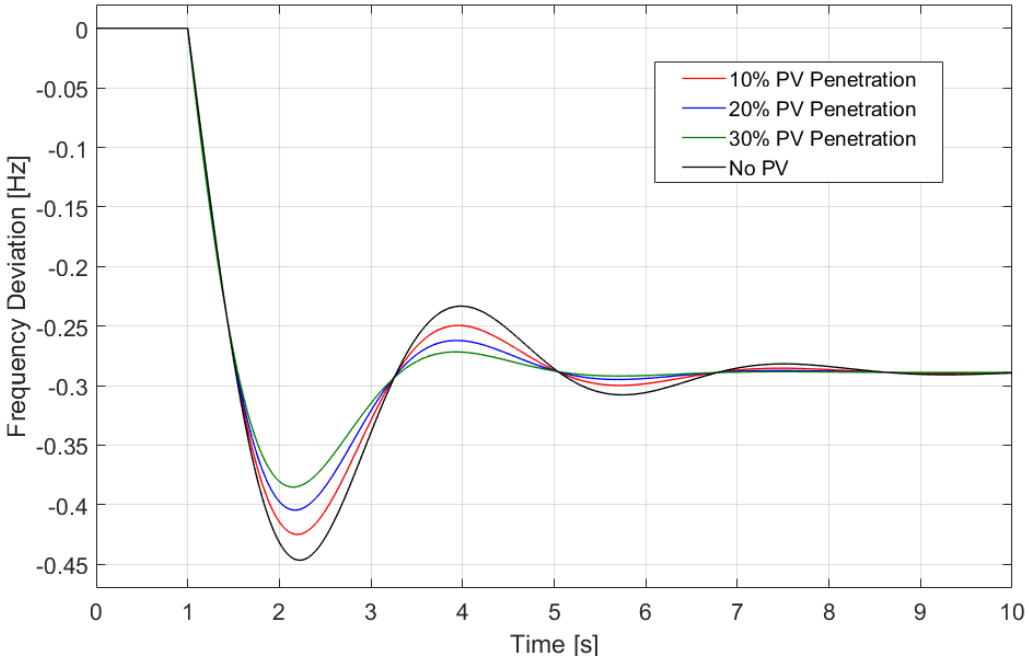

Figure A - 1: Combined inertia (K_{in}=6) and Droop (D_g=20)

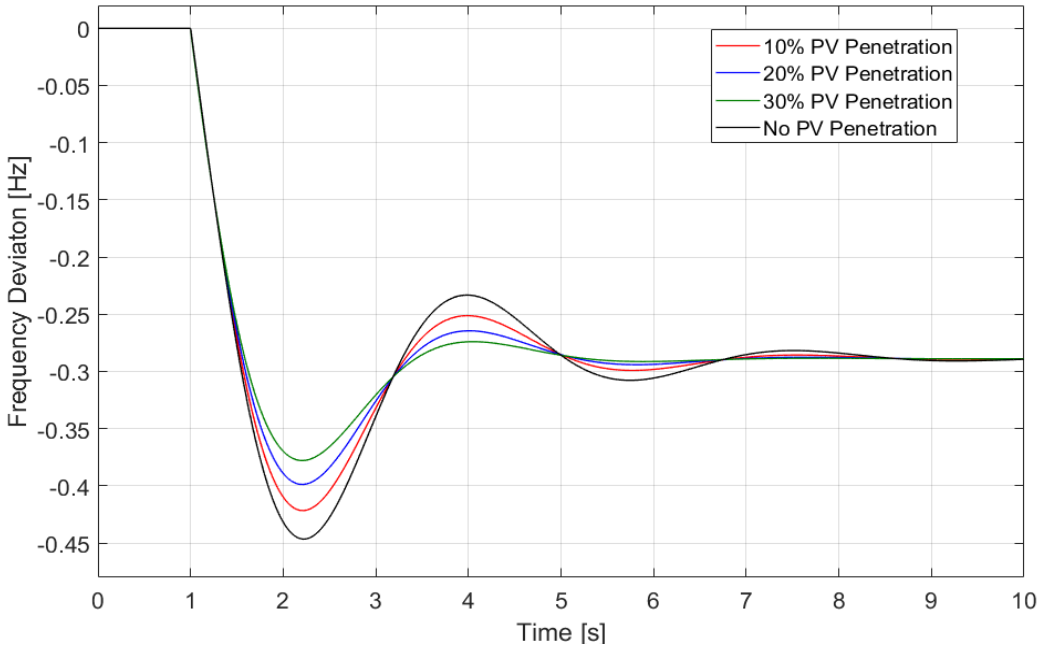

Figure A - 2: Combined inertia (K_{in}=8) and Droop (D_g=20)

Figure A-3 and Figure A-4 give the responses to a 0.1pu change in load for a system with PVPP providing only inertia support. The responses when K_{in} 8 results in smaller nadir than the responses when K_{in} is 6. However, with only inertia support PVPP, the nadir increases with increasing penetration.

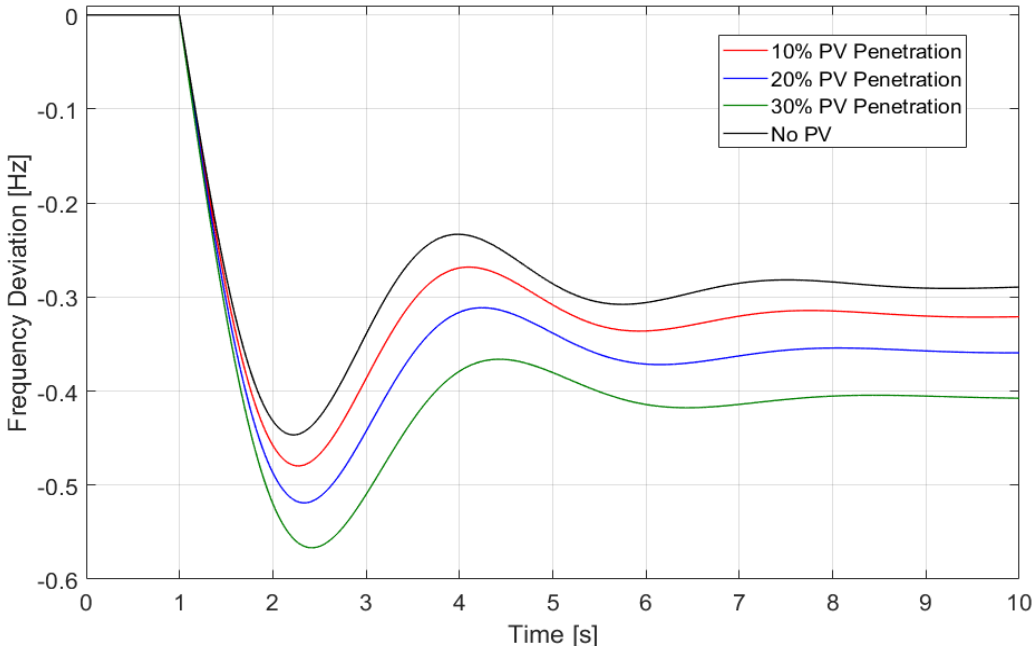

Figure A - 3: Inertia Support (K_{in}=6)

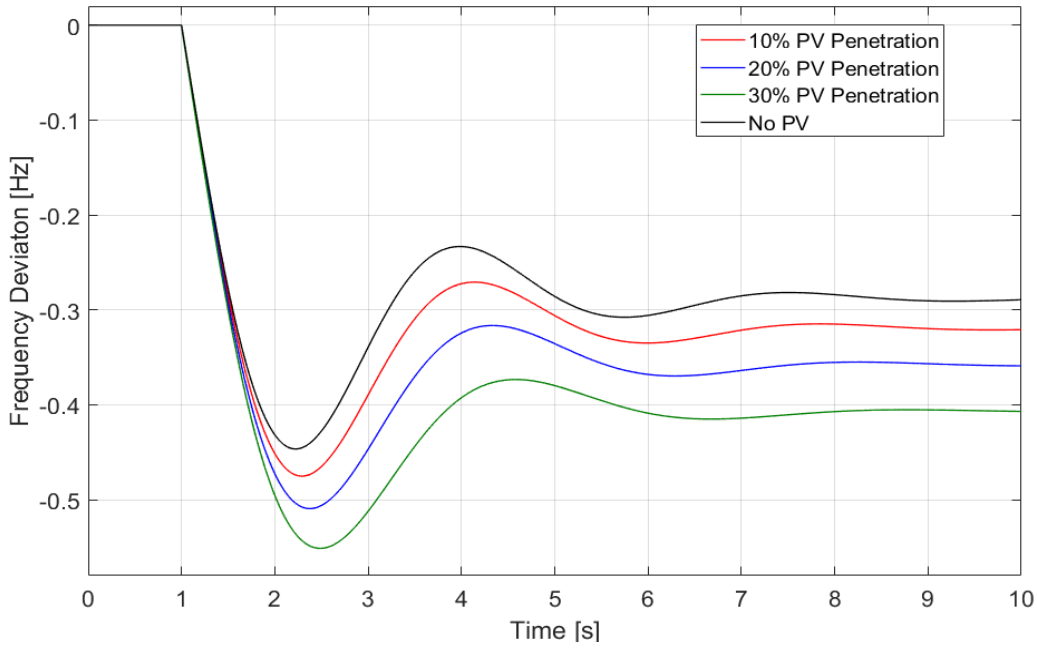

Figure A - 4: Inertia Support (K_{in}=6)